AD_____

AWARD NUMBER: W81XWH-07-1-0160

TITLE: ATF4, A Novel Mediator of the Anabolic Actions of PTH on Bone

PRINCIPAL INVESTIGATOR: Guozhi Xiao, M.D., Ph.D.

CONTRACTING ORGANIZATION: University of Pittsburgh
Pittsburgh, PA 15260

REPORT DATE: July 2010

TYPE OF REPORT: Annual

PREPARED FOR: U.S. Army Medical Research and Materiel Command
Fort Detrick, Maryland 21702-5012

REPORT DOCUMENTATION PAGE

Form Approved
OMB No. 0704-0188

1. REPORT DATE *(DD-MM-YYYY)*	**2. REPORT TYPE**	**3. DATES COVERED** *(From - To)*
01-Jul-2010	Annual	1 JUL 2009 - 30 JUN 2010

4. TITLE AND SUBTITLE
ATF4, A Novel Mediator of the Anabolic Actions of PTH on Bone

5a. CONTRACT NUMBER
W81XWH-07-1-0160

5b. GRANT NUMBER
PR064047

5c. PROGRAM ELEMENT NUMBER

6. AUTHOR(S)
Guozhi Xiao

Email: xiaog@upmc.edu

5d. PROJECT NUMBER

5e. TASK NUMBER

5f. WORK UNIT NUMBER

7. PERFORMING ORGANIZATION NAME(S) AND ADDRESS(ES)

University of Pittsburgh
Office of Research
350 Thackeray Hall
Pittsburgh, PA 15260

8. PERFORMING ORGANIZATION REPORT NUMBER

9. SPONSORING / MONITORING AGENCY NAME(S) AND ADDRESS(ES)
US Army Medical Research
And Materiel Command
Fort Detrick, MD 21702-5104

10. SPONSOR/MONITOR'S ACRONYM(S)

11. SPONSOR/MONITOR'S REPORT NUMBER(S)

12. DISTRIBUTION / AVAILABILITY STATEMENT

Approved for public release; distribution unlimited

13. SUPPLEMENTARY NOTES

14. ABSTRACT

During the last year of support (from July 1, 2009 to June 30, 2010), our studies have made significant progresses in all aspects of the study: 1) we demonstrate that ATF4 is essential for PTH promotion of osteoblast differentiation in vivo; 2) we have identified and characterized an ATF4-response element in mouse Osx promoter that is essential for ATF4 to induce Osx expression in osteoblasts and probably osteoblast differentiation; 3) we demonstrate that ATF4 is required for the anabolic actions of PTH in bone in adult OVX mice; 4) we have established that ATF4 is important for intermittent PTH to stimulate osteoblast-mediated bone formation in vivo; 5) we have revealed that ATF4 is essential for OVX induction of bone loss in vivo; and 6) we have identified and functionally characterized Erk/MAPK phosphorylation sites in Runx2, an ATF4-interacting factor identified by the project laboratory. In the next year of support, we will: i) identify and characterize PTH response phosphorylation site in ATF4; ii) determine the molecular mechanism whereby ATF4 promotes osteoblast proliferation and survival; and iii) determine the role of ATF4-Runx2 interactions in PTH-induced osteoblast function.

15. SUBJECT TERMS
ATF4, Runx2, PTH, anabolism, proliferation, apoptosis

16. SECURITY CLASSIFICATION OF:			**17. LIMITATION OF ABSTRACT**	**18. NUMBER OF PAGES**	**19a. NAME OF RESPONSIBLE PERSON**
a. REPORT	**b. ABSTRACT**	**c. THIS PAGE**			USAMRMC
U	U	U	UU	42	**19b. TELEPHONE NUMBER** *(include area code)*

Table of Contents

Page

This progress report covers research from the period 07/01/09-06/30/10

Introduction

Osteoporosis, or reduced bone mass, is a metabolic bone disease that affects millions of people including many of our service women and men now in the Armed Forces and VA patients in the United States. It causes a significant amount of morbidity and mortality in patients and is often diagnosed after a fracture occurs. Reducing the risk of osteoporotic and associated fractures of these patients will greatly improve their life quality and survival. Parathyroid hormone (PTH) is the most potent anabolic treatment of osteoporosis currently available. It not only dramatically improves bone mass, but also restores bone microarchitecture and increases bone diameter. All of these mechanisms contribute to increasing bone strength and reducing the risk for fractures. However, the molecular mechanisms whereby PTH increases bone formation are not well understood. Our central hypotheses in this study are: 1) PTH activates ATF4 by promoting its phosphorylation and protein-protein interactions with Runx2; and 2) ATF4 mediates the anabolic actions of PTH on bone. The long-tern goal of this study is to elucidate the molecular mechanisms underlying the anabolic actions of PTH on bone. Two Specific Aims have been proposed to determine the functional relationships between ATF4 and PTH actions in osteoblasts and bone: 1) determine the mechanism whereby PTH regulates ATF4 transcriptional activity; 2) establish whether the anabolic actions of PTH require ATF4 *in vivo*. Studies determine if ATF4 is required for the anabolic actions of PTH *in vivo* using ATF4-deficient mice. PTH anabolic activity is evaluated in wild type and *Atf4*$^{-/-}$ mice. PTH effects are measured using standard biochemical and histomorphometric criteria.

Body

Task 1: To determine the mechanism by which PTH regulates ATF4 and Runx2 transcriptional activity (1-36 months). During last year of support, we have made the following significant progress in this Task:

1) ATF4 is essential for PTH to increase osteoblast differentiation in vivo (P1).

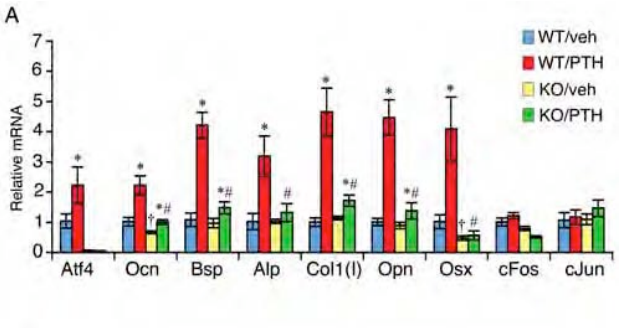

B

	WT/veh	WT/PTH	KO/veh	KO/PTH
IGF-1(ng/ml)	398 ± 57	412 ± 51	187 ± 7†	184 ± 4
FGF-2 (pg/ml)	8.6 ± 0.4	9.0 ± 0.2	6.3 ± 0.6†	7.4 ± 0.6

N = 5-8

Fig 1. Effects of PTH on expression of osteoblast marker genes in wt and ATF4 deficient mice. A, quantitative real-time PCR, total RNAs were isolated from tibiae and analyzed by quantitative real-time RT-PCR using specific primers for *Atf4, Ocn, Bsp, Col 1(I), ALP, Opn, Pthrp, c-Fos, and c-Jun* mRNAs, which were normalized to *Gapdh* mRNA. *P<0.05 (veh vs. PTH), $^{\#}$P<0.05 (wt-veh vs. *Atf4*$^{-/-}$-veh). B, plasma levels of IGF-1 and FGF-2 from mice using respective ELISA kits according to the manufacturer's instructions. *P<0.05 (veh vs. PTH), † P<0.05 (wt-veh vs. *Atf4*$^{-/-}$-veh), $^{\#}$P<0.05 (PTH/veh-wt vs. PTH/veh-*Atf4*$^{-/-}$).

We determined the effects of ATF4 deficiency on PTH induction of osteoblast differentiation markers in vivo. Total RNA was isolated from tibiae of *wt* and *Atf4*$^{-/-}$ mice treated with and without PTH for 28 d and expression levels of osteoblast differentiation marker genes were measured by quantitative real-time PCR analysis. As shown in Fig 1A, PTH dramatically increased the expression of genes known to be associated with osteoblast differentiation including *osteocalcin* (*Ocn*), *bone sialoprotein* (*Bsp*), *alkaline phosphatase* (*Alp*), *α1(I) collagen* (*Col1(I)*), *osteopontin* (*Opn*), and *osterix* (*Osx*). Importantly, this PTH regulation was either dramatically reduced or completely abolished in *Atf4*$^{-/-}$ tibiae. In contrast, c-Fos and c-Jun, both early PTH-induced genes, were not

induced by PTH in either wt or *Atf4*$^{-/-}$ tibiae. As shown in Fig 1B, the levels of IGF-1 and FGF-2 which have both been implicated in the anabolic actions of PTH in bone (1,2) were markedly reduced in plasma from *Atf4*$^{-/-}$ mice compared to wt mice ($P<0.05$, wt vs. *Atf4*$^{-/-}$). However, their levels were not significantly elevated by the treatment of intermittent PTH in both wt or *Atf4*$^{-/-}$ animals ($P>0.05$, veh vs. PTH).

2) Identification of a 132-bp ATF4-response element in proximal Osx promoter (P1).

As shown in our last year's report, we have demonstrated that ATF4 is a novel upstream activator of Osx, a key transcription factor for osteoblast differentiation. To define the mechanism whereby ATF4 regulates Osx, we examined the effect of ATF4 overexpression on Osx expression in MC-4 preosteoblast cells. As shown in Fig 2A, ATF4 dose-dependently increased levels of Osx protein (top) and mRNA (bottom). We next examined whether ATF4 up-regulates Osx by increasing gene transcription by using a -1003/+68 mouse Osx promoter (Fig 2B). Using COS-7 cells, which lack detectable Runx2, ATF4 had comparable activity to Runx2 in terms of its ability to activate promoter activity (approx. 1.8-fold). Together, ATF4 and Runx2 maximally activated the *Osx* promoter (3.2-fold induction). To further define the region of the Osx promoter necessary for ATF4 responsiveness, several constructs containing various deletion mutants of the mouse *Osx* promoter were transiently transfected into COS-7 cells with and without an ATF4 expression plasmid. Results showed that luciferase activity of both control and ATF4-transfected groups decreased with progressively larger 5' deletions. However, ATF4 stimulation was abrogated when a 132-bp region between bp -215 to -83 was deleted (Fig 2C). A putative ATF4-binding sequence (CTTCCTCA) at -201/-194 bp was identified in this region by using a TRANSFAC retrieval program. Introduction of a 3-bp substitution mutation to this core sequence (from CTTCCTCA to CTTgtaCA) completely abolished ATF4 activation (Fig 2D). As shown in Fig 2E, a DNA oligo probe from the Osx promoter that contains the TTACATCA core sequence bound to a factor(s) in nuclear extracts from COS-7 cells transfected with an ATF4 expression vector. Importantly, this binding (see arrow) was dramatically reduced by the addition of a specific antibody against ATF4 but not by normal control IgG or antibodies against cFos (an AP1 family member) or ATF2.

3) PTH stimulation of Osx gene transcription requires an ATF4 response element (P1).

To study the mechanism whereby PTH regulates *Osx*, we next evaluated the effect of PTH on mouse -1003/+68 *Osx* promoter activity in MC-4 preosteoblast cells. As illustrated in Fig 2F, PTH stimulated promoter activity in a dose-dependent manner with a detectable response seen at a PTH concentration of 10^{-10} M. Measurable activation of the *Osx* promoter was observed 0.5 h after PTH addition with maximal induction occurring between 4-6 h (Fig 2G). PTH-stimulated Osx protein expression was entirely blocked by PKA inhibition (Fig 2H). The 132-bp ATF4-responsive element identified above was also required for PTH induction of promoter (Fig 2I). Furthermore, the same 3-bp substitution mutation that abrogates ATF4 activation dramatically reduced PTH-dependent activation (Fig 2J), indicating that this element is critical for the actions of PTH on this promoter. *5) ATF4 is recruited to the endogenous Osx promoter in a PTH-dependent manner (P1).* To determine whether ATF4 is associated with the endogenous *Osx* promoter in vivo, we performed chromatin immunoprecipitation (ChIP) assays using MC-4 cells with and without PTH treatment. As shown in Fig 2K and L, ATF4 specifically interacted with a chromatin fragment of the proximal *Osx* promoter that contains the ATF4-binding site identified above. Furthermore, this interaction was dramatically stimulated by PTH treatment. ATF4 also bound to an ATF4-binding site (OSE1)-containing chromatin fragment of the proximal *mOG2* promoter in a PTH-dependent manner (primers P3/P4). In contrast, ATF4 antibody failed to immunoprecipitate a 3' chromatin fragment in the transcribed region of the *mOG2* gene that contains no ATF4-binding sites (primers P5/P6).

4) Identification and characterization of Erk/MAPK phosphorylation sites in Runx2 (P2).

We used a combination of in vitro and in vivo phosphorylation analysis, mass spectroscopy and functional assays to identify two sites at S301 and S319 within the proline/serine/threonine domain of Runx2 that are required for MAPK regulation. These sites are phosphorylated by activated Erk1 in vitro and in cell culture. In addition to

confirming Erk-dependent phosphorylation at S319, mass spectroscopy identified two other Erk-phosphorylated sites at S43 and S510. Furthermore, introduction of S301,319A mutations rendered Runx2 resistant to MAPK-dependent activation and reduced its ability to stimulate osteoblast-specific gene expression and differentiation after transfection into Runx2-null calvarial cells and mesenchymal cells. In contrast, S301,319E Runx2 mutants had enhanced transcriptional activity that was minimally dependent on MAPK signaling, consistent with the addition of a negative charge mimicking serine phosphorylation. These results emphasize the important role played by Runx2 phosphorylation in the control of osteoblast gene expression and provide a mechanism to explain how physiological signals acting on bone through the ERK/MAPK pathway can stimulate osteoblast-specific gene expression. Similar approaches are being used to identify and characterize potential PTH-responsive phosphorylation sites in ATF4 molecule.

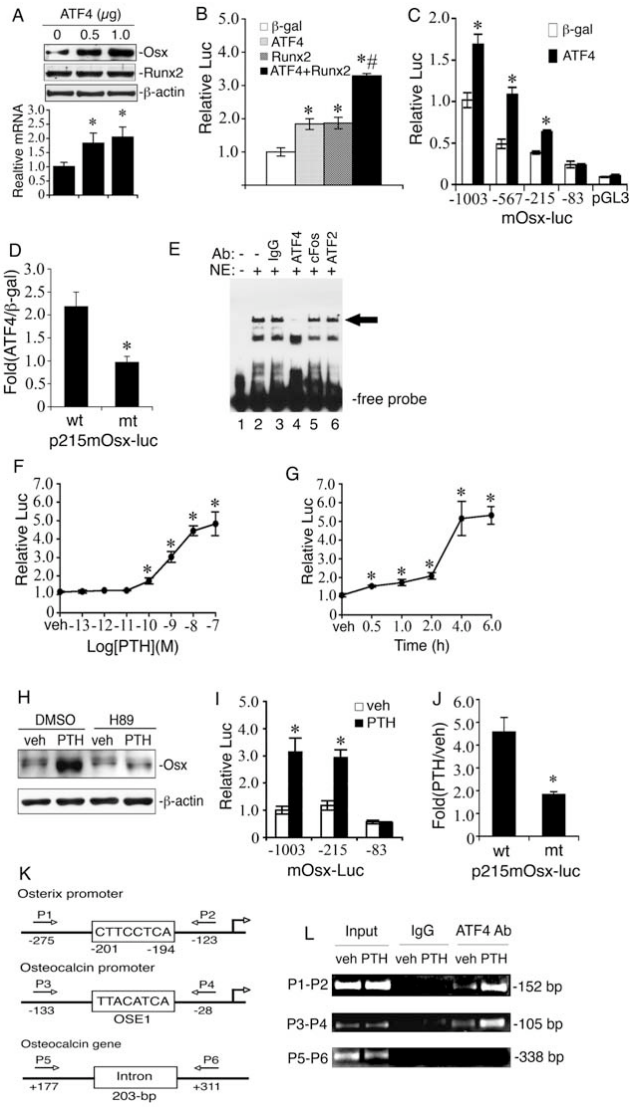

Fig 2. PTH activates Osx gene transcription via an ATF4-responsive element in the proximal Osx promoter. A, MC-4 cells were electroporated with indicated amount of ATF4 expression plasmid followed by Western blot. B, COS-7 cells were transfected with p1060mOsx-luc, pRL-SV40, and indicated expression vectors followed by dual lucferase assays. C, COS-7 cells were transfected with various deletion constructs and pRL-SV40 with and without ATF4 expression plasmid. D, COS-7 cells transfected with p215mOsx-luc or the same plasmid containing a 3-bp substitution mutation in the putative ATF4-binding site and pRL-SV40 with and without ATF4 expression plasmid. E, EMSA, labeled wild-type DNA probe was incubated with 2 μg nuclear extracts from COS-7 cells transfected with pCMV/ATF4 plasmid in the presence of normal control IgG (lane 3), ATF4 antibody (lane 4), cFos antibody (lane 5), and ATF2 antibody (lane 6). Experiments were repeated 3-4 times and qualitatively identical results were obtained. F and G, MC-4 cells transfected with p1003mOsx-luc and pRL-SV40 were treated with indicated concentration of PTH for 6 h (F) or with 10^{-7} M PTH for indicated times (G). H, MC-4 cells were treated with and without 10^{-7} M PTH in the presence and absence of 10 μM of H89 for 6 h. I, MC-4 cells transfected as in Fig 2C were treated with and without 10^{-7} M PTH for 6 h. J, MC-4 cells transfected as in Fig. 2D were treated with and without 10^{-7} M PTH for 6 h. K, a schematic illustration of putative ATF4 binding sites in the 5' flanking regions of the *Osx* and *osteocalcin* gene promoters and *osteocalcin* gene. L, ChIP assay of the *Osx* promoter in MC-4 cells treated with and without 10^{-7} M PTH for 6 h. $^{*}P<0.05$ (β-gal vs. ATF4, Runx2, and ATF4 plus Runx2, or veh vs. PTH), $^{\#}P<0.05$ (ATF4 plus Runx2 vs. β-gal, ATF4, or Runx2).

<u>*Task 2: To establish whether the anabolic actions of PTH require ATF4 (6-48 months).*</u> During the last year of support, we have made the following significant progress on this task:

1) Ablation of the Atf4 gene impairs PTH stimulation of trabecular, but not cortical bone in 7-month-old ovariectomized (OVX) mice (P1).

The experiments described in our previous study established a critical role of ATF4 in the anabolic effects of PTH on long bones, vertebrae, and calvariae in rapidly growing mice. However, it is possible that results obtained from growing animals may be different from those in adults due to possible effects of PTH and/or ATF4 on animal growth or influences of animal growth on the anabolic response to PTH, either of which could complicate the interpretation of the results. In contrast, adult mice have a mature skeleton in which these possible complications can be avoided. Furthermore, the OVX mouse provides a model that may be more relevant to the clinical applications of PTH in the treatment of osteoporosis. For these reasons, we evaluated whether ATF4 is required for the anabolic response to PTH in 7-month-old OVX mice. OVX surgery was successful as demonstrated by significant reduction in BV/TV (65 percent), Tb.N (27 percent), and Tb.Th (18 percent) and increased Tb.Sp (37 percent) relative to sham surgery (P<0.05, wt-sham vs. wt-OVX) (Fig 5). OVX surgery did not reduce Cort.Th, which is consistent with results from rats, As shown in Fig 3 A-C, similar to results from growing mice, ablation of the *Atf4* gene significantly decreased BV/TV and Tb.N and increased Tb.Sp in adult OVX mice. In further agreement with results in young mice, *Atf4*$^{-/-}$ animals exhibited a clearly attenuated response to PTH. For example, while PTH increased BV/TV by 7.8-fold in wt mice, this value was only increased 4.2-fold in *Atf4*$^{-/-}$ animals. Similarly, while PTH still stimulated formation of trabecular bone in *Atf4*$^{-/-}$ trabeculae, the magnitude of this response was significantly reduced compared to wt control (P<0.05, PTH/veh-wt vs. PTH/veh- *Atf4*$^{-/-}$). In contrast to result from growing mice, Cort.Th was not reduced by ablation of the *Atf4* gene in adult OVX mice (0.21±0.01 mm in wt vs. 0.19±0.02 mm in *Atf4*$^{-/-}$, P>0.05 wt vs. *Atf4*$^{-/-}$). Also, PTH was much less effective in stimulating Cort.Th in adult OVX mice (24%) than in growing mice (95%) (Figs 1 and 3 in P1). Furthermore, no difference in stimulation of cortical thickness by PTH was observed when wt and *Atf4*$^{-/-}$ groups were compared (24% wt vs. 21% *Atf4*$^{-/-}$)(P>0.05, PTH/veh-wt vs. PTH/veh-*Atf4*$^{-/-}$).

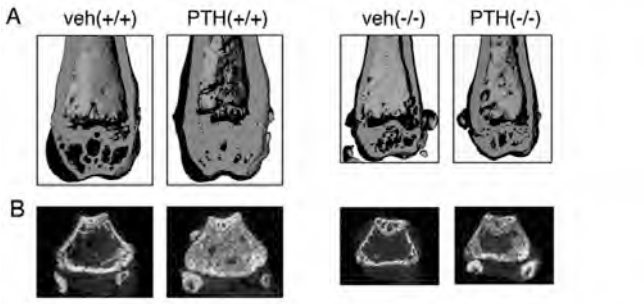

C

	veh(+/+)	PTH(+/+)	veh(-/-)	PTH(-/-)
BV/TV(%)	4.2±1.0	32.8±2.1*	2.7±0.8†	11.3±4.2*#
Tb.N(/mm)	1.6±0.21	2.7±0.32*	1.3±0.28†	1.8±0.26*#
Tb.Th(μm)	62.8±3.6	126±20*	62.4±9.2	92.5±11.8*#
Tb.Sp(mm)	0.64±0.1	0.43±0.07*	0.82±0.16†	0.59±0.1*#
Cort.Th(mm)	0.21±0.01	0.26±0.02*	0.19±0.02	0.23±0.02*

N = 8-10

Fig 3. Effects of ATF4 deficiency on PTH stimulation in adult OVX bone. A, three-dimensional (3D) reconstruction from μCT scan of distal femurs of adult OVX mice. B, sagittal view of 2D distal femur at 1.7-2.0 mm from the chondro-osseous junction. C, BV/TV, Tb. N, Tb.Th, Tb.Sp, and Cort.Th. *P<0.05 (veh vs. PTH), † P<0.05 (wt-veh vs. *Atf4*$^{-/-}$-veh), #P<0.05 (PTH/veh-wt vs. PTH/veh-*Atf4*$^{-/-}$).

2) ATF4 is critical for PTH to increase bone formation in vivo (P1).

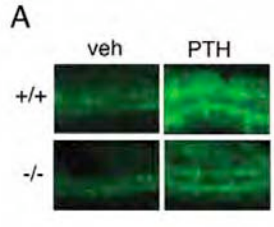

B

	MAR(μM/day)
+/+(veh)	4.20 ± 0.37
+/+(PTH)	7.37 ± 1.16*
-/-(veh)	3.39 ± 0.84†
-/-(PTH)	5.68 ± 1.20*#

N = 6-7

Fig 4. ATF4 deficiency impairs both basal and PTH-stimulated bone formation in vivo. Calcein double labeling of metaphyseal trabecular bone (magnification, x200). *P<0.05 (veh vs. PTH), † P<0.05 (wt-veh vs. *Atf4*$^{-/-}$-veh), #P<0.05 (PTH/veh-wt vs. PTH/veh-*Atf4*$^{-/-}$).

To determine if ATF4 is required for PTH to increase bone formation in vivo, we performed calcein double labeling experiments. As shown in Fig 4 A and B, results from calcein double labeling of 7-month old OVX wt and *Atf4*$^{-/-}$ tibia revealed that the PTH-stimulated increase in mineral apposition rate (MAR), an indicator of osteoblast function, was significantly reduced by ATF4 deficiency (P<0.05, PTH/veh-wt vs. PTH/veh-*Atf4*$^{-/-}$).

3) ATF4-deficient mice display a resistance to OVX-induced bone (P1).

Interestingly, as shown in Fig 5, OVX surgery significantly reduced bone mass in wt mice. This reduction was completely abolished in *Atf4*$^{-/-}$ animals (P>0.05, *Atf4*$^{-/-}$ -sham vs. *Atf4*$^{-/-}$ -OVX). This result suggests that ATF4 may play an important role in OVX induction of bone loss. Current study in the project laboratory is to define the molecular mechanism underlying this important finding.

	Sham(+/+)	OVX(+/+)	Sham(-/-)	OVX(-/-)
BV/TV(%)	12±1.2	3.4±0.5*	1.8±0.08†	2.0±0.12
Tb.N(/mm)	2.2±0.24	1.5±0.06*	1.4±0.07†	1.3±0.01
Tb.Th(μm)	77.2±6.0	62.4±1.2*	59.3±11†	57.4±0.8
Tb.Sp(mm)	0.46±0.04	0.62±0.24*	0.71±0.03†	0.83±0.23
Cort.Th(mm)	0.2±0.05	0.21±0.01	0.17±0.01†	0.18±0.01

N = 3

Fig 5. Effects of OVX surgery on bone parameters in wt and Atf4$^{-/-}$ mice. Four-month-old female mice were first ovariectomized. After two months, femurs were isolated for μCT analysis. *P<0.05 (sham vs. OVX), † P<0.05 (sham(+/+) vs. sham (-/-)).

Key Research Accomplishments

- We have demonstrated that ATF4 is essential for PTH promotion of osteoblast differentiation in vivo.
- We have identified and characterized an ATF4-response element in mouse Osx promoter that is essential for ATF4 to induce Osx expression in osteoblasts and probably osteoblast differentiation.
- We have demonstrated that ATF4 is required for the anabolic actions of PTH in bone in adult OVX mice.
- We have established that ATF4 is important for intermittent PTH to stimulate osteoblast-mediated bone formation in vivo.
- We have revealed that ATF4 is essential for OVX induction of bone loss in vivo.
- We have identified and functionally characterized Erk/MAPK phosphorylation sites in Runx2, an ATF4-interacting factor identified by the project laboratory.

Reportable Outcomes

Peer-reviewed paper:

P1. Yu S, Franceschi RT, Luo M, Fan J, Jiang D, Cao H, Lai Y, Zhang J, Patrene K, Hankenson KD, Roodman GD, Xiao G. Critical role of activating transcription factor 4 in the anabolic actions of PTH in bone. PLoS One. 2009, Oct 23;4(10):e7583. PMID: 19851510
(This paper was listed as the No. 1 "**Not to be Missed**" paper in the November (2009) issue of the IBMS BoneKEy, BoneKEy is published by the International Bone & Mineral Society, link: http://www.bonekey-ibms.org/).

P2. Ge C, Xiao G (co-first author), Jiang D, Yang Q, Hatch NE, and Franceschi RT. Identification and functional characterization of extracellular-regulated kinase/MAPK phosphorylation sites in the Runx2 transcription factor. J Biol Chem, 2009; 284(47):32533-43, PMID: 19801668

Abstracts:

A1. Yu S, Franceschi RT, Luo M, Fan J, Jiang D, Cao H, Lai Y, Zhang J, Patrene K, Hankenson K, Roodman GD, Xiao G. Activating transcription factor 4 mediates the anabolic actions of parathyroid hormone in bone. J. Bone Min. Res, 2009, 24

Conclusion

During the last year of support, our studies establish that: i) ATF4 is essential for intermittent PTH to increase osteoblast differentiation in vivo; ii) ATF4 promotes osteoblast differentiation at least in part via upregulation of Osx, a key transcription factor for osteoblast differentiation and bone formation; iii) ATF4 is critical for PTH to increase bone formation in vivo; iv) ATF4 may play a role in OVX induction of bone loss; and v) Erk/MAPK, which is known to be activated by PTH signaling in osteoblasts, phosphorylates and activates Runx2.

The knowledge obtained from these studies will significantly enhance our understanding of the molecular mechanism underlying the actions of PTH in osteoblasts and bone and define new potential therapeutic targets for improved treatment of osteoporosis and other metabolic bone diseases.

References

1. Miyakoshi N, Kasukawa Y, Linkhart TA, Baylink DJ, Mohan S 2001 Evidence that anabolic effects of PTH on bone require IGF-I in growing mice. Endocrinology **142**(10)**:**4349-56.
2. Hurley MM, Okada Y, Xiao L, Tanaka Y, Ito M, Okimoto N, Nakamura T, Rosen CJ, Doetschman T, Coffin JD 2006 Impaired bone anabolic response to parathyroid hormone in Fgf2-/- and Fgf2+/- mice. Biochem Biophys Res Commun **341**(4)**:**989-94.

Appendices

One peer-reviewed research paper: P1, P2
Two national meeting abstracts: A1, A2

OPEN ACCESS Freely available online

PLoS one

Critical Role of Activating Transcription Factor 4 in the Anabolic Actions of Parathyroid Hormone in Bone

Shibing Yu[1], Renny T. Franceschi[4,5], Min Luo[1], Jie Fan[2], Di Jiang[4], Huiling Cao[1], Tae-Geon Kwon[7], Yumei Lai[3], Jian Zhang[6], Kenneth Patrene[1], Kurt Hankenson[8], G. David Roodman[1], Guozhi Xiao[1]*

1 Department of Medicine, University of Pittsburgh, Pittsburgh, Pennsylvania, United States of America, **2** Department of Surgery, University of Pittsburgh, Pittsburgh, Pennsylvania, United States of America, **3** Department of Pharmacology and Chemical Biology, University of Pittsburgh, Pittsburgh, Pennsylvania, United States of America, **4** Department of Periodontics and Oral Medicine, University of Michigan, Ann Arbor, Michigan, United States of America, **5** Department of Biological Chemistry, School of Dentistry, University of Michigan, Ann Arbor, Michigan, United States of America, **6** Department of Medicine, School of Medicine, University of Michigan, Ann Arbor, Michigan, United States of America, **7** Department of Oral and Maxillofacial Surgery, School of Dentistry, Kyungpook National University, Daegu, Korea, **8** Department of Animal Biology, School of Veterinary Medicine, University of Pennsylvania, Philadelphia, Pennsylvania, United States of America

Abstract

Parathyroid hormone (PTH) is a potent anabolic agent for the treatment of osteoporosis. However, its mechanism of action in osteoblast and bone is not well understood. In this study, we show that the anabolic actions of PTH in bone are severely impaired in both growing and adult ovariectomized mice lacking bone-related activating transcription factor 4 (ATF4). Our study demonstrates that ATF4 deficiency suppresses PTH-stimulated osteoblast proliferation and survival and abolishes PTH-induced osteoblast differentiation, which, together, compromise the anabolic response. We further demonstrate that the PTH-dependent increase in osteoblast differentiation is correlated with ATF4-dependent up-regulation of Osterix. This regulation involves interactions of ATF4 with a specific enhancer sequence in the Osterix promoter. Furthermore, actions of PTH on Osterix require this same element and are associated with increased binding of ATF4 to chromatin. Taken together these experiments establish a fundamental role for ATF4 in the anabolic actions of PTH on the skeleton.

Citation: Yu S, Franceschi RT, Luo M, Fan J, Jiang D, et al. (2009) Critical Role of Activating Transcription Factor 4 in the Anabolic Actions of Parathyroid Hormone in Bone. PLoS ONE 4(10): e7583. doi:10.1371/journal.pone.0007583

Editor: Paul A. Bartell, Pennsylvania State University, United States of America

Received April 25, 2009; **Accepted** October 5, 2009; **Published** October 23, 2009

Funding: This work was supported by a NIH Grant DK072230 and a Department of Defense Grant W81XWH-07-1-0160 (to GX). The funders had no role in the study design, data collection and analysis, decision to publish, or preparation of the manuscript.

Competing Interests: The authors have declared that no competing interests exist.

* E-mail: xiaog@upmc.edu

Introduction

Parathyroid hormone (PTH) is a major regulator of calcium homeostasis and has both catabolic and anabolic effects on osteoblasts and bone that depend on the temporal pattern of administration. Continuous administration of PTH decreases bone mass whereas intermittent administration increases bone mass [1–6]. The mechanism(s) responsible for these differing effects are poorly understood. The anabolic activity of PTH has been attributed to both direct actions of this hormone on osteoprogenitor cells as well as indirect effects mediated by the production of growth factors such as insulin-like growth factor-1 (IGF-1) and basic fibroblast growth factor-2 (FGF-2) [7,8]. Most cellular actions of PTH are mediated by the PTH-1 receptor, a G protein-coupled receptor that is expressed in osteoblasts [9,10]. Binding of PTH to its receptor activates multiple intracellular signaling pathways that involve cAMP, inositol phosphates, intracellular Ca^{2+}, protein kinases A and C [11], and the extracellular signal-related (ERK)/mitogen-activated protein kinase (MAPK) pathway [12,13]. Activation of these signal transduction pathways ultimately affects cellular behavior. In this regard, the anabolic actions of PTH on bone have been attributed to increased proliferation of osteopregenitors/osteoblasts [2,14,15] and/or decreased osteoblast apoptosis [6,16,17].

Although a number of transcription factors including cAMP response element binding protein (CREB) [18,19], AP1 family members [20–22], and Runx2 [20,23] have been implicated in the molecular actions of PTH in osteoblasts, genetic studies have not strongly linked any of these factors in the anabolic actions of this hormone. To better understand the anabolic actions of PTH, it is essential that the downstream signals induced by this hormone be identified and evaluated for possible roles in bone formation. The *osteocalcin* (*Ocn*) promoter has been an important tool for unraveling the mechanisms mediating osteoblast-specific gene expression and was used to identify a number of important transcription factors and cofactors involved in *Ocn* gene expression [24–28]. Because the *Ocn* gene is regulated by PTH [29,30], we have used it as a model system for identifying new transcriptional mediators of PTH action. We previously demonstrated that the OSE1 (osteoblast-specific element 1) in the proximal *mOG2* promoter [24] is necessary and sufficient for PTH induction of this gene [31]. The OSE1 core sequence (TTACATCA) was subsequently identified as a DNA binding site for the ATF4 transcription factor. The critical role of ATF4 in osteoblast differentiation and bone development was established using *Atf4*-deficient mice [26]. At the cellular level, ATF4 is critical for proliferation and differentiation as well as survival in osteoblasts [32,33]. We recently showed that ATF4 is also required for PTH induction of *Ocn* expression in osteoblasts [34]. Specifically, PTH elevated levels of ATF4 mRNA and protein in a dose and time-dependent manner and increased binding of ATF4 to OSE1 DNA. Furthermore, PTH stimulation of *Ocn* expression was lost by siRNA downregulation of ATF4 in

MC-4 cells and in primary bone marrow stromal cells from *Atf4*$^{-/-}$ mice. Collectively, these studies demonstrate that ATF4 is a novel downstream mediator of PTH signaling.

Osterix (Osx, or Sp7), a zinc-finger-containing transcription factor of the sp family, is essential for osteoblast differentiation and bone formation [35]. Since Osx is not detected in mice lacking Runx2 [35], a master regulator of osteoblast differentiation [25,36–38], it functions downstream of Runx2. However, the molecular mechanisms whereby the Osx gene is transcriptionally regulated are not well understood.

In the present study, we used ATF4-deficient mice to determine whether ATF4 is more generally required for the in vivo anabolic actions of PTH in bone as well as explore the mechanism used by PTH to regulate ATF4 activity. As will be shown, loss of ATF4 greatly attenuated the anabolic effects of PTH. Furthermore, ATF4 may participate in the PTH response by regulating the expression of the Osterix transcription factor.

Results

The anabolic effects of PTH on bone are severely impaired in growing Atf4-deficient mice

We first evaluated our hypothesis that ATF4 mediates the anabolic actions of PTH in bone using a relatively simple "growing mouse" model system, that has been widely used for studying the anabolic actions of PTH, PTHrP, FGF2, and IGF-1 in bone [2–4,8,39,40]. The advantages of this system are that it is less time consuming and costly versus adult ovarectomized mouse models. Furthermore, because young growing animals have relatively high osteoblast activity, they are more sensitive to PTH than adults [2,11,14,16–18,41–43]. Mice were treated with vehicle or PTH and sacrificed 24 h after the last PTH injection. PTH-dependent anabolic activity was evaluated in these mice using standard biochemical and histomorphometric criteria. *Atf4*$^{-/-}$ mice grew more slowly than wild type (wt) animals. The growth rate was slightly but significantly increased by PTH treatment during d 6–18 in wt but not *Atf4*$^{-/-}$ animals (Fig. S1A). *Atf4*$^{-/-}$ femurs were also shorter than *wt* or *Atf4*$^{+/-}$ femurs. Consistent with results from a previous study [3], PTH did not alter the length of femurs (Fig. S1B). However, it did significantly increase the dry ash weight per femur in wt and *Atf4*$^{+/-}$ but not in *Atf4*$^{-/-}$ mice (Fig. S1C). Serum Pi and calcium concentration (Fig. S1D and E) were not markedly affected by PTH or ATF4 deficiency. Faxitron X-ray analysis of femurs revealed that *wt* and *Atf4*$^{+/-}$ mice responded to PTH with markedly increased radiopacity throughout the whole femur, with the most dramatic increase in the metaphyseal region (Fig. S2, top and middle). In contrast, PTH only slightly increased the radiopacity in the same region of *Atf4*$^{-/-}$ femurs (Fig. S2, bottom). As shown in Fig. 1, quantitative μCT analysis of femur histomorphometric parameters showed that *Atf4*$^{-/-}$ mice had a significant reduction in bone volume/tissue volume (BV/TV), trabecular number (Tb.N), and cortical thickness (Cort.Th) and a marked increase in trabecular space (Tb.Sp) compared with the *wt* or *Atf4*$^{+/-}$ littermates. These data confirmed an essential role of ATF4 in bone that was previously demonstrated by the Karsenty group [26]. As expected, in *wt* femurs, intermittent PTH increased BV/TV, Tb.N, and Tb.Th by 5.4-fold, 2.7-fold, and 1.5-fold, respectively, and decreased Tb.Sp by 60 percent. Similar effects were also seen in *Atf4*$^{+/-}$ mice (Fig. 1B). In contrast, the PTH response was greatly attenuated in *Atf4*$^{-/-}$ mice where the following PTH responses were observed; BV/TV, 2.2-fold increase; Tb.N, 1.7-fold increase; Tb.Th, 1.1-fold increase; Tb.Sp, 36 percent decrease. In all cases, the magnitude of PTH-stimulated changes on BV/TV, Tb.N, Tb.Sp was dramatically reduced in *Atf4*$^{-/-}$ mice relative to *wt* or *Atf4*$^{+/-}$ mice ($P<0.05$, PTH/veh-wt vs. PTH/veh-*Atf4*$^{-/-}$). Furthermore, PTH-stimulated increases in Cort.Th and Tb.Th were completely lost in *Atf4*$^{-/-}$ femurs. Because PTH similarly affected all trabecular and cortical parameters in *Atf4*$^{+/+}$ and *Atf4*$^{+/-}$ mice, subsequent experiments compared the PTH effects on bone only between *wt* and *Atf4*$^{-/-}$ mice.

We next measured effects of *Atf4* gene ablation on PTH stimulation of tibiae, vertebrae, and calvariae. The anabolic effect of PTH on wt tibiae was so dramatic that the majority of the bone marrow cavity was replaced by newly formed bone (Fig. 2A and B). In *Atf4*$^{-/-}$ tibiae, while PTH still induced a small increase in trabecular area, the magnitude of stimulation was significantly reduced (5-fold in wt vs. 2.2-fold in *Atf4*$^{-/-}$)($P<0.05$, PTH/veh-wt vs. PTH/veh-*Atf4*$^{-/-}$)(Fig. 2C-E). Likewise, the PTH-stimulated increase in the trabeculae of vertebrae (L5) was markedly reduced in *Atf4*$^{-/-}$ mice (3-fold in wt vs. 2-fold in *Atf4*$^{-/-}$) ($P<0.05$, PTH/veh-wt vs. PTH/veh-*Atf4*$^{-/-}$)(Fig. 2F–J). When histological sections of calvariae were compared, PTH increased the width of the calvariae by 1.8-fold in *wt* mice, a response that was abolished in *Atf4*$^{-/-}$ animals (Fig. 2K–O).

Ablation of the Atf4 gene impairs PTH stimulation of trabecular, but not cortical bone in 7-month-old ovariectomized (OVX) mice

The experiments described above clearly establish a critical role of ATF4 in the anabolic effects of PTH on long bones, vertebrae, and calvariae in rapidly growing mice. However, it is possible that results obtained from growing animals may be different from those in adults due to possible effects of PTH and/or ATF4 on animal growth or influences of animal growth on the anabolic response to PTH, either of which could complicate the interpretation of the results. In contrast, adult mice have a mature skeleton in which these possible complications can be avoided. Furthermore, the OVX mouse provides a model that may be more relevant to the clinical applications of PTH in the treatment of osteoporosis. For these reasons, we next evaluated whether ATF4 is required for the anabolic response to PTH in 7-month-old OVX mice. OVX surgery was successful as demonstrated by significant reduction in BV/TV (65 percent), Tb.N (27 percent), and Tb.Th (18 percent) and increased Tb.Sp (37 percent) relative to sham surgery ($P<0.05$, wt-sham vs. wt-OVX) (Fig. S3). OVX surgery did not reduce Cort.Th, which is consistent with results from rats [44], Interestingly, OVX surgery did not significantly reduce bone parameters in *Atf4*$^{-/-}$ animals ($P>0.05$, *Atf4*$^{-/-}$ -sham vs. *Atf4*$^{-/-}$ -OVX). As shown in Fig. 3 A–C, similar to results from growing mice, ablation of the *Atf4* gene significantly decreased BV/TV and Tb.N and increased Tb.Sp in adult OVX mice. In further agreement with results in young mice, *Atf4*$^{-/-}$ animals exhibited a clearly attenuated response to PTH. For example, while PTH increased BV/TV by 7.8-fold in wt mice, this value was only increased 4.2-fold in *Atf4*$^{-/-}$ animals. Similarly, while PTH still stimulated formation of trabecular bone in *Atf4*$^{-/-}$trabeculae, the magnitude of this response was significantly reduced compared to wt control ($P<0.05$, PTH/veh-wt vs. PTH/veh- *Atf4*$^{-/-}$). In contrast to result from growing mice, Cort.Th was not reduced by ablation of the *Atf4* gene in adult OVX mice (0.21 ± 0.01 mm in wt vs. 0.19 ± 0.02 mm in *Atf4*$^{-/-}$, $P>0.05$ wt vs. *Atf4*$^{-/-}$). Also, PTH was much less effective in stimulating Cort.Th in adult OVX mice (24%) than in growing mice (95%) (Figs. 1 and 3). Furthermore, no difference in stimulation of cortical thickness by PTH was observed when wt and *Atf4*$^{-/-}$ groups were compared (24% wt vs. 21% *Atf4*$^{-/-}$)($P>0.05$, PTH/veh-wt vs. PTH/veh-*Atf4*$^{-/-}$). As shown in Fig. 3D and E, results from calcein double labeling of 7-month old OVX wt and *Atf4*$^{-/-}$ tibia revealed that the PTH-stimulated increase in mineral

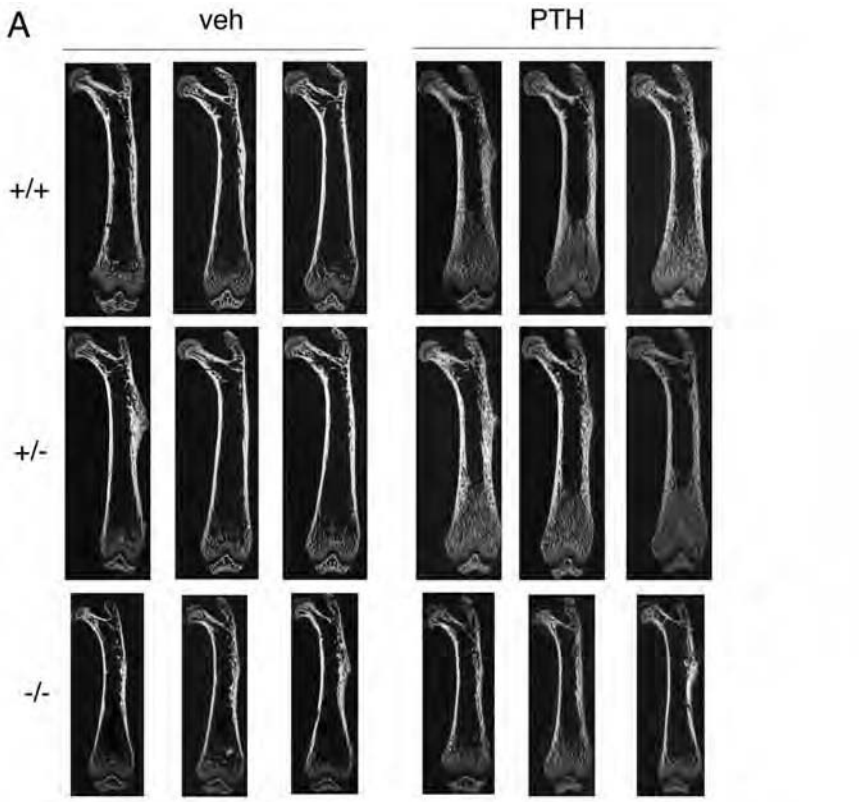

B

	veh(+/+)	PTH(+/+)	veh(+/-)	PTH(+/-)	veh(-/-)	PTH(-/-)
BV/TV(%)	6.2±0.4	33.4±6.6*	6.5±0.5	37.2±4.6*	3.9±0.8†	8.6±4.0*#
Tb.N(/mm)	1.5±0.08	4.02±0.8*	1.5±0.1	4.7±0.65*	1.3±0.08†	2.2±0.6*#
Tb.Th(μm)	50.4±5.1	75.5±12*	54.1±2.6	76.8±4.4*	48.3±6.9	54.4±4.2#
Tb.Sp(mm)	0.67±0.04	0.27±0.1*	0.66±0.05	0.25±0.04*	0.78±0.06†	0.5±0.13*#
Cort.Th(mm)	0.19±0.06	0.37±0.01*	0.17±0.01	0.4±0.08*	0.14±0.02†	0.14±0.03#

N = 6-12

Figure 1. PTH-stimulated bone was significantly reduced or lost in Atf4$^{-/-}$ femurs. A, two-dimensional (2D) reconstruction from μCT scan of femurs from growing *wt*, *Atf4*$^{+/-}$ and *Atf4*$^{-/-}$ mice treated with and without intermittent PTH for 28 d. B, quantitative analysis of bone volume/tissue volume (BV/TV), trabecular number (Tb. N), trabecular thickness (Tb.Th), trabecular space (Tb.Sp), and cortical thickness (Cort. Th). *P<0.05 (veh vs. PTH), † P<0.05 (wt-veh vs. *Atf4*$^{-/-}$-veh), #P<0.05 (PTH/veh-wt vs. PTH/veh-*Atf4*$^{-/-}$).
doi:10.1371/journal.pone.0007583.g001

apposition rate (MAR), an indicator of osteoblast function, was significantly reduced by ATF4 deficiency (P<0.05, PTH/veh-wt vs. PTH/veh-*Atf4*$^{-/-}$).

ATF4 deficiency significantly reduces basal and PTH-stimulated proliferation in osteoblasts/preosteoblasts

PTH and PTHrP are both known to increase the proliferation and numbers of osteoblasts [14,15,17,45]. ATF4 is also a positive regulator of osteoblast proliferation and can be up-regulated by PTH in these cells [33,34]. To determine whether ATF4 plays a role in PTH regulation of osteoblast proliferation, sections of tibiae and calvariae from wt and *Atf4*$^{-/-}$ mice treated with and without intermittent PTH were analyzed for in vivo cell proliferation using a Zymed BrdU immunostaining kit. As shown in Fig. 4A, B, and E, in wt mice, PTH increased the percentage of proliferating osteoblasts/preosteoblasts of tibial trabeculae by 2.8-fold relative to vehicle-treated control. Ablation of the *Atf4* gene resulted in a 50% decline in basal proliferation. In addition, the PTH-stimulated increase in proliferation was decreased by 40 percent (Fig. 4C–E). Similarly, PTH-induced proliferation in calvarial periosteal osteoblasts was also significantly reduced by ATF4 deficiency (Fig. 4F–J). As expected, very few osteocytes were BrdU-positive in both tibiae and calvariae. Note: basal proliferation rate of calvarial periosteal osteoblasts was significantly higher than that of tibial trabecular osteoblasts (28% vs. 4%). Therefore, ATF4 is critical for basal and PTH-stimulated proliferation of osteoblasts/preosteoblasts in vivo.

PTH fails to reduce apoptotic death in Atf4$^{-/-}$ osteoblasts/osteocytes

Mature osteoblasts synthesize and deposit a mineralizing extracellular matrix and become osteocytes. Both osteoblasts and osteocytes can be lost through apoptosis. PTH signaling increases

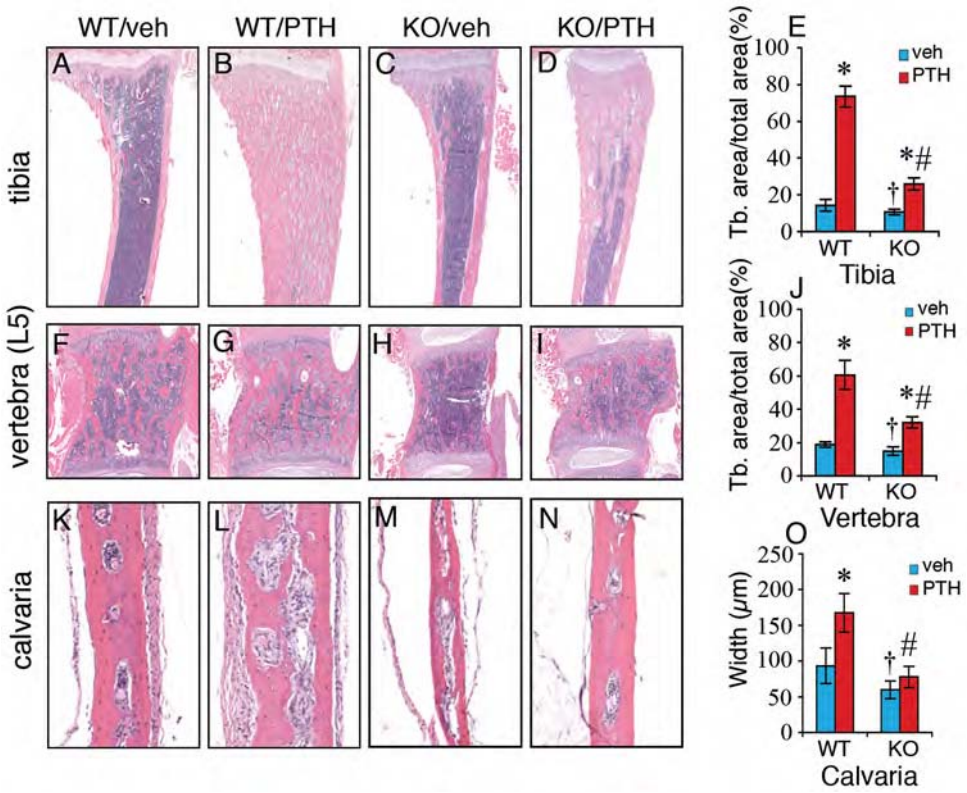

Figure 2. PTH-stimulated bone is severely impaired in Atf4$^{-/-}$ tibiae, vertebrae, and calvariae. Representative H&E stained sections of tibiae (A–E), vertebrae (L5) (F–J), and calvariae (K–O) are shown. Trabecular bone area versus total area of tibiae (E) and vertebrae (J) was measured using an Image Pro Plus 6.2 software. The calvarial width was obtained from 20 random measurements throughout the whole calvaria using a SPOT Advanced imaging software (O). *P<0.05 (veh vs. PTH), † P<0.05 (wt-veh vs. *Atf4*$^{-/-}$-veh), #P<0.05 (PTH/veh-wt vs. PTH/veh-*Atf4*$^{-/-}$).
doi:10.1371/journal.pone.0007583.g002

the survival of osteoblasts and osteocytes by reducing apoptosis [6,16,17,45]. Our recent study shows that ATF4 is anti-apoptotic in osteoblasts [33]. To determine whether ATF4 plays a role in PTH-mediated anti-apoptosis, sections of tibiae were stained with TUNEL and apoptotic cells were assessed. As shown in Fig. 4K and L, ATF4 deficiency significantly increased the basal levels of apoptosis. As expected, PTH dramatically reduced apoptotic death of tibial trabecular osteoblasts/osteocytes by 48 percent, which is consistent with results from previous studies [6,16,17,45]. Importantly, the PTH-stimulated decrease in apoptotic death was completely abolished in *Atf4*$^{-/-}$ trabeculae (Fig. 4M–O). ATF4 was similarly required for PTH to inhibit apoptosis in cortical osteocytes of tibiae (Fig. 4P). Collectively, ATF4 is essential for PTH-mediated inhibition of apoptosis in osteoblasts/osteocytes in vivo.

PTH-induced increase in expression of osteoblast differentiation marker genes is dramatically reduced or completely abolished in Atf4$^{-/-}$ animals

We next determined the effects of ATF4 deficiency on PTH induction of osteoblast differentiation markers in vivo. Total RNA was isolated from tibiae of *wt* and *Atf4*$^{-/-}$ mice treated with and without PTH for 28 d and expression levels of osteoblast differentiation marker genes were measured by quantitative real-time PCR analysis. As shown in Fig. 5A, PTH dramatically elevated the expression of genes known to be associated with osteoblast differentiation including *osteocalcin* (*Ocn*) (2.2-fold), *bone sialoprotein* (*Bsp*) (4.2-fold), *alkaline phosphatase* (*Alp*) (3.2-fold), *α1(I) collagen* (*Col1(I)*)(4.7-fold), *osteopontin* (*Opn*) (4.6-fold), and *osterix* (*Osx*) (4.1-fold). Importantly, this PTH regulation was either dramatically reduced or completely abolished in *Atf4*$^{-/-}$ tibiae. ATF4 deficiency also reduced basal *Ocn* and *Osx* mRNA levels. Consistent with our previous report [34], PTH increased *Atf4* mRNA 2.2-fold in wt tibiae, while *Atf4* was undetectable in *Atf4*$^{-/-}$ animals. In contrast, c-Fos and c-Jun, both early PTH-induced genes, were not induced by PTH in either wt or *Atf4*$^{-/-}$ tibiae. As shown in Fig. 5B, the levels of IGF-1 and FGF-2 which have both been implicated in the anabolic actions of PTH in bone [7,8] were markedly reduced in plasma from *Atf4*$^{-/-}$ mice compared to wt mice (P<0.05, wt vs. *Atf4*$^{-/-}$). However, their levels were not significantly elevated by the treatment of intermittent PTH in both wt or *Atf4*$^{-/-}$ animals (P>0.05, veh vs. PTH).

Intermittent PTH increases in vivo Osx expression in osteoblasts through a pathway requiring ATF4

Our above results demonstrate that ATF4 is essential for the major anabolic actions of PTH on bone and is also required for PTH-dependent induction of osteoblast differentiation. To begin to address the mechanism underlying this response, we measured the expression of Osterix (Osx) and Runx2 proteins, two critical transcription factors that regulate osteoblast differentiation. Initially, we used immunohistochemistry (IHC) to measure Osx in the tibiae and calvariae of wt and *Atf4*$^{-/-}$ mice with or without 28 d anabolic PTH treatment. As shown in Fig. 6, in wt-vehicle-treated tibiae, Osx-positive osteoblasts were only identified in the trabeculae and cortical endosteum close to the growth plate (Fig. 6A1, B1, and D1) and were almost undetectable in the same

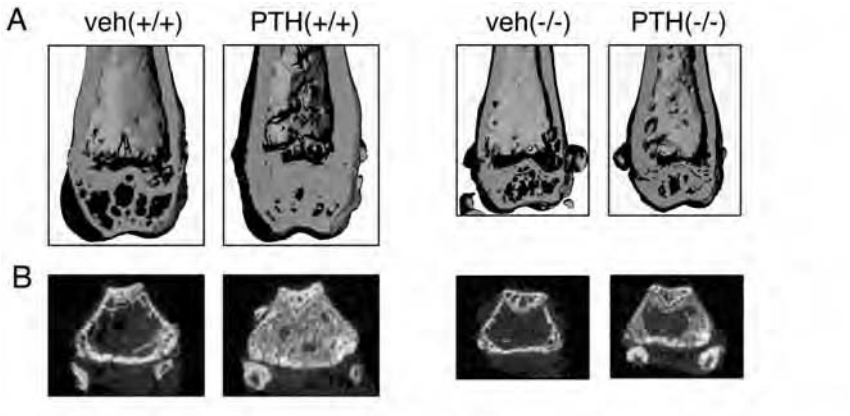

C

	veh(+/+)	PTH(+/+)	veh(-/-)	PTH(-/-)
BV/TV(%)	4.2±1.0	32.8±2.1*	2.7±0.8†	11.3±4.2*#
Tb.N(/mm)	1.6±0.21	2.7±0.32*	1.3±0.28†	1.8±0.26*#
Tb.Th(μm)	62.8±3.6	126±20*	62.4±9.2	92.5±11.8*#
Tb.Sp(mm)	0.64±0.1	0.43±0.07*	0.82±0.16†	0.59±0.1*#
Cort.Th(mm)	0.21±0.01	0.26±0.02*	0.19±0.02	0.23±0.02*

N = 8-10

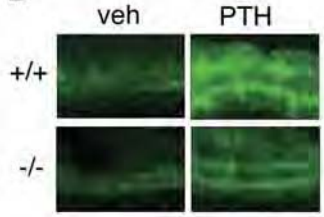

E

	MAR(μM/day)
+/+(veh)	4.20 ± 0.37
+/+(PTH)	7.37 ± 1.16*
-/-(veh)	3.39 ± 0.84†
-/-(PTH)	5.68 ± 1.20*#

N = 6-7

Figure 3. Effects of ATF4 deficiency on PTH stimulation in adult OVX bone. A, three-dimensional (3D) reconstruction from μCT scan of distal femurs of adult OVX mice. B, sagittal view of 2D distal femur at 1.7–2.0 mm from the chondro-osseous junction. C, BV/TV, Tb. N, Tb.Th, Tb.Sp, and Cort.Th. D, calcein double labeling of metaphyseal trabecular bone (magnification,x200). *P<0.05 (veh vs. PTH), † P<0.05 (wt-veh vs. *Atf4*$^{-/-}$-veh), #P<0.05 (PTH/veh-wt vs. PTH/veh-*Atf4*$^{-/-}$).
doi:10.1371/journal.pone.0007583.g003

regions close to the marrow (Fig. 6C1), indicating that cells in these areas are still in the immature (preosteoblast) state. In contrast, in the wt-PTH group, Osx-positive osteoblasts were identified on all surfaces of trabeculae and endosteum throughout the tibia. PTH increased the total number of Osx-positive cells per tibial section by 3.2-fold in wt mice (Panel 2). ATF4 deficiency reduced the numbers of Osx-positive cells by 50 percent (Panel 3). Strikingly, although PTH slightly increased bone volume in *Atf4*$^{-/-}$ bone (Fig. 1 and 2), it failed to elevate the numbers of Osx-positive cells in *Atf4*$^{-/-}$ tibiae. Similar results were obtained in calvariae (Fig. 6E). The IHC staining was highly specific since no signal was detected in the non-immune IgG control group (Panel 5). Consistent with IHC results, as shown in Fig. 6I, Western blot analysis using protein extracts showed that PTH dramatically elevated the level of Osx protein in wt tibiae. In contrast, Osx was not detected by Western blot in extracts from *Atf4*$^{-/-}$ animals (Fig. 6I). The level of Runx2 protein was slightly up-regulated by PTH in the wt group, but not in *Atf4*$^{-/-}$ group. Unlike Osx, the basal level of Runx2 was not reduced by ATF4 deficiency. PTH1R protein, the major receptor for PTH and PTHrP signaling in osteoblasts, was expressed in endosteal osteoblasts of tibiae (Fig. 6F) and periosteal osteoblasts of calvariae and hypertrophic chrodrocytes in the growth plate area (unpublished data). The signal for PTH1R protein was weak in trabecular osteoblasts that actively form new bone (unpublished data). In contrast to results from a previous study showing that PTH1R is down-regulated by PTH in cultured osteoblasts [46], PTH1R was slightly increased by intermittent PTH treatment in vivo as measured by IHC and Western blot analysis. Importantly, ATF4 deficiency did not reduce the level of PTH1R (Fig. 6F and I). In addition, primary calvarial osteoblasts from wt and *Atf4*$^{-/-}$ mice displayed an identical cAMP accumulation curve in response to treatment of increasing concentrations of PTH in vitro. Taken together, these results indicate that the impaired anabolic response of skeleton to PTH observed in *Atf4*$^{-/-}$ animals cannot be explained by a reduction in the level of PTH1R and/or cAMP production. These results clearly demonstrate that: i) intermittent PTH stimulates the expression of Osx and, to a lesser extent,

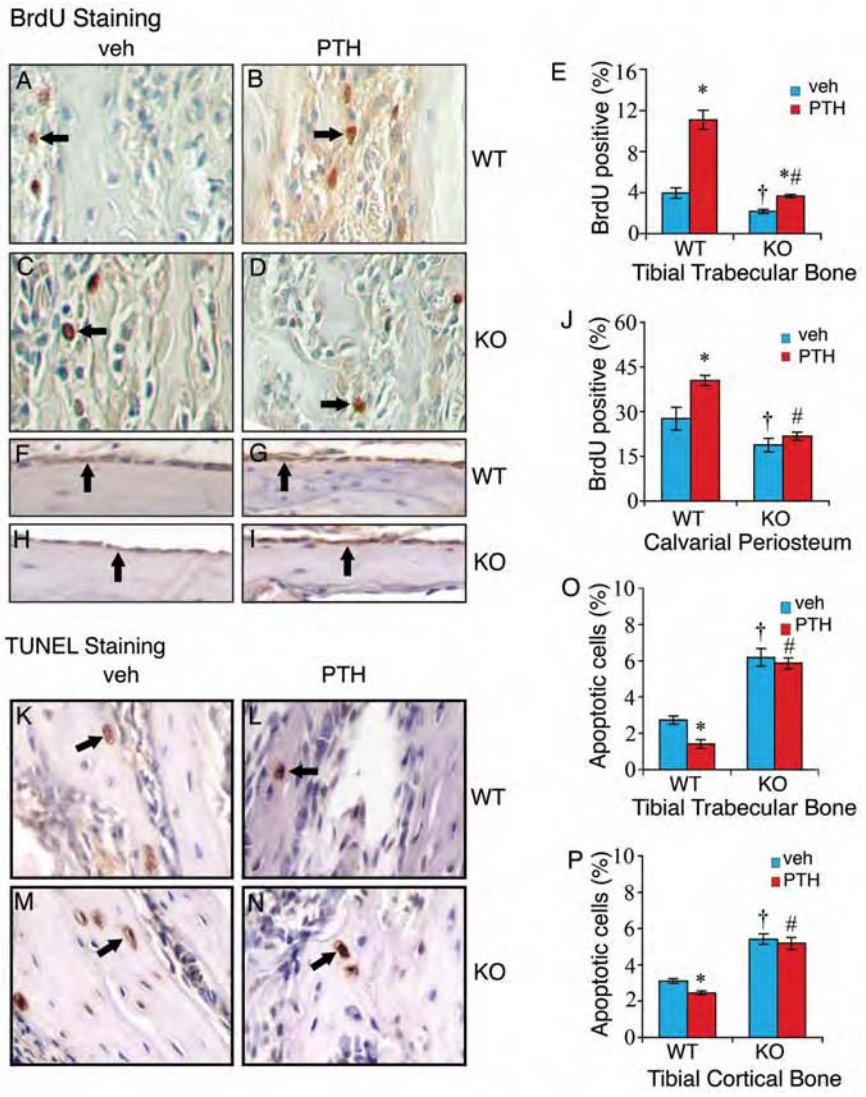

Figure 4. Effects of PTH on osteoblast proliferation and survival in wt and Atf4$^{-/-}$ bone. A–J, BrdU staining, sections of tibiae (A–D) and calvariae (F–I) were stained using a Zymed BrdU immunostaining kit. Proliferating cells were stained brown (arrows) and non-proliferating cells were stained blue. Proliferating cells on tibial trabecular surface or osteoid (E) or calvarial periosteal surface (J) were counted and normalized to total cells from the same area. K–P, TUNEL staining, sections of tibiae were stained using the ApopTag Peroxidase *In Situ* Apoptosis Detection Kit. Apoptotic osteoblasts and osteocytes (arrows) were stained brown and non-apoptotic cells were stained blue. Apoptotic osteoblasts and osteocytes in the trabecular (O) and cortical bone (P) of tibiae were counted and normalized to total osteoblasts and osteocytes from the same area. *P<0.05 (veh vs. PTH), † P<0.05 (wt-veh vs. *Atf4*$^{-/-}$-veh), #P<0.05 (PTH/veh-wt vs. PTH/veh-*Atf4*$^{-/-}$).
doi:10.1371/journal.pone.0007583.g004

Runx2, ii) PTH fails to stimulate Osx/Runx2 expression in the absence of ATF4, and iii) ATF4 is also required for basal level Osx expression.

Identification of a 132-bp ATF4-response element in proximal Osx promoter

Osx is not detected in *Runx2*$^{-/-}$ mice [35], indicating that Runx2 functions upstream of this factor and is essential for Osx expression. However, the results described above showed that ATF4 deficiency dramatically reduced the level of Osx protein without decreasing Runx2, suggesting that Runx2 is not sufficient for the maximal expression of Osx and that ATF4 has an important role in Osx expression. To define the mechanism whereby ATF4 regulates Osx, we examined the effect of ATF4 overexpression on Osx expression in MC-4 preosteoblast cells. As shown in Fig. 7A, ATF4 dose-dependently increased levels of Osx protein (top) and mRNA (bottom). We next examined whether ATF4 up-regulates Osx by increasing gene transcription by using a −1003/+68 mouse Osx promoter (Fig. 7 B). Using COS-7 cells, which lack detectable Runx2, ATF4 had comparable activity to Runx2 in terms of its ability to activate promoter activity (approx. 1.8-fold). Together, ATF4 and Runx2 maximally activated the *Osx* promoter (3.2-fold induction). To further define the region of the Osx promoter necessary for ATF4 responsiveness, several constructs containing various deletion mutants of the mouse *Osx* promoter were transiently transfected into COS-7 cells with and without an ATF4 expression plasmid. Results showed that luciferase activity of both control and ATF4-transfected groups decreased with progressively larger 5′ deletions. However, ATF4 stimulation was abrogated when a 132-bp region between bp −215 to −83 was deleted (Fig. 7C). A putative ATF4-binding sequence (CTTCCTCA) at −201/−194 bp was identified in this

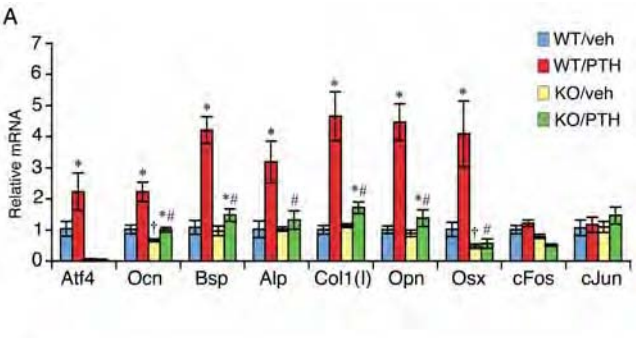

B

	WT/veh	WT/PTH	KO/veh	KO/PTH
IGF-1(ng/ml)	398 ± 57	412 ± 51	187 ± 7†	184 ± 4
FGF-2 (pg/ml)	8.6 ± 0.4	9.0 ± 0.2	6.3 ± 0.6†	7.4 ± 0.6

N = 5-8

Figure 5. Effects of PTH on expression of osteoblast marker genes in wt and ATF4 deficient mice. A, quantitative real-time PCR, total RNAs were isolated from tibiae and analyzed by quantitative real-time RT-PCR using specific primers for *Atf4*, *Ocn*, *Bsp*, *Col 1(I)*, *ALP*, *Opn*, *Pthrp*, *c-Fos*, *and c-Jun* mRNAs, which were normalized to *Gapdh* mRNA. *P<0.05 (veh vs. PTH), #P<0.05 (wt-veh vs. *Atf4*$^{-/-}$-veh). B, plasma levels of IGF-1 and FGF-2 from mice using respective ELISA kits according to the manufacturer's instructions. *P<0.05 (veh vs. PTH), †P<0.05 (wt-veh vs. *Atf4*$^{-/-}$-veh), #P<0.05 (PTH/veh-wt vs. PTH/veh-*Atf4*$^{-/-}$).
doi:10.1371/journal.pone.0007583.g005

region by using a TRANSFAC retrieval program. Introduction of a 3-bp substitution mutation to this core sequence (from CTTCCTCA to CTTgtaCA) completely abolished ATF4 activation (Fig. 7D). As shown in Fig. 7E, a DNA oligo probe from the Osx promoter that contains the TTACATCA core sequence bound to a factor(s) in nuclear extracts from COS-7 cells transfected with an ATF4 expression vector. Importantly, this binding (see arrow) was dramatically reduced by the addition of a specific antibody against ATF4 but not by normal control IgG or antibodies against cFos (an AP1 family member) or ATF2.

PTH stimulation of Osx gene transcription requires an ATF4 response element

To study the mechanism whereby PTH regulates *Osx*, we next evaluated the effect of PTH on mouse −1003/+68 *Osx* promoter activity in MC-4 preosteoblast cells. As illustrated in Fig. 7F, PTH stimulated promoter activity in a dose-dependent manner with a detectable response seen at a PTH concentration of 10^{-10} M (significance at P<0.01). Measurable activation of the *Osx* promoter was observed 0.5 h after PTH addition with maximal induction occurring between 4–6 h (Fig. 7G). PTH-stimulated Osx protein expression was entirely blocked by PKA inhibition (Fig. 7H). The 132-bp ATF4-responsive element identified above was also required for PTH induction of promoter (Fig. 7I). Furthermore, the same 3-bp substitution mutation that abrogates ATF4 activation dramatically reduced PTH-dependent activation (Fig. 7J), indicating that this element is critical for the actions of PTH on this promoter.

ATF4 is recruited to the endogenous Osx promoter in a PTH-dependent manner

To determine whether ATF4 is associated with the endogenous *Osx* promoter in vivo, we performed chromatin immunoprecipitation (ChIP) assays using MC-4 cells with and without PTH treatment. As shown in Fig. 7K and L, ATF4 specifically interacted with a chromatin fragment of the proximal *Osx* promoter that contains the ATF4-binding site identified above. This interaction was not detected in primary calvarial osteoblasts from *Atf4*$^{-/-}$ mice (data not shown). Furthermore, this interaction was dramatically stimulated by PTH treatment. Supporting our previous demonstration that the OSE1 site in the *mOG2* promoter mediates PTH induction of the gene [31,34], ATF4 also bound to an ATF4-binding site (OSE1)-containing chromatin fragment of the proximal *mOG2* promoter in a PTH-dependent manner (primers P3/P4). In contrast, ATF4 antibody failed to immunoprecipitate a 3′ chromatin fragment in the transcribed region of the *mOG2* gene that contains no ATF4-binding sites (primers P5/P6).

Discussion

Our goals in this study were: 1) to determine whether the bone-related transcription factor ATF4 plays a role in the anabolic effects of PTH in bone, and 2) if so, to define the relevant mechanisms. Our results clearly show that PTH-stimulated increases in osteoblast proliferation, volume of long bones, vertebrae, and calvariae as well as decreases in apoptosis are all dramatically reduced or completely abolished in *Atf4*-deficient mice. Equally importantly, PTH-induced bone in *Atf4*$^{-/-}$ mice cannot mature due to a severe defect in osteoblast differentiation as manifested by a defect in Osx expression. Therefore, this study establishes a critical role for ATF4 in the anabolic actions of PTH in bone.

In agreement with results from previous studies [14,47], we find that intermittent PTH dramatically increases trabecular and cortical bone volume. This PTH response is achieved at least in part by stimulating the proliferation of osteoblasts and preosteoblasts and/or by inhibiting apoptotic death of osteoblasts and osteocytes in vivo [2,6,45,47]. Effects of PTH on osteoblast proliferation and survival can be reproduced in cultured osteoblasts [15,16,48]. Importantly, this study demonstrates that ATF4 plays a pivotal role in PTH stimulation of cell proliferation in osteoblasts and preosteoblasts and attenuation of apoptosis in osteoblasts and osteocytes in vivo. PTH can increase osteoblast proliferation at least in part through ATF4-mediated expression of cyclin D1 [33] because both factors are up-regulated by PTH in osteoblasts [15,34]. The mechanism whereby ATF4 blocks apoptosis in osteoblasts remains unknown. ATF4 deficiency also increases apoptosis in lens fiber cells in a p53-dependent manner. The embryonic lens in double homozygous *p53/Atf4*$^{-/-}$ mice does not undergo apoptosis, which suggests possible involvement of p53 in this process [49,50].

Accumulating evidence supports the concept that, in addition to increasing osteoblast cell number, intermittent PTH also stimulates osteoblast differentiation [4,51–53]. In agreement with these results, the present study clearly demonstrates that: i) PTH dramatically increases the in vivo expression of osteoblast differentiation marker genes, including *Ocn*, *Bsp*, *Alp*, *Opn*, and *Col1(I)*; and ii) PTH strikingly elevates the numbers of Osx-positive osteoblasts (i.e., mature or differentiating osteoblasts) and level of Osx protein as demonstrated by both IHC and Western blot analysis. Because PTH is able to stimulate the expression of many osteoblast differentiation marker genes in cultured osteoblast-like cells [12,30,31,54–57], it is likely that intermittent PTH also activates these genes in vivo via a similar molecular mechanism. Although part of the increased osteoblast activity in PTH-treated animals is likely explained by a PTH-dependent increase in

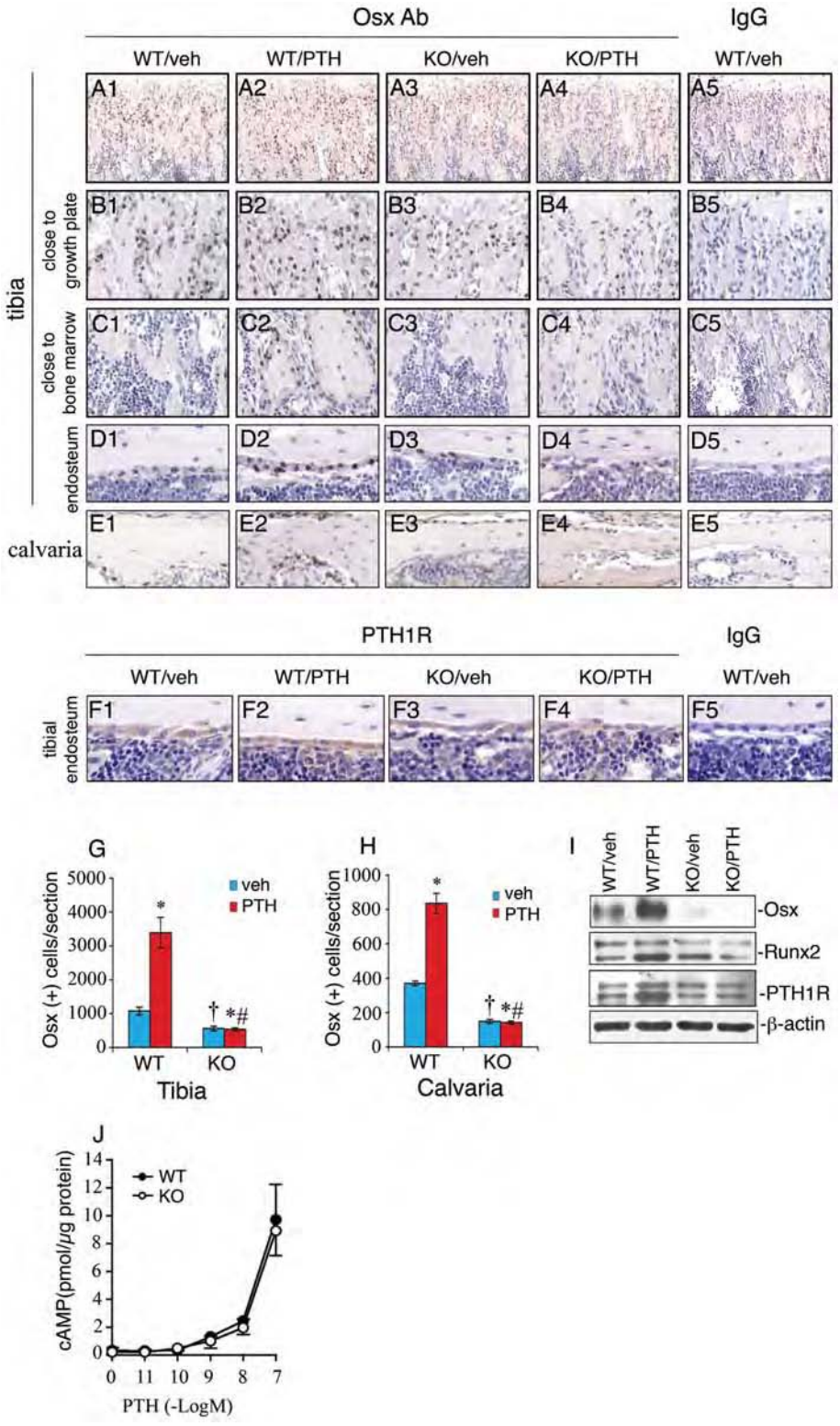

Figure 6. PTH fails to promote osteoblast maturation/differentiation in the absence of ATF4. A–E, IHC analysis of Osx expression, sections of tibiae (A–D) and calvariae (E) were immunohistochemically stained using a specific antibody against Osx protein. The nuclei of Osx-positive cells (i.e., osteoblasts) were stained brown. The nuclei of preosteoblasts and other cells are stained blue. The total numbers of Osx-positive osteoblasts per tibial (G) or calvarial (H) section were counted under microscope. F, sections of tibiae were stained using an antibody against PTH1R protein. I, Western blot analysis, protein extracts were isolated from tibiae and analyzed for Osx, Runx2, and PTH1R proteins. *$P<0.05$ (veh vs. PTH), $^{\dagger}P<0.05$ (wt-veh vs. *Atf4*$^{-/-}$-veh), $^{\#}P<0.05$ (PTH/veh-wt vs. PTH/veh-*Atf4*$^{-/-}$). J, cAMP assay, primary calvarial osteoblasts from 3-d-old wt or *Atf4*$^{-/-}$ mice were isolated, seeded at density of 5×10^4 on 96-well plate, and treated with vehicle or increasing concentrations of human recombinant PTH(1-34) for 5 min followed by measurement of cAMP.
doi:10.1371/journal.pone.0007583.g006

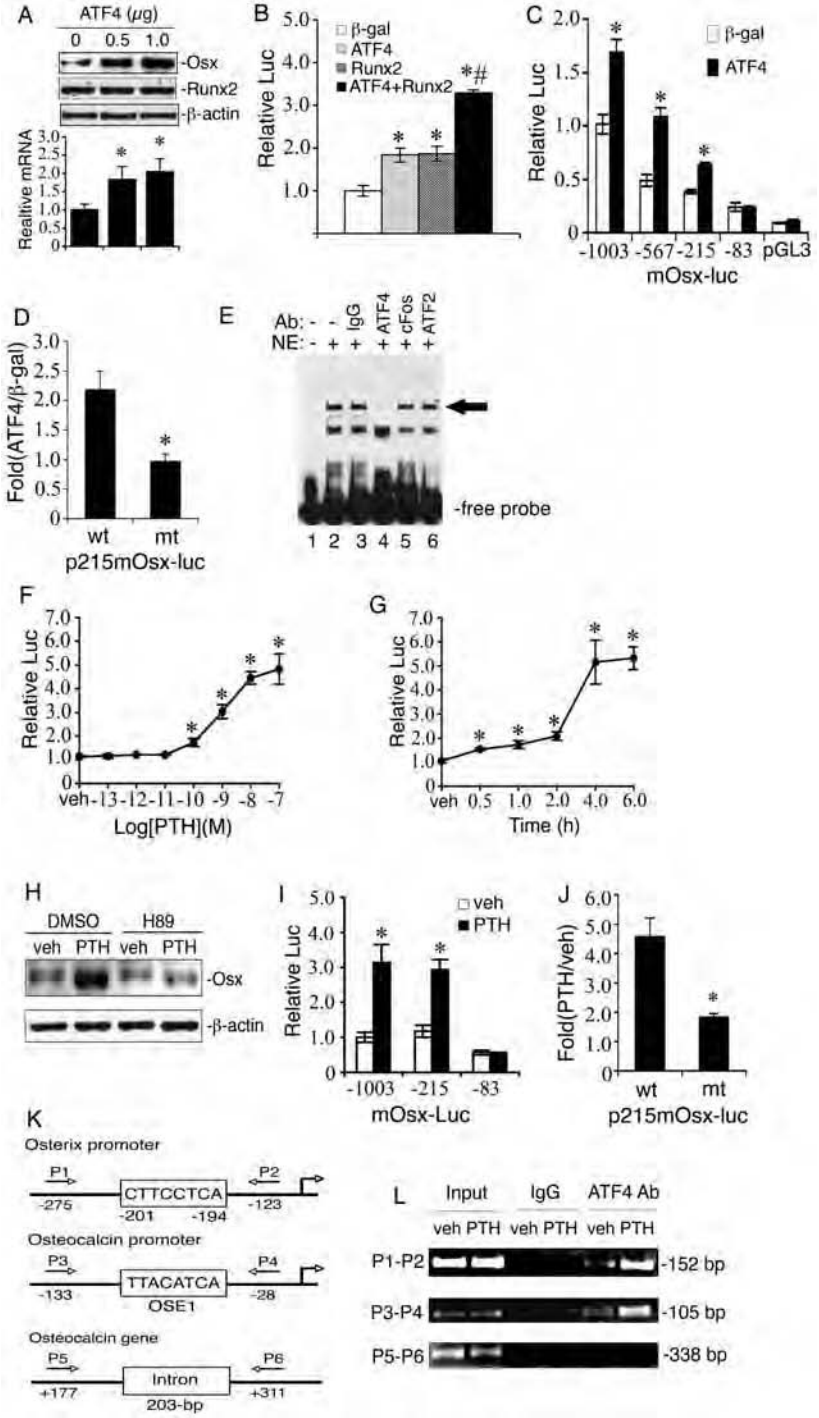

Figure 7. PTH activates Osx gene transcription via an ATF4-responsive element in the proximal Osx promoter. A, MC-4 cells were electroporated with indicated amount of ATF4 expression plasmid followed by Western blot. B, COS-7 cells were transfected with p1060mOsx-luc, pRL-SV40, and indicated expression vectors followed by dual lucferase assays. C, COS-7 cells were transfected with various deletion constructs and pRL-SV40 with and without ATF4 expression plasmid. D, COS-7 cells transfected with p215mOsx-luc or the same plasmid containing a 3-bp substitution mutation in the putative ATF4-binding site and pRL-SV40 with and without ATF4 expression plasmid. E, EMSA, labeled wild-type DNA probe was incubated with 2 μg nuclear extracts from COS-7 cells transfected with pCMV/ATF4 plasmid in the presence of normal control IgG (lane 3), ATF4 antibody (lane 4), cFos antibody (lane 5), and ATF2 antibody (lane 6). Experiments were repeated 3–4 times and qualitatively identical results were obtained. F and G, MC-4 cells transfected with p1003mOsx-luc and pRL-SV40 were treated with indicated concentration of PTH for 6 h (F) or with 10^{-7} M PTH for indicated times (G). H, MC-4 cells were treated with and without 10^{-7} M PTH in the presence and absence of 10 μM of H89 for 6 h. I, MC-4 cells transfected as in Fig. 7C were treated with and without 10^{-7} M PTH for 6 h. J, MC-4 cells transfected as in Fig. D were treated with and without 10^{-7} M PTH for 6 h. K, a schematic illustration of putative ATF4 binding sites in the 5′ flanking regions of the *Osx* and *osteocalcin* gene promoters and *osteocalcin* gene. L, ChIP assay of the *Osx* promoter in MC-4 cells treated with and without 10^{-7} M PTH for 6 h. *P<0.05 (β-gal vs. ATF4, Runx2, and ATF4 plus Runx2, or veh vs. PTH), #P<0.05 (ATF4 plus Runx2 vs. β-gal, ATF4, or Runx2).
doi:10.1371/journal.pone.0007583.g007

osteoblast proliferation and/or reduction of apoptosis, our studies suggest that PTH also increases osteoblast differentiation by rapidly up-regulating Osx.

Importantly, experiments from the current study show that effects of PTH on osteoblast differentiation are mediated by ATF4. Although PTH increased osteoblast proliferation in *Atf4*$^{-/-}$ animals as evidenced by significant increases in bone volume and nuclear BrdU labeling (Figs. 1–3), expression of osteoblast marker genes and numbers of Osx-positive osteoblasts were either dramatically reduced or completely abolished in *Atf4*$^{-/-}$ animals. Furthermore, since the basal levels of osteoblast differentiation markers are either slightly reduced or not changed at all in *Atf4*$^{-/-}$ animals, the impaired differentiation response to PTH cannot be explained by a nonspecific blockage in osteoblast differentiation associated with ATF4 deficiency. Instead, ATF4 appears to have a unique role in the PTH-dependent component of osteoblast differentiation.

Further support for the concept that PTH actions are mediated by ATF4 comes from mechanistic studies. Specifically, we showed that PTH is a potent inducer of Osx expression in vivo and this response is completely abolished by ATF4 deficiency. Furthermore, PTH directly activated *Osx* gene transcription in cultured osteoblast-like cells, a response that required an ATF4 response element located between −201 and −194 bp in the proximal mouse *Osx* promoter. Introduction of a 3-bp substitution mutation into this ATF4-binding site essentially eliminated the PTH response. ChIP assays demonstrated that ATF4 binds to an endogenous chromatin fragment near the putative ATF4-binding site in the proximal *Osx* promoter in MC-4 cells. Of particular significance, ATF4 binding to the *Osx* promoter is dramatically enhanced by PTH. Collectively, these studies establish a unique role for ATF4 in PTH-mediated induction of Osx and osteoblast differentiation.

Runx2 is absolutely required for Osx expression, osteoblast differentiation, and bone formation [35,58]. Nevertheless, ATF4 deficiency dramatically reduced the level of Osx protein without altering Runx2, suggesting that Runx2 is not sufficient for maximal Osx expression. ATF4 stimulated Osx gene transcription in COS-7 cells that lack Runx2 protein to an extent similar to that seen with Runx2. In addition, an ATF4 response element was identified in the proximal region of the mouse Osx promoter. These results demonstrate that both ATF4 and Runx2 are essential for the maximal expression of Osx and are reminiscent of our previous study showing cooperative interactions between these two factors in regulating the *Ocn* gene [59].

It should be noted that ATF4 deficiency did not completely block the anabolic actions of PTH since this hormone increased bone volume in both growing and adult OVX bones from *Atf4*$^{-/-}$ mice (Figs. 1–3). This suggests that other factors must be involved for the PTH response. c-Fos [3], cAMP response element binding protein (CREB) [16], a major downstream target for PTH/cAMP and calcium signals, cAMP-response element modulator (CREM)[60], and Runx2 [16,23], a master regulator of osteoblast differentiation and bone formation, have all been shown to mediate components of the PTH anabolic response. Interestingly, these factors are either structurally related to ATF4 (c-Fos and CREM) or can interact with this factor (Runx2 and c-Fos) [59,61–65]. Most recently, low-density lipoprotein-related protein 6 (LRP6)[66], a major component of the Wnt signaling pathway, has been implicated in the anabolic actions of PTH in bone. It would be interesting to determine whether ATF4 mediates the PTH anabolic response via interactions with these factors or signaling pathways.

PTH signaling may regulate ATF4 via several mechanisms. First, PTH up-regulates *Atf4* gene expression in cultured osteoblasts as demonstrated by our recent study [34] as well as in vivo (Fig. 5). Second, PTH post-translationally activates ATF4 via PKA [34], a major route for PTH signaling in osteoblasts. PKA phosphorylation of ATF4 at its Ser254 residue mediates β-adrenergic induction of *Rankl* mRNA expression in osteoblasts [67]. ATF4 can also be directly phosphorylated and activated by RSK2 [26], a growth factor-regulated serine-threonine protein kinase activated by the Ras-Mitogen-Activated Protein Kinase (MAPK) pathway. This phosphorylation is critical for ATF4 activity as well as bone formation [26]. Because PTH signaling activates Erk/MAPK [48], an immediate upstream activator of RSK2, ATF4 can be activated via the PTH-MAPK-RSK2 signaling pathway. Lastly, PTH promotes ATF4-Runx2 interactions which are critical for osteoblast function and bone formation [59,61,63]. This notion is supported by the fact that PTH up-regulates both factors in osteoblasts [23,34].

Based on findings from this and other studies, we proposed a working model for ATF4 to mediate PTH stimulation of osteoblast function and bone formation (Fig. 8). Binding of PTH to its receptor, PTH1R, activates PKA and probably other intracellular signaling pathways, leading to up-regulation/activation of ATF4. ATF4 subsequently increases proliferation of osteoblasts and/or preosteoblasts via modulation of cyclin D1 protein, and attenuates apoptotic death in osteoblasts and osteocytes, resulting in a significant increase in the numbers of osteoblasts and/or osteocytes. At the same time, ATF4 together with Runx2 maximally activates Osx expression and increases osteoblast differentiation. The resulting increases in osteoblast number and

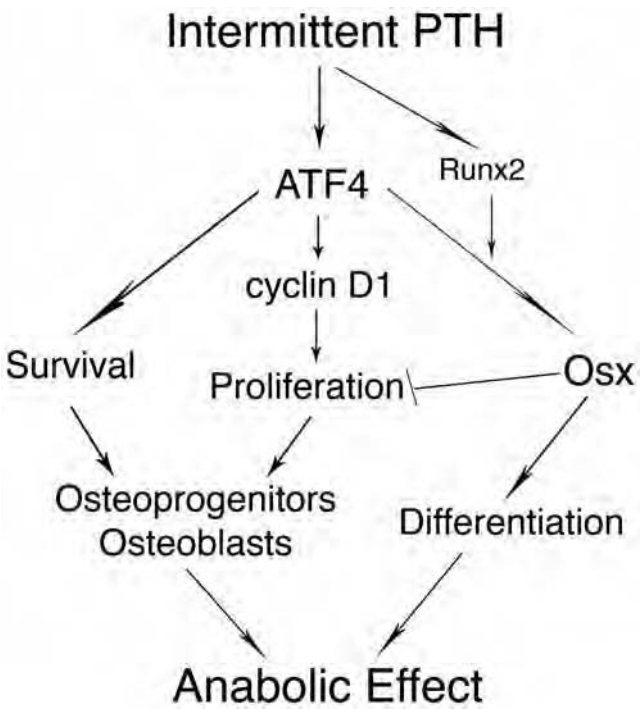

Figure 8. Proposed model for ATF4 mediation of PTH stimulation of bone formation. Binding of PTH to PTH1R activates PKA and leads to up-regulation of ATF4. ATF4 subsequently increases proliferation and survival of osteoblasts. At the same time, ATF4 together with Runx2 maximally activates Osx expression and increases osteoblast differentiation. These increases in osteoblast number and differentiation lead to massive bone formation. Osx also negatively regulates osteoblast proliferation, thus preventing excess bone formation.
doi:10.1371/journal.pone.0007583.g008

differentiation lead to bone formation. Osx also negatively regulates osteoblast proliferation, thus preventing excess bone formation [68].

Since ATF4 is known to regulate the expression of RANKL in osteoblasts and thereby osteoclast differentiation [67,69], it will be interesting to determine if ATF4 is also required for the catabolic actions of PTH in bone.

In summary, this study establishes a critical role for ATF4 in the anabolic actions of PTH in bone. ATF4 is necessary for PTH to increase both osteoblast numbers and differentiation. Therefore, ATF4 may provide a potential new therapeutic target for improving bone mass and for treating metabolic bone diseases such as osteoporosis.

Materials and Methods

Reagents

Tissue culture media and fetal bovine serum were obtained from HyClone (Logan, UT). H89, DMSO, PTH1R antibody, mouse monoclonal antibody against β-actin were purchased from Sigma (St Louis, MO). Other reagents were obtained from the following sources: antibodies against ATF4 (for Western blot), Runx2, normal control IgGs and horseradish peroxidase-conjugated mouse or goat IgG from Santa Cruz (Santa Cruz, CA), and Osterix antibody from Abcam Inc. (Cambridge, MA). ATF4 antibody used for EMSA was raised against epitope QETN-KEPPQTVNPIGHLPESLIK (St Louis, MO). All other chemicals were of analytical grade.

Atf4-deficient mice

Breeding pairs of *Atf4* heterozygous mice were described previously [34] and used to generate *Atf4* wild-type (wt) ($Atf4^{+/+}$), heterozygous ($Atf4^{+/-}$) and homozygous mutant ($Atf4^{-/-}$) mice for this study. All research protocols were approved by the Institutional Animal Care and Use Committee of the VA Pittsburgh Healthcare System, where this study was conducted.

In vivo PTH administration

For the "growing mouse model", five-day-old mice were given daily subcutaneous injections of vehicle (saline) or hPTH(1–34) (60 ng/g body weight, Bachem, Torrance, CA) for 28 d. For the "adult OVX mouse model", four-month-old female mice were anesthetized and ovariectomized as follows: A 1-cm midline incision was made through the skin. The "white line" will be visualized on the peritoneum and a second incision was made along the white line through the peritoneum. Using long, straight forceps, the left ovary was isolated and the connective tissue between the ovary and kidney was dissected away. Straight forceps with flat ends was used to pinch the uterine horn while another set of straight forceps was used to tear the ovary away from the uterine horn. The same was done on the right ovary. 6-0 PDS (Polydioxanone Sutures, 6/0) was used to tie around the uterine horn to provide hemostasis if necessary. 6-0 PDS was used to close the innermost layer. Sterile surgical staples were used to close the incision. Two months later mice were given daily subcutaneous injections of vehicle or hPTH(1-34) (100 ng/g body weight) for 28 d. Mice were euthanized 24 h after last PTH injection. The effects of these PTH dosing regimens on bone were determined by both biochemical and histomorphometric criteria.

Gross evaluation and serum biochemistry

Body weight was recorded every another day. The length of the femurs was measured using an electronic digital caliper. Faxitron X-ray analysis of femurs was conducted at 27 kv and 7.5 seconds (Faxitron X-Ray Corp., Wheeling, IL). Femurs were ashed at 800°C for 4 h and weighed. Serum calcium and Pi concentrations were determined using kits from Pointe Scientific, Inc (Canton, MI) following the manufacture's instructions (Sigma Diagnostics).

Bone morphometric analyses by micro-computerized tomography (μCT)

Upon termination of PTH or vehicle treatment, mice were sacrificed and femurs were isolated. Fixed non-demineralized femurs were used for μCT analysis at the Center for Bone Biology using a VIVACT40 (SCANCO Medical AG) following the standards of techniques and terminology recommended by American Society for Bone and Mineral Research [70]. For trabecular bone parameters, transverse CT slices were obtained in the region of interest in the axial direction from the trabecular bone 0.1 mm below the growth plate (bottom of the primary spongiosa) to the mid-femur. Contours were defined and drawn close to the cortical bone. The trabecular bone was then removed and analyzed separately. 3D analysis was then performed on trabecular bones slices. A 3-mm section was used to obtain mid-femoral cortical bone thickness. The analysis of the specimens involves the following bone measurements: bone volume fraction (BV/TV, %), trabecular number (Tb. N), trabecular thickness (Tb. Th), trabecular spacing (Tb. Sp), and cortical thickness (Cort.Th).

Histological evaluation

Tibiae, lumbar vertebrae (L5), and calvariae were fixed in PBS buffered 10% formalin at 4°C for 24 h, decalcified in 10% EDTA (pH 7.4) for 10–14 d, and embedded in paraffin. Longitudinal sections of tibiae and vertebrae were cut at 4 μm and stained with hematoxylin and eosin (H&E). Trabecular area of tibial sections was measured in the proximal metaphysis beginning immediately below the chondro-osseous junction to the mid-tibia. Calvariae were bisected perpendicular to the sagittal suture through the central portion of the parietal bones, parallel to lamboidal and coronal sutures, and embedded in paraffin to obtain sections of a standard area according to the method described by Zhao et al. [71]. Trabecular area versus total bone area was measured using an Image Pro Plus 6.2 software (Media Cybernetics, Inc, Bethesda, MD). The calvarial width was the average value from 20 random measurements of each calvaria (at least 6 samples per group) using a SPOT Advanced imaging software (provided with the purchase of the Olympus BX41 microscope).

Measurement of mineral apposition rate (MAR)

Mice were injected with calcein subcutaneously (20 mg/kg) at 6 and 2 d before sacrifice. Undecalcified tibia were fixed in 70% ethanol, embedded in methylmethacrylate and sectioned at 10 μm. Calcein labeling was visualized using a Nikon E800 fluorescence microscope. The metaphyseal trabecular bone projected into the marrow space was evaluated and the distance between the all double-labeled areas was measured at a magnification of 200x. MAR was calculated as mean distance between the double labels divided by the number of the days between the calcein injections. Histomorphometric analysis was performed using BioQuant image analysis software (R&M Bio Metrics, Nashville, TN, USA).

In vivo proliferation assay

Mice were injected intraperitoneally with 100 μg bromodeoxyuridine (BrdU)/12 μg fluorodeoxyuridine (FdU) per gram of body weight 12 h before sacrifice. After sacrifice, sections of tibiae and calvariae were obtained. To identify actively proliferating cells,

nuclei that have incorporated BrdU were detected using a Zymed BrdU immunostaining kit according to the manufacturer's instruction (Invitrogen, Carlsbad, CA). BrdU-positive cells (brown) on the calvarial periosteal surface or in the osteoid of tibiae were counted and normalized to the total numbers in the same area [33]. BrdU-positive hematopoietic cells in marrow were not counted.

In situ apoptosis detection

This assay is based on the classical TUNEL assay to examine apoptosis by detecting DNA fragmentation. 4-μm sections of tibiae were prepared and stained using the ApopTag Peroxidase *In Situ* Apoptosis Detection Kit according to the manufacturer's instruction (Millipore, Billerica, MA). Apoptotic osteoblasts and osteocytes in tibiae were counted and normalized to the total cells from the same area.

Immunohistochemistry (IHC)

Tibiae and calvariae were fixed, decalcified, and embedded in paraffin. Sections of tibiae and calvariae were stained with antibodies against Osx (Abcam Inc, Cambridge, MA) and PTH1R (Sigma, St. Louis, MO) using the EnVision^{+}System-HRP (DAB) kit (Dako North America, Inc, Carpinteria, CA) according to the manufacturer's instructions. Briefly, slides were baked at 55°C for 45 min, deparaffinized in three washes of xylene, and rehydrated in a decreasing ethanol gradient. Antigen retrieval was performed using 0.1% trypsin for 10 min at 37°C in a humidified chamber. Endogenous peroxidases were deactivated with 3% H_2O_2 in 1x PBS for 10 min, and sections were blocked in blocking solution for 30 min at room temperature. Sections were incubated with primary antibody (1:200 dilution for both osterix and PTH1R) in blocking solution for 2 hours at 4°C. Sections were washed in PBS three times and incubated with a donkey-anti-rabbit IgG-HRP secondary antibody solution for 30 min at room temperature. After washing with PBS three times, HRP activity was detected using a DAB substrate solution for 5 min at room temperature. Sections were counter-stained with a Mayer's hematoxylin solution.

Measurement of plasma levels of IGF-1 and FGF-2 by ELISA

Blood plasma samples were prepared from whole-blood samples from mice of each group and plasma levels of IGF-1 and FGF-2 were measured by using ELISA kits (human FGF basic Quantikine ELISA Kit, cat#: DFB50, and mouse IGF-I Quantikine ELISA Kit, cat#: MG100, both from R&D Systems Inc, Minnepolis, MN 55413) according to the manufacturer's instructions.

cAMP assay

Primary osteoblasts from calvariae of 3-d-old wt or *Atf4*$^{-/-}$ mice were isolated as described previously [72]. Cells were seeded at a desity of 5×10^4/well on 96-well plate and treated with vehicle or increasing concentrations of human recombinant PTH(1-34) for 5 min. Cells were then lysed with lysis reagent 1B and cell lysates used for cAMP assay using a cAMP Biotrak Enzymeimmunoassay (EIA) kit (cat #: RPN225, GE Healthcare Biosciences Corp, Piscataway, NJ) according to the manufacturer's instructions and the protein concentrations were measured using a BCA protein assay kit (Pierce). cAMP was normalized to total protein.

Quantitative real-time RT/PCR and Western blot analysis

RNA isolation, reverse transcription (RT), regular PCR, and quantitative real-time PCR analysis were performed as previously described [34]. The DNA sequences of mouse primers used for real-time PCR were summarized in Table 1. Western blot analysis was performed as previously described [33]. RNAs or protein extracts from at least six specimens in each group were used.

DNA constructs and site-directed mutagenesis, transfection

pCMV/β-gal, pCMV/ATF4, and pCMV/Runx2 were previously described [62]. mOsx-luc containing different mouse *Osx* promoter elements (−1003/+68, −567/+68, −215/+68, and −83/+68) driving a firefly luciferase reporter gene were constructed in the project laboratory by PCR subcloning promoter fragments using mouse tail DNA as a template into pGL3-luc vector (Promega, Madison, WI). Mutant p215mOsx-luc which contains a 3-bp substitution mutation in a putative ATF4-binding at positions −198, −197 and −196 (from CTTCCTCA to CTTgtaCA) was generated from the wild-type p215mOsx-luc by PCR amplification using a QuickChange^{TM} XL Site-Directed Mutagenesis Kit (Stratagene, La Jolla, CA) using the following primers: 5′-GGT ACC CCT CCC TCT CTC GCC TTg taC ATT GGA TCC GGA GTC TTC TCC GC-3′ (forward); 5′-GCG GAG AAG ACT CCG GAT CCA ATG tac AAG GCG AGA GAG GGA GGC GGT ACC-3′ (reverse). Sequence accuracy was confirmed by automatic DNA sequencing. For all transfection experiments, the amount of plasmid DNAs (reporter plasmid, 0.25 μg; normalization plasmid pRL-SV4, 10 ng; and expression plasmid, 1.0 μg) was balanced as necessary with β-galactosidase expression plasmid such that the total DNA was constant in each group. Experiments were performed in triplicates and repeated 3–4 times.

Nuclear extracts preparation and electrophoretic mobility shift assay (EMSA)

Nuclear extracts were prepared from COS-7 cells transfected with pCMV/ATF4 plasmids as previously described [73]. The DNA sequences of the oligonucleotides used for EMSA were as follows: GAT CCC TGC CTC CCT CTC TCG CCT TCC TCA TTG GAT CCG GAG TCT TCG. DNA oligonucleotide was labeled using a Biotin 3′ end DNA Labeling Kit (cat #: 89818, Pierce Biotechnology Inc., Rockford, IL). Two μg of nuclear extracts and 20 fmol biotin-labeled DNA probe were incubated in 1x binding buffer for 30 min at room temperature.

Table 1. real-time PCR primers.

Gene name	5′ primer	3′ primer
Alp	TCCCACGTTTTCACATTCGG	CCCGTTACCATATAGGATGGCC
Atf4	GAGCTTCCTGAACAGCGAAGTG	TGGCCACCTCCAGATAGTCATC
Bsp	AAGAGGAAGAAAATGAGAACGA	GCTTCTTCTCCGTTGTCTCC
cFos	AATGGTGAAGACCGTGTCAGGA	CCCTTCGGATTCTCCGTTTCT
cJun	GCCAACATGCTCAGGGAACAGGTG	GCCCCTCAGCCCTGACAGTCTG
Col I(1)	AGATTGAGAACATCCGCAGCC	TCCAGTACTCTCCGCTCTTCCA
Gapdh	CAGTGCCAGCCTCGTCCCGTAGA	CTGCAAATGGCAGCCCTGGTGAC
Ocn	TAGTGAACAGACTCCGGCGCTA	TGTAGGCGGTCTTCAAGCCAT
Opn	CCAATGAAAGCCATGACCACA	CGTCAGATTCATCCGAGTCCAC
Osx	AGAGGTTCACTCGCTCTGACGA	TTGCTCAAGTGGTCGCTTCTG
Pth1r	GATGCGGACGATGTCTTTACC	GGCGGTCAAATACCTCC

doi:10.1371/journal.pone.0007583.t001

Table 2. PCR primers used in ChIP assay.

Oligo name	Sequence
P1	CCCTCCCAGATCCCTTCTTT
P2	GGCTGCTCTCTGTCTGTAGGG
P3	CACAGCATCCTTTGGGTTTGAC
P4	TATCGGCTACTCTGTGCTCTCTGA
P5	TAGTGAACAGACTCCGGCGCTA
P6	TGTAGGCGGTCTTCA AGCCAT

doi:10.1371/journal.pone.0007583.t002

For supershift assay, 1 μg of IgG or indicated antibodies were first incubated with nuclear extracts prior to addition of DNA probe. Protein–DNA complexes were separated on 4% polyacrylamide gels in 1x TBE buffer, and transferred onto Biodyne B Nylon Membrane (cat #: 77016, Pierce). The membrane was blocked in 1x blocking buffer, washed five times with 1x wash buffer, and visualized by a Chemiluminescent Nucleic Acid detection Module (cat #: 89880, Pierce, Rockford, IL).

Chromatin immunoprecipitation (ChIP)

ChIP assays were performed using ATF4 antibody or control IgG as described previously [62]. PCR primer pairs (Table 2) were generated to detect DNA segments located near a putative ATF4-binding site (CTTCCTCAT) at −201/−193 (primers P1 and P2) determined by the TRANSFAC retrieval program in the 5′ flanking region of the *Osx* promoter, a previously identified ATF4-binding site (OSE1) in *osteocalcin* gene 2 (mOG2) promoter (primers 3 and 4), and a mOG2 gene region (+177/+311) that contains no ATF4-binding sites (primers P5 and P6) [62]. PCR products were run on 3% agarose gel and stained with ethidium bromide. Purified input chromatin was used to perform parallel PCRs with the respective primer pairs.

Statistical analysis

Data was analyzed with a GraphPad Prism software (4.0). A one-way ANOVA analysis was used followed by the Tukey test. Students' *t* test was used to test for differences between two groups of data as needed. Data of Figs. 1, 2, 4, and 5 and S1-2 were from growing mice and Figs. 3 and S3 from 7-month-old OVX mice. For H&E, IHC, BrdU, and TUNEL studies, two to three sections per specimen and at least six specimens in each group were used. Results were expressed as means ± standard deviation (SD). Differences with a $P<0.05$ was considered as statistically significant.

Supporting Information

Figure S1 Effects of PTH on animal growth, length and ash weight of femurs, and serum Pi and calcium concentrations and alkaline activity in wt and Atf4−/− mice. A, growth curve, B, length of femur, C, dry ash weight of femur, D, serum Pi, E, serum calcium. *$P<0.05$ (veh vs. PTH), † $P<0.05$ (wt-veh vs. Atf4-/--veh).
Found at: doi:10.1371/journal.pone.0007583.s001 (1.78 MB DOC)

Figure S2 Faxitron X-ray analysis of femurs from vehicle and PTH-treated growing wt, Atf4+/−, and Atf4-/− mice. Faxitron X-ray analysis was conducted at 27 kv and 7.5 seconds. Representative microradiographic images of femurs are shown.
Found at: doi:10.1371/journal.pone.0007583.s002 (1.45 MB TIF)

Figure S3 Effects of OVX surgery on bone parameters in wt and Atf4−/− mice. Four-month-old female mice were first ovariectomized. After two months, femurs were isolated for μCT analysis. *$P<0.05$ (sham vs. OVX), † $P<0.05$ (sham(+/+) vs. sham (−/−)).
Found at: doi:10.1371/journal.pone.0007583.s003 (0.16 MB DOC)

Acknowledgments

We thank Professors Laurie K. McCauley (University of Michigan Ann Arbor) and Chuanyue Wu (University of Pittsburgh) for critical reading of this manuscript. Thanks to Dr. Sengyong Yang of University of Pittsburgh for assistance of EMSA. Thanks to Dr. Deborah L. Galson of University of Pittsburgh for valuable suggestions and discussion.

Author Contributions

Conceived and designed the experiments: SY JF JZ DR GX. Performed the experiments: SY ML DJ HC TGK YL KP KH GX. Analyzed the data: SY RF TGK DR GX. Wrote the paper: RF GX.

References

1. Neer RM, Arnaud CD, Zanchetta JR, Prince R, Gaich GA, et al. (2001) Effect of parathyroid hormone (1-34) on fractures and bone mineral density in postmenopausal women with osteoporosis. N Engl J Med 344: 1434–1441.
2. Miao D, He B, Karaplis AC, Goltzman D (2002) Parathyroid hormone is essential for normal fetal bone formation. J Clin Invest 109: 1173–1182.
3. Demiralp B, Chen HL, Koh AJ, Keller ET, McCauley LK (2002) Anabolic actions of parathyroid hormone during bone growth are dependent on c-fos. Endocrinology 143: 4038–4047.
4. Iida-Klein A, Zhou H, Lu SS, Levine LR, Ducayen-Knowles M, et al. (2002) Anabolic action of parathyroid hormone is skeletal site specific at the tissue and cellular levels in mice. J Bone Miner Res 17: 808–816.
5. Iida-Klein A, Lu SS, Kapadia R, Burkhart M, Moreno A, et al. (2005) Short-term continuous infusion of human parathyroid hormone 1-34 fragment is catabolic with decreased trabecular connectivity density accompanied by hypercalcemia in C57BL/J6 mice. J Endocrinol 186: 549–557.
6. Jilka RL, Weinstein RS, Bellido T, Roberson P, Parfitt AM, et al. (1999) Increased bone formation by prevention of osteoblast apoptosis with parathyroid hormone. J Clin Invest 104: 439–446.
7. Miyakoshi N, Kasukawa Y, Linkhart TA, Baylink DJ, Mohan S (2001) Evidence that anabolic effects of PTH on bone require IGF-I in growing mice. Endocrinology 142: 4349–4356.
8. Hurley MM, Okada Y, Xiao L, Tanaka Y, Ito M, et al. (2006) Impaired bone anabolic response to parathyroid hormone in Fgf2−/− and Fgf2+/− mice. Biochem Biophys Res Commun 341: 989–994.
9. Partridge NC, Alcorn D, Michelangeli VP, Kemp BE, Ryan GB, et al. (1981) Functional properties of hormonally responsive cultured normal and malignant rat osteoblastic cells. Endocrinology 108: 213–219.
10. McCauley LK, Koh AJ, Beecher CA, Cui Y, Decker JD, et al. (1995) Effects of differentiation and transforming growth factor beta 1 on PTH/PTHrP receptor mRNA levels in MC3T3-E1 cells. J Bone Miner Res 10: 1243–1255.
11. Swarthout JT, D'Alonzo RC, Selvamurugan N, Partridge NC (2002) Parathyroid hormone-dependent signaling pathways regulating genes in bone cells. Gene 282: 1–17.
12. Carpio L, Gladu J, Goltzman D, Rabbani SA (2001) Induction of osteoblast differentiation indexes by PTHrP in MG-63 cells involves multiple signaling pathways. Am J Physiol Endocrinol Metab 281: E489–499.
13. Swarthout JT, Doggett TA, Lemker JL, Partridge NC (2001) Stimulation of extracellular signal-regulated kinases and proliferation in rat osteoblastic cells by parathyroid hormone is protein kinase C- dependent. J Biol Chem 276: 7586–7592.
14. Calvi LM, Adams GB, Weibrecht KW, Weber JM, Olson DP, et al. (2003) Osteoblastic cells regulate the haematopoietic stem cell niche. Nature 425: 841–846.
15. Datta NS, Pettway GJ, Chen C, Koh AJ, McCauley LK (2007) Cyclin D1 as a Target for the Proliferative Effects of PTH and PTHrP in Early Osteoblastic Cells. J Bone Miner Res 22: 951–964.
16. Bellido T, Ali AA, Plotkin LI, Fu Q, Gubrij I, et al. (2003) Proteasomal Degradation of Runx2 Shortens Parathyroid Hormone-induced Anti-apoptotic

Signaling in Osteoblasts: A PUTATIVE EXPLANATION FOR WHY INTERMITTENT ADMINISTRATION IS NEEDED FOR BONE ANABOLISM. J Biol Chem 278: 50259–50272.
17. Chen HL, Demiralp B, Schneider A, Koh AJ, Silve C, et al. (2002) Parathyroid hormone and parathyroid hormone-related protein exert both pro- and anti-apoptotic effects in mesenchymal cells. J Biol Chem 277: 19374–19381.
18. Pearman AT, Chou WY, Bergman KD, Pulumati MR, Partridge NC (1996) Parathyroid hormone induces c-fos promoter activity in osteoblastic cells through phosphorylated cAMP response element (CRE)-binding protein binding to the major CRE. J Biol Chem 271: 25715–25721.
19. Gonzalez GA, Montminy MR (1989) Cyclic AMP stimulates somatostatin gene transcription by phosphorylation of CREB at serine 133. Cell 59: 675–680.
20. Selvamurugan N, Chou WY, Pearman AT, Pulumati MR, Partridge NC (1998) Parathyroid hormone regulates the rat collagenase-3 promoter in osteoblastic cells through the cooperative interaction of the activator protein-1 site and the runt domain binding sequence. J Biol Chem 273: 10647–10657.
21. McCauley LK, Koh AJ, Beecher CA, Rosol TJ (1997) Proto-oncogene c-fos is transcriptionally regulated by parathyroid hormone (PTH) and PTH-related protein in a cyclic adenosine monophosphate-dependent manner in osteoblastic cells. Endocrinology 138: 5427–5433.
22. McCauley LK, Koh-Paige AJ, Chen H, Chen C, Ontiveros C, et al. (2001) Parathyroid hormone stimulates fra-2 expression in osteoblastic cells in vitro and in vivo. Endocrinology 142: 1975–1981.
23. Krishnan V, Moore TL, Ma YL, Helvering LM, Frolik CA, et al. (2003) Parathyroid hormone bone anabolic action requires cbfa1/runx2-dependent signaling. Mol Endocrinol 17: 423–435.
24. Ducy P, Karsenty G (1995) Two distinct osteoblast-specific cis-acting elements control expression of a mouse osteocalcin gene. Mol Cell Biol 15: 1858–1869.
25. Ducy P, Zhang R, Geoffroy V, Ridall AL, Karsenty G (1997) Osf2/Cbfa1: a transcriptional activator of osteoblast differentiation [see comments]. Cell 89: 747–754.
26. Yang X, Matsuda K, Bialek P, Jacquot S, Masuoka HC, et al. (2004) ATF4 Is a Substrate of RSK2 and an Essential Regulator of Osteoblast Biology; Implication for Coffin-Lowry Syndrome. Cell 117: 387–398.
27. Banerjee C, Hiebert SW, Stein JL, Lian JB, Stein GS (1996) An AML-1 consensus sequence binds an osteoblast-specific complex and transcriptionally activates the osteocalcin gene. Proc Natl Acad Sci U S A 93: 4968–4973.
28. Banerjee C, McCabe LR, Choi JY, Hiebert SW, Stein JL, et al. (1997) Runt homology domain proteins in osteoblast differentiation: AML3/CBFA1 is a major component of a bone-specific complex. J Cell Biochem 66: 1–8.
29. Boudreaux JM, Towler DA (1996) Synergistic induction of osteocalcin gene expression: identification of a bipartite element conferring fibroblast growth factor 2 and cyclic AMP responsiveness in the rat osteocalcin promoter. J Biol Chem 271: 7508–7515.
30. Yu XP, Chandrasekhar S (1997) Parathyroid hormone (PTH 1-34) regulation of rat osteocalcin gene transcription [see comments]. Endocrinology 138: 3085–3092.
31. Jiang D, Franceschi RT, Boules H, Xiao G (2004) Parathyroid Hormone Induction of the Osteocalcin Gene: REQUIREMENT FOR AN OSTEOBLAST-SPECIFIC ELEMENT 1 SEQUENCE IN THE PROMOTER AND INVOLVEMENT OF MULTIPLE SIGNALING PATHWAYS. J Biol Chem 279: 5329–5337.
32. Yang X, Karsenty G (2004) ATF4, the osteoblast accumulation of which is determined post-translationally, can induce osteoblast-specific gene expression in non-osteoblastic cells. J Biol Chem 279: 47109–47114.
33. Zhang X, Yu S, Galson DL, Luo M, Fan J, et al. (2008) Activating transcription factor 4 is critical for proliferation and survival in primary bone marrow stromal cells and calvarial osteoblasts. J Cell Biochem 105: 885–895.
34. Yu S, Franceschi RT, Luo M, Zhang X, Jiang D, et al. (2008) Parathyroid hormone increases activating transcription factor 4 expression and activity in osteoblasts: requirement for osteocalcin gene expression. Endocrinology 149: 1960–1968.
35. Nakashima K, Zhou X, Kunkel G, Zhang Z, Deng JM, et al. (2002) The novel zinc finger-containing transcription factor osterix is required for osteoblast differentiation and bone formation. Cell 108: 17–29.
36. Otto F, Thornell AP, Crompton T, Denzel A, Gilmour KC, et al. (1997) Cbfa1, a candidate gene for cleidocranial dysplasia syndrome, is essential for osteoblast differentiation and bone development [see comments]. Cell 89: 765–771.
37. Mundlos S, Otto F, Mundlos C, Mulliken JB, Aylsworth AS, et al. (1997) Mutations involving the transcription factor CBFA1 cause cleidocranial dysplasia [see comments]. Cell 89: 773–779.
38. Komori T, Yagi H, Nomura S, Yamaguchi A, Sasaki K, et al. (1997) Targeted disruption of Cbfa1 results in a complete lack of bone formation owing to maturational arrest of osteoblasts [see comments]. Cell 89: 755–764.
39. Hock JM, Gera I, Fonseca J, Raisz LG (1988) Human parathyroid hormone-(1-34) increases bone mass in ovariectomized and orchidectomized rats. Endocrinology 122: 2899–2904.
40. Tanaka S, Sakai A, Tanaka M, Otomo H, Okimoto N, et al. (2004) Skeletal unloading alleviates the anabolic action of intermittent PTH(1-34) in mouse tibia in association with inhibition of PTH-induced increase in c-fos mRNA in bone marrow cells. J Bone Miner Res 19: 1813–1820.
41. Cole JA (1999) Parathyroid hormone activates mitogen-activated protein kinase in opossum kidney cells. Endocrinology 140: 5771–5779.
42. Dempster DW, Cosman F, Parisien M, Shen V, Lindsay R (1993) Anabolic actions of parathyroid hormone on bone. Endocr Rev 14: 690–709.
43. Calvi LM, Sims NA, Hunzelman JL, Knight MC, Giovannetti A, et al. (2001) Activated parathyroid hormone/parathyroid hormone-related protein receptor in osteoblastic cells differentially affects cortical and trabecular bone. J Clin Invest 107: 277–286.
44. Mosekilde L, Danielsen CC, Sogaard CH, McOsker JE, Wronski TJ (1995) The anabolic effects of parathyroid hormone on cortical bone mass, dimensions and strength—assessed in a sexually mature, ovariectomized rat model. Bone 16: 223–230.
45. Miao D, He B, Jiang Y, Kobayashi T, Soroceanu MA, et al. (2005) Osteoblast-derived PTHrP is a potent endogenous bone anabolic agent that modifies the therapeutic efficacy of administered PTH 1-34. J Clin Invest 115: 2402–2411.
46. Koh AJ, Beecher CA, Rosol TJ, McCauley LK (1999) 3′,5′-Cyclic adenosine monophosphate activation in osteoblastic cells: effects on parathyroid hormone-1 receptors and osteoblastic differentiation in vitro. Endocrinology 140: 3154–3162.
47. Jilka RL (2007) Molecular and cellular mechanisms of the anabolic effect of intermittent PTH. Bone 40: 1434–1446.
48. Chen C, Koh AJ, Datta NS, Zhang J, Keller ET, et al. (2004) Impact of the mitogen-activated protein kinase pathway on parathyroid hormone-related protein actions in osteoblasts. J Biol Chem 279: 29121–29129.
49. Tanaka T, Tsujimura T, Takeda K, Sugihara A, Maekawa A, et al. (1998) Targeted disruption of ATF4 discloses its essential role in the formation of eye lens fibres. Genes Cells 3: 801–810.
50. Hettmann T, Barton K, Leiden JM (2000) Microphthalmia due to p53-mediated apoptosis of anterior lens epithelial cells in mice lacking the CREB-2 transcription factor. Dev Biol 222: 110–123.
51. Wang YH, Liu Y, Buhl K, Rowe DW (2005) Comparison of the action of transient and continuous PTH on primary osteoblast cultures expressing differentiation stage-specific GFP. J Bone Miner Res 20: 5–14.
52. Schmidt IU, Dobnig H, Turner RT (1995) Intermittent parathyroid hormone treatment increases osteoblast number, steady state messenger ribonucleic acid levels for osteocalcin, and bone formation in tibial metaphysis of hypophysectomized female rats. Endocrinology 136: 5127–5134.
53. Kaback LA, Soung do Y, Naik A, Geneau G, Schwarz EM, et al. (2008) Teriparatide (1-34 human PTH) regulation of osterix during fracture repair. J Cell Biochem 105: 219–226.
54. Boguslawski G, Hale LV, Yu XP, Miles RR, Onyia JE, et al. (2000) Activation of osteocalcin transcription involves interaction of protein kinase A- and protein kinase C-dependent pathways. J Biol Chem 275: 999–1006.
55. Ogata Y, Nakao S, Kim RH, Li JJ, Furuyama S, et al. (2000) Parathyroid hormone regulation of bone sialoprotein (BSP) gene transcription is mediated through a pituitary-specific transcription factor-1 (Pit-1) motif in the rat BSP gene promoter. Matrix Biol 19: 395–407.
56. Wang BL, Dai CL, Quan JX, Zhu ZF, Zheng F, et al. (2006) Parathyroid hormone regulates osterix and Runx2 mRNA expression predominantly through protein kinase A signaling in osteoblast-like cells. J Endocrinol Invest 29: 101–108.
57. van der Horst G, Farih-Sips H, Lowik CW, Karperien M (2005) Multiple mechanisms are involved in inhibition of osteoblast differentiation by PTHrP and PTH in KS483 Cells. J Bone Miner Res 20: 2233–2244.
58. Karsenty G (2000) Role of Cbfa1 in osteoblast differentiation and function. Semin Cell Dev Biol 11: 343–346.
59. Xiao G, Jiang D, Ge C, Zhao Z, Lai Y, et al. (2005) Cooperative Interactions between Activating Transcription Factor 4 and Runx2/Cbfa1 Stimulate Osteoblast-specific Osteocalcin Gene Expression. J Biol Chem 280: 30689–30696.
60. Liu F, Lee SK, Adams DJ, Gronowicz GA, Kream BE (2007) CREM deficiency in mice alters the response of bone to intermittent parathyroid hormone treatment. Bone 40: 1135–1143.
61. Dobreva G, Chahrour M, Dautzenberg M, Chirivella L, Kanzler B, et al. (2006) SATB2 is a multifunctional determinant of craniofacial patterning and osteoblast differentiation. Cell 125: 971–986.
62. Yu S, Jiang Y, Galson DL, Luo M, Lai Y, et al. (2008) General transcription factor IIA-gamma increases osteoblast-specific osteocalcin gene expression via activating transcription factor 4 and runt-related transcription factor 2. J Biol Chem 283: 5542–5553.
63. Tominaga H, Maeda S, Hayashi M, Takeda S, Akira S, et al. (2008) CCAAT/Enhancer-binding Protein {beta} Promotes Osteoblast Differentiation by Enhancing Runx2 Activity with ATF4. Mol Biol Cell.
64. D'Alonzo RC, Selvamurugan N, Karsenty G, Partridge NC (2001) Physical interaction of the activator protein-1 factors, c-Fos and c- Jun, with Cbfa1 for collagenase-3 promoter activation. J Biol Chem 18: 18.
65. Hess J, Porte D, Munz C, Angel P (2001) AP-1 and Cbfa/runt physically interact and regulate parathyroid hormone- dependent MMP13 expression in osteoblasts through a new osteoblast- specific element 2/AP-1 composite element. J Biol Chem 276: 20029–20038.
66. Wan M, Yang C, Li J, Wu X, Yuan H, et al. (2008) Parathyroid hormone signaling through low-density lipoprotein-related protein 6. Genes Dev 22: 2968–2979.
67. Elefteriou F, Ahn JD, Takeda S, Starbuck M, Yang X, et al. (2005) Leptin regulation of bone resorption by the sympathetic nervous system and CART. Nature 434: 514–520.

68. Zhang C, Cho K, Huang Y, Lyons JP, Zhou X, et al. (2008) Inhibition of Wnt signaling by the osteoblast-specific transcription factor Osterix. Proc Natl Acad Sci U S A 105: 6936–6941.
69. Elefteriou F, Benson MD, Sowa H, Starbuck M, Liu X, et al. (2006) ATF4 mediation of NF1 functions in osteoblast reveals a nutritional basis for congenital skeletal dysplasiae. Cell Metab 4: 441–451.
70. Parfitt AM, Drezner MK, Glorieux FH, Kanis JA, Malluche H, et al. (1987) Bone histomorphometry: standardization of nomenclature, symbols, and units. Report of the ASBMR Histomorphometry Nomenclature Committee. J Bone Miner Res 2: 595–610.
71. Zhao W, Byrne MH, Wang Y, Krane SM (2000) Osteocyte and osteoblast apoptosis and excessive bone deposition accompany failure of collagenase cleavage of collagen. J Clin Invest 106: 941–949.
72. Ducy P, Starbuck M, Priemel M, Shen J, Pinero G, et al. (1999) A Cbfa1-dependent genetic pathway controls bone formation beyond embryonic development. Genes Dev 13: 1025–1036.
73. Xiao G, Cui Y, Ducy P, Karsenty G, Franceschi RT (1997) Ascorbic acid-dependent activation of the osteocalcin promoter in MC3T3-E1 preosteoblasts: requirement for collagen matrix synthesis and the presence of an intact OSE2 sequence. Mol Endocrinol 11: 1103–1113.

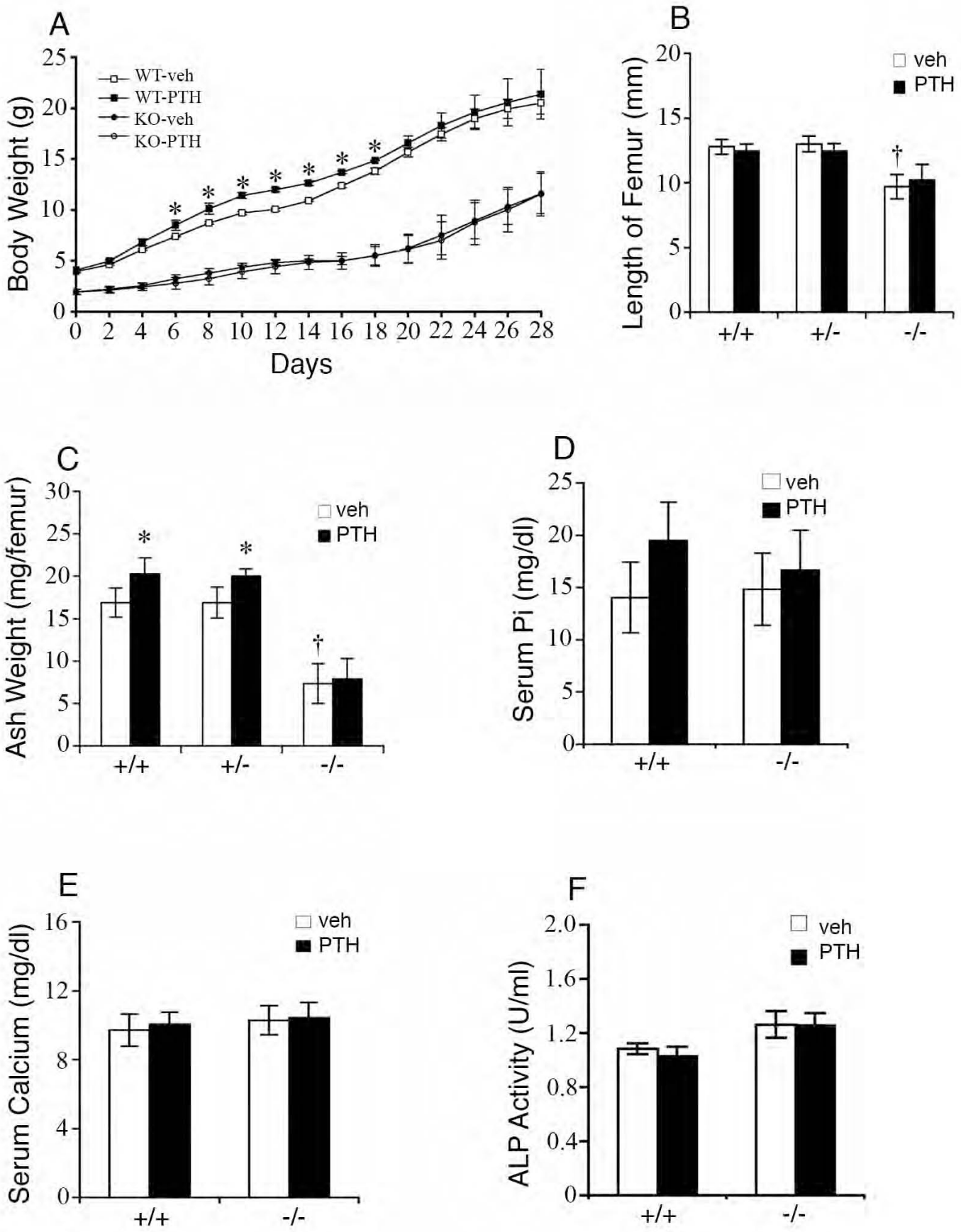
A
Body Weight (g)
Days
WT-veh
WT-PTH
KO-veh
KO-PTH
B
Length of Femur (mm)
veh
PTH
+/+
+/-
-/-
C
Ash Weight (mg/femur)
D
Serum Pi (mg/dl)
E
Serum Calcium (mg/dl)
F
ALP Activity (U/ml)

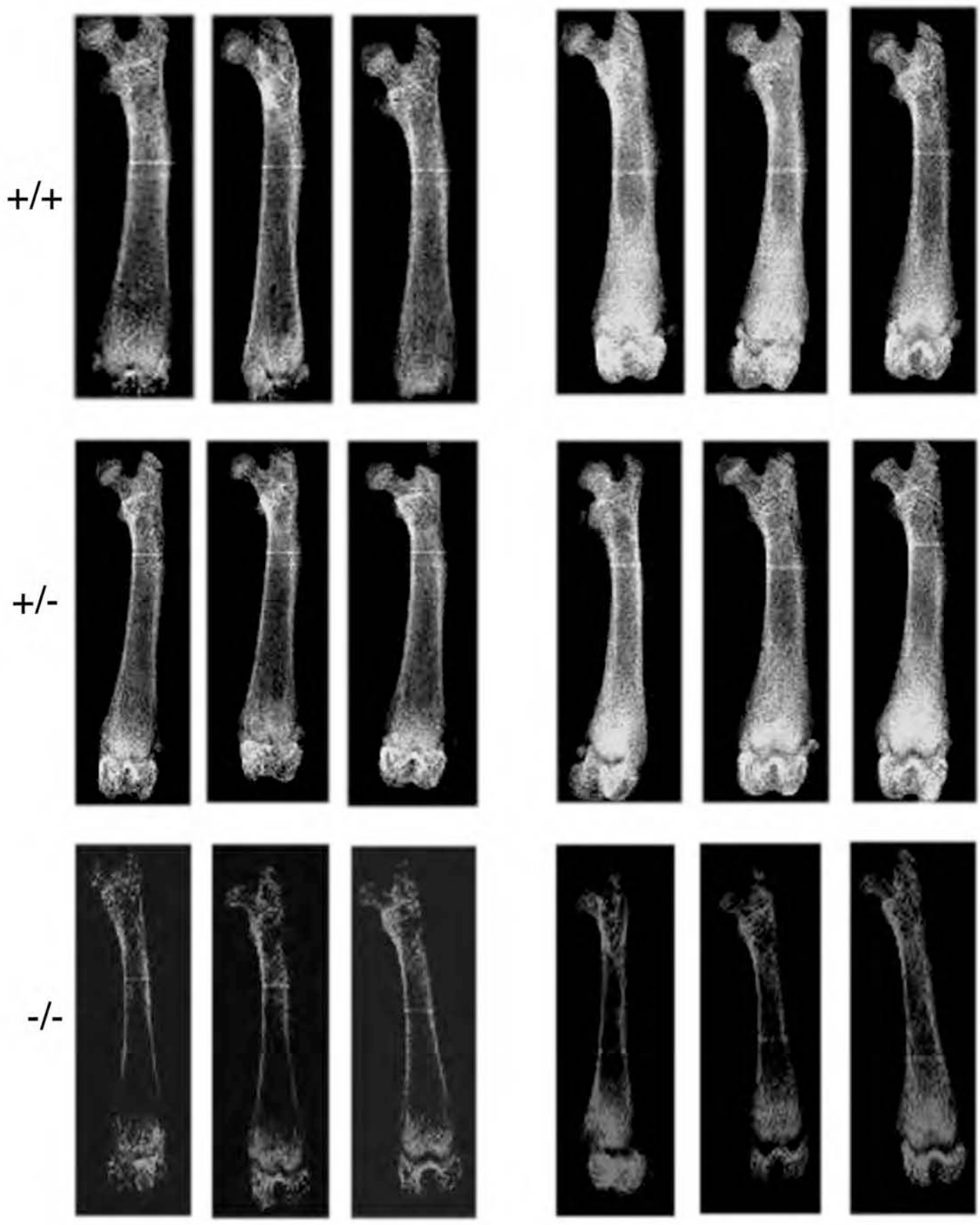
veh
PTH
+/+
+/-
-/-

	Sham(+/+)	OVX(+/+)	Sham(-/-)	OVX(-/-)
BV/TV(%)	12±1.2	3.4±0.5*	1.8±0.08†	2.0±0.12
Tb.N(/mm)	2.2±0.24	1.5±0.06*	1.4±0.07†	1.3±0.01
Tb.Th(μm)	77.2±6.0	62.4±1.2*	59.3±11†	57.4±0.8
Tb.Sp(mm)	0.46±0.04	0.62±0.24*	0.71±0.03†	0.83±0.23
Cort.Th(mm)	0.2±0.05	0.21±0.01	0.17±0.01†	0.18±0.01

N = 3

Supplemental Material can be found at:
http://www.jbc.org/content/suppl/2009/09/30/M109.040980.DC1.html

THE JOURNAL OF BIOLOGICAL CHEMISTRY VOL. 284, NO. 47, pp. 32533–32543, November 20, 2009

Identification and Functional Characterization of ERK/MAPK Phosphorylation Sites in the Runx2 Transcription Factor*[S]

Received for publication, July 3, 2009, and in revised form, September 28, 2009 Published, JBC Papers in Press, September 30, 2009, DOI 10.1074/jbc.M109.040980

Chunxi Ge[‡1], Guozhi Xiao[§1], Di Jiang[‡], Qian Yang[‡], Nan E. Hatch[‡], Hernan Roca[‡], and Renny T. Franceschi[‡¶2]

From the [‡]Department of Periodontics and Oral Medicine, School of Dentistry, and [¶]Department of Biological Chemistry, School of Medicine, University of Michigan, Ann Arbor, Michigan 48109-1078 and the [§]Department of Medicine, University of Pittsburgh, Pittsburgh, Pennsylvania 15240

The Runx2 transcription factor is required for commitment of mesenchymal cells to bone lineages and is a major regulator of osteoblast-specific gene expression. Runx2 is subject to a number of post-transcriptional controls including selective proteolysis and phosphorylation. We previously reported that Runx2 is phosphorylated and activated by the ERK/MAPK pathway (Xiao, G., Jiang, D., Thomas, P., Benson, M. D., Guan, K., Karsenty, G., and Franceschi, R. T. (2000) *J. Biol. Chem.* 275, 4453–4459). In this study, we used a combination of *in vitro* and *in vivo* phosphorylation analysis, mass spectroscopy, and functional assays to identify two sites at Ser[301] and Ser[319] within the proline/serine/threonine domain of Runx2 that are required for this regulation. These sites are phosphorylated by activated ERK1 *in vitro* and in cell culture. In addition to confirming ERK-dependent phosphorylation at Ser[319], mass spectroscopy identified two other ERK-phosphorylated sites at Ser[43] and Ser[510]. Furthermore, introduction of S301A,S319A mutations rendered Runx2 resistant to MAPK-dependent activation and reduced its ability to stimulate osteoblast-specific gene expression and differentiation after transfection into Runx2-null calvarial cells and mesenchymal cells. In contrast, S301E,S319E Runx2 mutants had enhanced transcriptional activity that was minimally dependent on MAPK signaling, consistent with the addition of a negative charge mimicking serine phosphorylation. These results emphasize the important role played by Runx2 phosphorylation in the control of osteoblast gene expression and provide a mechanism to explain how physiological signals acting on bone through the ERK/MAPK pathway can stimulate osteoblast-specific gene expression.

The bone cell lineage is controlled by a hierarchy of transcription factors that are expressed in a defined temporal sequence. Runx2, an essential factor for both hypertrophic cartilage and bone formation, is expressed very early in skeletal development, first appearing coincident with the formation of mesenchymal condensations (1). Subsequent development of the osteoblast lineage requires at least two additional factors; Osterix, which is essential for subsequent progression of the osteoblast lineage, and ATF4, which regulates osteoblast activity, particularly in postnatal animals (2, 3). Runx2 expression continues during the later stages of bone development and persists in regions of active bone remodeling throughout life. Skeletal development in Runx2-deficient mice fails to progress beyond the cartilage anlage stage, whereas dominant-negative suppression of Runx2 even in postnatal animals inhibits osteoblast activity and bone formation (4). Thus, Runx2 is required for both the initial formation of osteoblasts and hypertrophic chondrocytes during development and for sustained osteoblast differentiation during bone remodeling.

Consistent with its multiple roles in bone formation, Runx2 is highly regulated. In addition to transcriptional control by factors such as bone morphogenetic proteins (5), Runx2 activity is controlled both by its interaction with a number of accessory nuclear factors and by post-translational modifications, including phosphorylation. We have been particularly interested in this latter regulation and proposed that Runx2 is phosphorylated and activated by a ERK[3]/MAPK-dependent pathway initiated by the interaction of osteoprogenitors with a type I collagen-containing extracellular matrix (ECM) via $\alpha 2\beta 1$ integrins (6, 7). This collagen-integrin interaction is necessary for subsequent osteoblast-specific gene expression and differentiation (7–9). Consistent with this model, steady-state Runx2 phosphorylation and DNA binding activity increase with osteoblast differentiation, whereas pharmacological inhibition of the ERK/MAPK pathway rapidly inhibits ECM and BMP-induced gene expression (10–12). In related studies, FGF2 treatment of osteoblasts, which is known to stimulate both ERK/MAPK and protein kinase C pathways, increases Runx2 phosphorylation and *Ocn* expression in a MAPK-dependent manner (13). Furthermore, manipulation of the MAPK pathway by overexpression of constitutively active or dominant-negative mutants of MEK1, respectively, increases or decreases osteocalcin gene expression and Runx2 phosphorylation (6). ERK/MAPK signaling is also important for *in vivo* bone development. Transgenic overexpression of constitutively active or dominant-negative MEK1 in mouse osteoblasts, respectively, stimulates or inhibits Runx2 phosphorylation and skeletal maturation. Furthermore,

* This work was supported, in whole or in part, by National Institutes of Health Grants DE11723 and DE12211 (to R. T. F.) and Grant DK072230 and Department of Defense Grant W81XWH-07-1-0160 (to G. X.).

[S] The on-line version of this article (available at http://www.jbc.org) contains supplemental Fig. S1.

[1] Both authors contributed equally to this study.

[2] To whom correspondence should be addressed: University of Michigan School of Dentistry, 1011 N. University Ave., Ann Arbor, MI 48109-1078. Fax: 734-763-5503; E-mail: rennyf@umich.edu.

[3] The abbreviations used are: ERK, extracellular signal-regulated kinase; MAPK, mitogen-activated protein kinase; ECM, extracellular matrix; MEK, mitogen-activated protein kinase/extracellular signal-regulated kinase kinase; OSE2, osteoblast-specific element 2; Mek(sp), constitutively active MEK1 mutant; FGF, fibroblast growth factor; HA, hemagglutinin; aa, amino acid; FBS, fetal bovine serum; MS, mass spectrometry.

the cleidocranial dysplasia phenotype of Runx2 heterozygous null mice can be partially rescued by crossing these animals with mice expressing constitutively active MEK1, consistent with the *in vivo* actions of the ERK/MAPK pathway being at least in part mediated by Runx2 (14).

In addition to the work from our laboratory cited above (6–14), a number of studies from other groups support the concept that ECM-integrin binding, MAPK activation, and Runx2 phosphorylation are important for osteoblast differentiation. The requirement for $\alpha1\beta1$ and $\alpha2\beta1$ collagen-binding integrins in osteoblast differentiation and BMP responsiveness was demonstrated by both *in vitro* and *in vivo* analysis (15–18). Also, ERK/MAPK signaling was shown to be necessary for differentiation of human osteoblasts and marrow stromal cells (19, 20). A number of groups also confirmed that Runx2 can be phosphorylated and activated by MAPK inducers. During the osteoblastic differentiation of human marrow stromal cells, Runx2 levels remain relatively unchanged, but DNA binding increases as does Runx2 phosphorylation (21). Also, mechanical loading of osteoblasts, mediated in part through $\alpha2\beta1$ integrins, induces MAPK activity (22, 23). Similarly, loading of periodontal ligament cells (osteoprogenitor-like cells) increases Runx2 phosphorylation and binding to OSE2 DNA via an ERK/MAPK-dependent process (24). In osteomimetic prostate cancer cells, differentiation is accompanied by ERK1/2 activation, increased Runx2-DNA binding, and *Ocn* expression, responses that were all blocked by MAPK inhibition (25). Last, insulin-like growth factor-1, which activates phosphatidylinositol 3-kinase and, subsequently, ERK/MAPK pathways, stimulates Runx2-OSE2 binding and phosphorylation in vascular endothelial cells (26) as well as differentiation of marrow stromal cells (27, 28). Thus, ERK/MAPK-dependent phosphorylation of Runx2 likely plays an important role in the response of osteoblasts to a variety of signals initiated by cell-ECM binding, hormone/growth factor signaling, and mechanical loading.

To further understand how the ERK/MAPK pathway regulates Runx2 transcriptional activity, in the present study we identify amino acid residues in Runx2 that are phosphorylated in a ERK/MAPK-dependent manner and show that these sites are necessary for osteoblast-specific gene expression and differentiation.

EXPERIMENTAL PROCEDURES

Reagents—The reagents used in this study were obtained from the following sources: tissue culture medium and fetal bovine serum from Invitrogen; U0126 from Calbiochem; mouse anti-Runx2 antibody from MBL; phosphoserine antibody from ABCam; and M2 and M2 horseradish peroxidase-conjugated antibody from Sigma.

DNA Constructs and Viral Expression Vectors—The 0.6-kb mouse osteocalcin gene 2-Luc reporter plasmid and a constitutively active MEK1 expression vector were previously described (29–31). A series of Runx2 expression plasmids encoding HA- or FLAG-tagged full-length type II Runx2 (N-terminal sequence: MASN) or several N- and C-terminal deletions were generated by PCR and subcloning into the pCMV5 expression vector. Serine mutants of full-length and aa 1–330 Runx2 were generated using the QuikChange site-directed mutagenesis kit (Stratagene). A cDNA encoding Runx2 with a biotinylation tag was generated by adding the sequence, MASSLRQILDSQK-MEWRSNAGGS, to the N terminus of mouse Runx2. This sequence is specifically recognized by bacterial BirA biotin ligase (32). Plasmids containing cDNAs encoding the biotinylation tag and BirA were a generous gift from Dr. John Strouboulis (Alexander Fleming Biomedical Sciences Research Center, Athens, Greece). Adenoviruses encoding wild type and mutant Runx2, and biotinylation tagged Runx2, BirA, and Mek(sp) (constitutively active MEK1) were constructed by first subcloning the respective cDNA into pAdloxp and then generating viruses using Cre-Lox recombination as previously described (33).

Cell Culture—C3H10T1/2, COS7, and HEK293 cells were obtained from the American Type Culture Collection and maintained in Dulbecco's modified Eagle's medium containing 10% FBS and 1% antibiotics. An mTERT-immortalized calvarial cell line from Runx2$^{-/-}$ mice (34) was a generous gift from Drs. Jane Lian and Gary Stein (University of Massachusetts Medical Center, Worcester, MA) and maintained in minimal essential medium-α, 10% FBS. MC3T3-E1 clone 4 (MC-4) cells, previously developed in this laboratory (35), were also maintained in minimal essential medium-α, 10% FBS. To induce differentiation, C3H10T1/2, mTERT cells, and MC-4 cells were grown in minimal essential medium-α, 10% FBS containing 50 μg/ml ascorbic acid as previously described (12, 34, 36).

Transfections—COS7 cells were plated at a density of 5×10^4 cells/cm^2 on 35-mm dishes and transfected using Lipofectamine (Invitrogen). Each transfection contained 0.5 μg of the indicated plasmid and 0.05 μg of pRL-SV40 containing a cDNA for *Renilla reniformis* luciferase to control transfection efficiency. Cells were harvested and assayed using a dual luciferase assay kit (Promega) with a Monolight 2010 luminometer (Pharmingen). For mTERT cells, transfection was accomplished using FuGENE 6 reagent (Roche). For studies where effects of more sustained Runx2 expression were analyzed, C3H10T1/2 cells were transduced with adenovirus expression vectors as previously described (36).

Western Blot Analysis—Whole cell extracts were prepared by dissolving cell layers in SDS sample buffer. Samples were fractionated by SDS-PAGE on 4–12% precast minigels (Invitrogen) and electrophoretically transferred to nitrocellulose membranes (Schleicher & Schuell). Primary antibodies were used at the following dilutions (Runx2, 1:500; M2, 1:2000; phosphoserine, 1:500). Secondary antibody was used at a dilution of 1:10,000. Immunoreactivity was detected using ECL chemiluminescence reagents (Amersham Biosciences).

RNA Analysis—RNA was isolated using TRIzol reagent (Invitrogen) and further purified by DNase I treatment and an RNeasy kit (Qiagen). Reverse transcriptase reactions were conducted with 2 μg of total RNA, TaqMan reverse transcriptase reagents, and an oligo(dT) primer (Applied Biosystems)). PCR was performed using an ABI Prism 7700 sequence detection system. Glyceradehyde-3-phosphate dehydrogenase mRNA was used as an endogenous control.

Metabolic Labeling and Immunoprecipitation of Runx2—COS7 cells were transfected with Runx2 expression plasmids, cultured for 30 h, and preincubated in phosphate-free Dulbec-

co's modified Eagle's medium, 0.1% FBS for 12 h. Labeling was conducted for 4 h in phosphate-free Dulbecco's modified Eagle's medium containing 200 μCi/ml [^{32}P]orthophosphate (phosphorus-32 or [^{35}S]methionine/cysteine Tran^{35}S-label, Amersham Biosciences). Nuclear extracts were prepared as previously described (12) and precleared twice with 50 μl of protein A/G-agarose beads. Appropriate antibodies were added and incubated for 2 h at 4 °C with gentle rocking. Immune complexes were then collected by the addition 30 μl of protein A/G-agarose beads and incubation for 1 h at 4 °C followed by centrifugation. Precipitates were washed five times with 1× washing buffer (20 mM HEPES, pH 7.6, 50 mM KCl, 1 mM dithiothreitol, 0.25% Nonidet P-40, 5 mM sodium fluoride, 1 mM EGTA, 5 mM $MgCl_2$). The immunoprecipitated complexes were suspended in SDS sample buffer and analyzed by SDS-PAGE and autoradiography or Western blot analysis using the indicated antibodies. ^{32}P incorporation was measured using a Packard A2024 InstantImager.

In Vitro Phosphorylation—Synthetic peptides were prepared by the University of Michigan Protein Structure Facility. Each peptide (1 μg) was incubated with 10 μCi of [γ-^{32}P]ATP and 1 unit of activated MAPK (Calbiochem) in a buffer containing 25 mM Tris-HCl, pH 7.4, 10 mM $MgCl_2$, 1 mM dithiothreitol, 40 μM ATP, and 0.5 mM EGTA in a final volume of 25 μl. Samples were incubated at 25 °C for 30 min. Reactions were terminated by addition of 25 μl of 2× SDS sample buffer and samples were analyzed by electrophoresis on 15% SDS gels. For *in vitro* Runx2 phosphorylation, biotinylated Runx2 was purified on streptavidin beads as described below and directly phosphorylated by incubation of beads under the same conditions used for peptide phosphorylation, except that [γ-^{32}P]ATP was omitted.

Runx2 Purification and Identification of Phosphorylation Sites by Mass Spectroscopy—An adenovirus expression system for biotinylation tagging of Runx2 was developed (32). COS7 cells were transduced with adenovirus encoding Runx2 cDNA with an N-terminal biotinylation sequence and AdBirA (adenovirus expressing bacterial biotin protein ligase) with or without AdMek(sp). After 48 h, cell lysates were adsorbed to streptavidin magnetic beads and purified Runx2 was resolved by SDS-PAGE using a 4–12% gradient gel. The Runx2 gel band was alkylated with iodoacetamide and peptide fragments were generated by in-gel digestion with pepsin. Samples were analyzed by LC/MS/MS using a ThermoFisher LTQ Orbitrap XL (NextGenSciences, Ann Arbor, MI). The Orbitrap MS scan was performed at 60,000 full-width at half-maximum resolution and searched using a local copy of Mascot. Phosphorylated peptides containing P-serine were then identified. In certain cases, product ion data were used to confirm identification of the phosphorylation site.

Statistical Analysis—All statistical analyses were performed using SPSS 16.0 Software. Unless indicated otherwise, each reported value is the mean ± S.D. of triplicate independent samples. Statistical significance was assessed using a one-way analysis of variance.

RESULTS

ERK/MAPK-dependent Phosphorylation and Activation of Runx2 Require a Specific Region of the C-terminal Pro/Ser/Thr Domain—Fig. 1*A* shows a schematic of the domain structure of Runx2 with positions of potential phosphorylation sites to be discussed in this study. Activation of the ERK/MAPK pathway by overexpression of a constitutively active form of MEK1 or by treatment with FGF2 was previously shown to stimulate *Ocn* mRNA expression and promoter activity via a mechanism requiring Runx2 (6, 13). An initial deletion analysis of the Runx2 coding sequence showed that removal of the entire C-terminal proline/serine/threonine-rich (Pro/Ser/Thr) domain (contains AD3 and RD regions encompassing amino acid residues 258–528 in the mouse sequence) rendered Runx2 completely resistant to MAPK regulation and phosphorylation. In contrast, deletion of the N-terminal AD1, AD2, and QA-rich regions (amino acids 1–108) lowered basal transcriptional

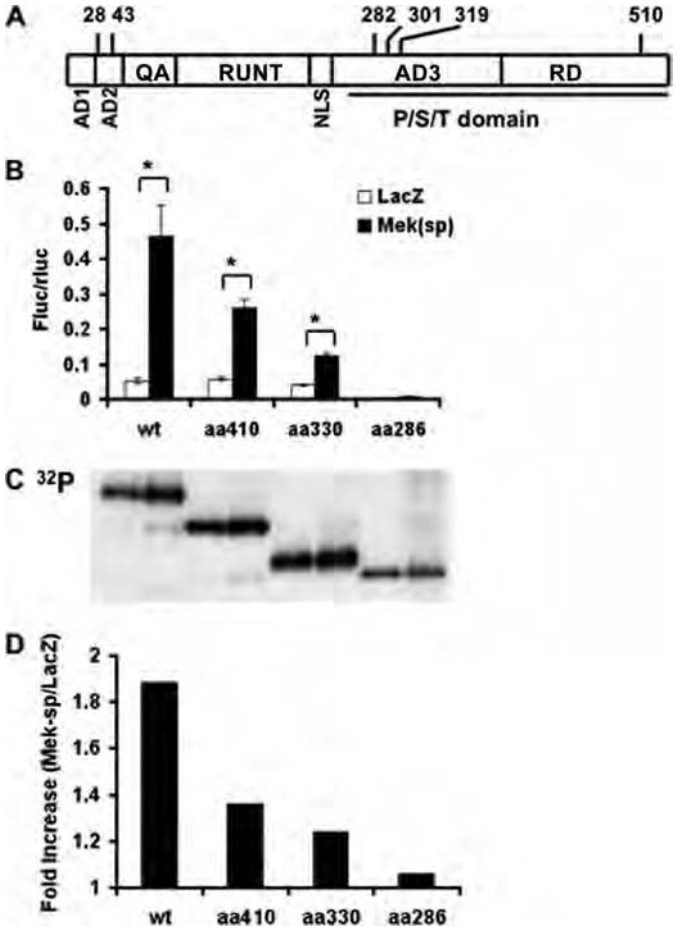

FIGURE 1. **Identification of a region in Runx2 necessary for ERK/MAPK-dependent transcriptional activation and phosphorylation.** *A*, schematic of the domain structure of Runx2 with relevant serine residues indicated. *AD1–3*, transcriptional activation domains; *QA*, glutamine/alanine-rich domain; *RUNT*, runt/DNA-binding domain; *NLS*, nuclear localization sequence; *P/S/T domain*, proline/serine/threonine-rich domain; *RD*, repressor domain (from Ref. 30). *B*, MAPK-dependent transcriptional activity. COS7 cells were transfected with wild type (*WT*) Runx2 or the indicated C-terminal deletions in the presence of control (LacZ) or Mek(sp) expression vectors and a 6OSE2-luc reporter as described under "Experimental Procedures." Firefly luciferase activity was normalized for transfection efficiency using a *R. reinformis* luciferase plasmid. *Asterisk*, significantly different from corresponding control, $p < 0.01$; *brackets* indicate comparisons made; *error bars*, ±S.D. *C* and *D*, Runx2 phosphorylation. COS7 cell cultures treated as in *B* were metabolically labeled with [^{32}P]orthophosphate or Tran^{35}S-label as described under "Experimental Procedures." Runx2 was immunoprecipitated (*C*) and ^{32}P incorporation was normalized to total ^{35}S-labeled protein in each group and expressed as fold-increase with Mek(sp) stimulation (*D*).

activity without affecting MAPK-dependent activation (6). Similarly, deletion of the Pro/Ser/Thr domain also rendered Runx2 unresponsive to activation by FGF2 (13).

To more precisely define regions of Runx2 necessary for MAPK responsiveness, we carried out a more detailed deletion analysis of the Pro/Ser/Thr domain (Fig. 1, *B–D*). Wild type Runx2 or several C-terminal deletions (to residues 410, 330, and 286) were transfected into COS7 cells in the presence or absence of constitutively active MEK1 (Mek(sp)) and a p6OSE2-luc Runx2 reporter gene. Samples were either assayed for luciferase activity (*panel B*) or were metabolically labeled with [^{32}P]orthophosphate and assayed for Runx2 phosphorylation by immunoprecipitation and autoradiography (*panels C* and *D*). C-terminal Runx2 deletions gradually reduced MAPK activation of Runx2 transcriptional activity from ~9-fold with wild type Runx2 to ~3-fold with the amino acid 330 deletion. Mek(sp) stimulation was completely lost with deletion to residue 286. Similarly, Mek(sp) stimulated total ^{32}P incorporation into wild type Runx2 by ~2-fold (*panel C*). This stimulation gradually decreased in the 410 and 330 deletions and was completely lost after deletion to residue 286. These results indicate that the minimal region for MAPK phosphorylation and activation of Runx2 is between amino acids 286 and 330. Subsequent analysis was restricted to this region although it is possible that more C-terminal sites may also participate in this regulation.

Identification of Runx2 Phosphorylation Sites—Inspection of the Runx2 peptide sequence in the 286–330 region (Fig. 2*A*) identified two putative proline-directed serine phosphorylation sites at residues 301 and 319 and an adjacent site at residue 282. A similar proline-directed threonine site was also seen (Thr^{326}). Incubation of peptides spanning the 264 to 337 region with active ERK1 and [γ-^{32}P]ATP revealed that Ser^{282}, Ser^{301}, and Ser^{319} were all phosphorylated *in vitro*, whereas Ser/Ala substitution at each site prevented phosphorylation. In contrast, Thr^{326} was not phosphorylated under these conditions (*i.e.* Introduction of an S319A mutation in the 316–337 peptide blocked phos-

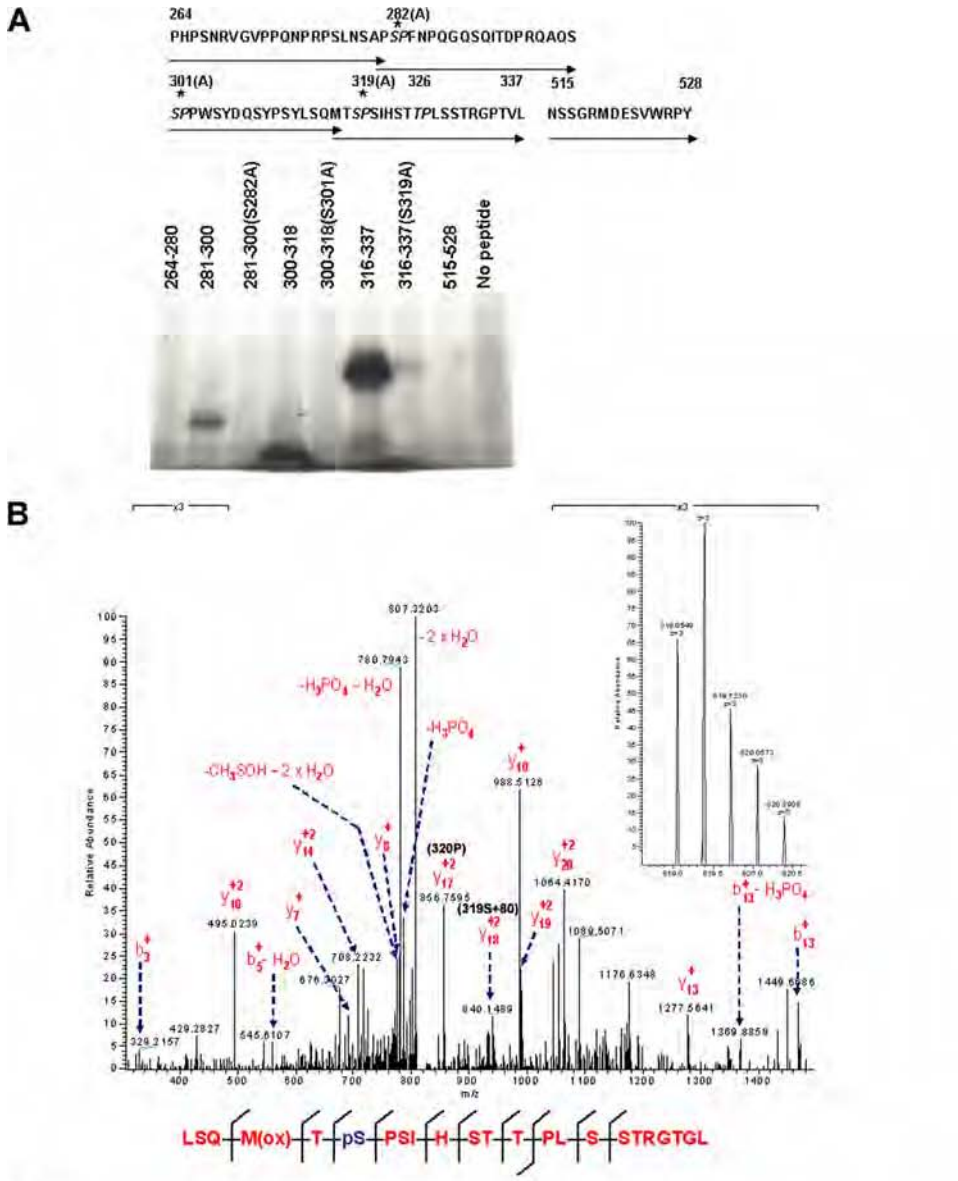

C

Measured Mass-groups	Residues from-to	Peptide sequence filtered by phosphate event	Correlation rate	Serine
In vivo Phophorylation	23-42	TSRRFSPPSSSLQPGKMSDV	95%	S28
	32-48	SSLQPGKMSDVSPVVAA	74%	S43
	276-292	LNSAPSPFNPQGQSOI	95%	S282
	313-337	YLSQMTSPSIHSTTPLSSTRGTGLP	95%	S319
	389-514	LLNPNLPNQNDGVDADGSHSSSPTVL	95%	S510
U0126 Treatment	23-43	SRRFSPPSSSLQPGKMSDVV	88%	S28
In vitro Phosphorylation	23-43	TSRRFSPPSSSLQPGKMSDVS	94%	S24, S28
	22-48	SRRFSPPSSSLQPGKMSDVSPVVAA	73%	S43
	313-337	YLSQMTSPSIHSTTPLSSTRGTGLP	94%	S319,S321
	337-356	LAITDVRPPISDDDTATSDF	77%	S347
	389-514	LLNPNLPNQNDGVDADGSHSSSPTVL	85%	S510

phorylation). Peptides containing residues 264–280 and 515–528 were also not phosphorylated.

More extensive analysis of Runx2 phosphorylation was conducted using mass spectroscopy. COS7 cells were transduced with adenovirus vectors expressing a biotinylation tagged Runx2, BirA (bacterial biotin protein ligase), and Mek(sp). Runx2 was then purified from cell lysates using streptavidin magnetic beads and LC/MS/MS analysis was carried out on pepsin-digested samples. As shown in Fig. 2*B*, five peptides were identified containing phosphoserine at residues 28, 43, 282, 319, and 510. The probability of a correct identification for each peptide was 95% with the exception of the peptide containing Ser^{43}, which had a correlation of 74%. In contrast, only phosphoserine 28 was identified in Runx2 purified from cells pretreated with the MAPK inhibitor, U0126. This indicates that other sites at Ser^{43}, Ser^{282}, Ser^{319}, and Ser^{510} are directly or indirectly dependent on ERK/MAPK activity for phosphorylation. To identify direct MAPK targets, nondenatured Runx2 purified from U0126-treated cells was phosphorylated directly on streptavidin beads with activated P-ERK *in vitro* and MS was repeated. In this case, phosphate was detected on Ser^{24}, Ser^{43}, Ser^{319}, Ser^{347}, and Ser^{510}. From this analysis, we conclude that the *in vivo* phosphorylation sites identified by MS, Ser^{43}, Ser^{319}, and Ser^{510} are probably direct ERK substrates, whereas Ser^{282} is likely phosphorylated by a second kinase activated by ERK. Because we also obtained functional evidence for the importance of Ser^{319} in Runx2 regulation (below), more extensive confirmation that this site is phosphorylated was obtained by analyzing product ion data for the LSQMTpSPSIHSTTPLSSTRGTGL peptide (residues 313–337). Both $[M + 2H]^{2+}$ and $[M + 3H]^{3+}$ charge states were analyzed ($[M + 3H]^{3+}$ is shown in the *left panel* of Fig. 2*C*). Analysis of product ion data (Fig. 2*C*, *right*) confirmed that this peptide was phosphorylated at Ser^{6} (Ser^{319}) within a mass accuracy of 2 ppm.

Surprisingly, although MS analysis consistently identified peptides containing 56–69% of the entire Runx2 sequence (62–76% if the N-terminal Gln/Ala region is excluded), peptides were never identified spanning the Ser^{301} region. Identified peptides contained 11 of the 12 proline-directed serine/threonine sites in Runx2, making Ser^{301} the only site not included in our analysis. Similar results were obtained using alternative protease digestions (trypsin/AspN *versus* pepsin). This suggests that the Ser^{301} region contains some abnormality in secondary structure, possibly due to post-translational modification, which prevents normal fragmentation and identification.

To further explore the possibility that the Ser^{301} site is phosphorylated *in vivo*, we used an indirect approach that takes advantage of the observation that activation of MAPK signaling stimulates a shift in the electrophoretic mobility of a truncated Runx2-(1–330) (Fig. 3*A*). For this experiment, wild type truncated Runx2-(1–330) or Runx2 containing an S301A mutation, an S319A mutation, or combined S301A,S319A mutations was transfected into COS7 cells with or without constitutively active Mek(sp) and ERK1 expression vectors and analyzed by SDS-PAGE. Activation of MAPK signaling clearly reduced the electrophoretic mobility of wild type Runx2-(1–330) and this mobility change was eliminated by treatment of samples with alkaline phosphatase. In contrast, no detectable MAPK-dependent change in mobility was seen with S301A, S319A mutations or the S301A,S319A double mutation. This is the result that would be expected if a detectable mobility shift requires phosphorylation on both Ser^{301} and Ser^{319}.

Although the larger size of full-length Runx2 (528 amino acid residues) precluded conducting mobility shift analysis, we obtained additional evidence for Ser^{301} and Ser^{319} phosphorylation using immunoprecipitation/immunoblotting with Runx2 and Ser(P) antibodies (Fig. 3*B*). COS7 cells were transfected with FLAG-tagged wild type, S301A, S319A, or S301A,S319A full-length Runx2 mutants in the presence or absence of Mek(sp) expression vector or in the presence of the MAPK inhibitor, U0126. Samples were then either immunoprecipitated with a specific anti-Runx2 (M2) antibody followed by Western blotting with antiphosphoserine antibody or, alternatively, immunoprecipitated with antiphosphoserine followed by probing with anti-Runx2 antibody. Cells transfected with WT Runx2 displayed a strong Runx2-associated P-serine signal that was further increased by Mek(sp). S301A or S319A mutations each reduced the P-serine signal to a similar extent, whereas the combined S301A,S319A double mutant displayed even weaker P-serine immunoreactivity. MAPK inhibition (+U0126) greatly reduced the P-serine signal in all groups and eliminated differences between WT and mutant Runx2 as would be expected if Ser^{301} and Ser^{319} were both phosphorylated in a MAPK-dependent manner. However, the fact that the double mutant still displayed a Mek(sp)-dependent increase in P-serine indicates that Runx2 contains additional direct or indirect MAPK phosphorylation sites, in agreement with our MS data.

In summary, multiple phosphorylation sites were identified in Runx2 including two sites in the aa 286–330 region. Definitive identification of Ser^{319} as a direct ERK substrate was established using a combination of *in vitro* peptide phosphorylation, MS/MS, and electrophoresis mobility shift analysis. Strong evidence was also obtained that Ser^{301} is phosphorylated by ERK (*in vitro* peptide phosphorylation, electrophoresis mobility shift analysis, and Ser(P)/Runx2 co-precipitation). However, it

FIGURE 2. **Runx2 phosphorylation sites.** *A*, *in vitro* peptide phosphorylation. Synthetic peptides were prepared containing amino acid residues 264–337 of the Runx2 sequence (indicated by *arrows*) or the indicated amino acid substitutions (*top panel*). Peptides were labeled with [γ-^{32}P]ATP using activated ERK1 and resolved by SDS-PAGE as described under "Experimental Procedures" (*lower panel*). *B*, MS/MS analysis of ERK/MAPK-related phosphorylation sites. COS7 cells were transduced with adenoviruses encoding biotinylation-tagged Runx2, BirA biotin transferase, and Mek(sp) with (U0126 treatment) or without (*in vivo* phosphorylation) MAPK inhibitor. Runx2 as then purified as described under "Experimental Procedures" and subjected to MS/MS analysis. For *in vitro* phosphorylation, an aliquot of Runx2 purified from U0126-treated cells was incubated with the activated MAPK before MS/MS analysis. Phosphopeptides were identified using Mascot software. *Correlation rate* indicates the probability that the indicated peptide identification in the Runx2 sequence is correct. *C*, verification of Ser^{319} phosphorylation. The peptic peptide LSQMTSPSIHSTTPLSSTRGRGL was selected to manually validate the phosphorylation event. Mascot search results indicated that acquired MS/MS spectra contain product ion data for both $[M + 2H]^{2+}$ and $[M + 3H]^{3+}$ charged states for this peptide. The full MS spectra of the $[M + 3H]^{3+}$ charged state is shown in the *left panel*. The *right panel* shows the annotated MS/MS spectra of $m/z = 819.05$ (+3). Diagnostic $Y_{17}{}^{+2}$ and $Y_{18}{}^{+2}$ ions are indicated with m/z values of 856.8 and 940.2, respectively, which confirms the presence of a phosphate on Ser^{319}.

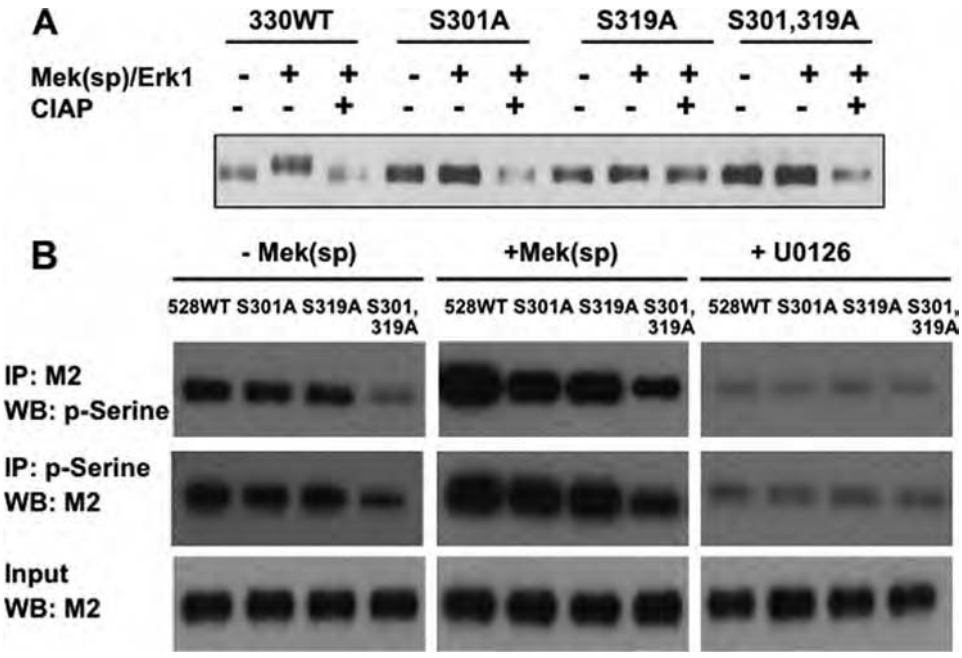

FIGURE 3. **Additional evidence for Runx2 phosphorylation at Ser^{301}.** *A*, analysis of electrophoretic mobility of wild type (*WT*) truncated Runx2-(1–330) and Ser^{301} and Ser^{319} mutants. The indicated truncated Runx2 mutants were expressed in COS7 cells in the presence or absence of Mek(sp) and ERK1 expression vectors. Cell lysates were analyzed by SDS-PAGE with or without prior treatment with calf intestinal alkaline phosphatase (*CIAP*). Runx2 was detected by Western blotting. *B*, anti-P-serine antibody reactivity with full-length Runx2. FLAG-tagged WT Runx2 or the indicated mutants were expressed in COS7 cells in the presence (+) or absence (−) of Mek(sp) or in the presence of the MAPK inhibitor (+*U0126*). Nuclear extracts were then either immunoprecipitated with M2 antibody and probed with an anti-P-serine monoclonal antibody or immunoprecipitated (*IP*) with anti-P-serine and probed with M2.

was not possible to detect peptide fragments containing the Ser^{301} region in MS/MS, precluding its identification using this approach.

Identification of an ERK Binding Region in Runx2—Consistent with the concept that Runx2 is an ERK/MAPK substrate, ERK was shown to bind Runx2 in co-immunoprecipitation assays (Fig. 4). ERK-Runx2 complexes were detected in nuclear extracts from MC-4 cells that have high endogenous levels of both proteins (*panel A*) as well as in COS7 cells transfected with affinity-tagged Runx2 (*panels B–D*). To identify the Runx2 region responsible for ERK binding, COS7 cells were transfected with wild type HA-tagged Runx2, Runx2 with S301A,S319A mutations, or Runx2 with several N-terminal deletions and interactions with endogenous ERK1/2 were examined. Cell lysates were immunoprecipitated with an anti-ERK1/2 antibody and precipitates were probed on Western blots with an anti-HA antibody (Fig. 4*B*, *top*). Wild type Runx2 was clearly coprecipitated with the anti-ERK antibody. Of the N-terminal deletions examined, only the Δ97 fragment was precipitated, whereas Δ232 and 242 deletions failed to interact with ERK. The reciprocal experiment (immunoprecipitation with HA antibody and probing blots with anti-ERK antibody, Fig. 4*B*, *second panel* from *top*) gave equivalent results. Similarly, when C-terminal deletions were examined using FLAG-tagged Runx2 (Fig. 4*C*), Runx2-ERK binding was retained down to and including the Δ330 deletion. This indicates that the ERK binding site is in the runt domain of Runx2. Interestingly, the S301A,S319A mutant Runx2 bound ERK normally, indicating that this interaction does not require intact phosphorylation sites.

Inspection of the runt domain region of Runx2 revealed that it contains a consensus ERK docking "D" site (GKSFTLTITVFTNPP) at aa 201–215 (37). To confirm its role in ERK complex formation, this region of Runx2 was deleted, resulting in complete loss of ERK binding (Fig. 4*D*). The D site deletion also almost completely blocked the ability of Mek(sp) to stimulate Runx2-dependent transcription of a 6OSE2-luc reporter (supplemental Fig. S1).

Functional Analysis of Phosphorylation Sites—We initially assessed the functionality of the above phosphorylation sites in the context of the Runx2-(1–330) fragment because this contained the minimal sequence for MAPK responsiveness. Ser/Ala mutants described above or Ser/Glu mutations were generated at each site individually or in combination, and wild type or mutated expression plasmids were transfected into COS7 cells with 6OSE2-luc +/−Mek(sp). As shown in Fig. 5*A*, the ability of Mek(sp) to stimulate transcriptional activity of Runx2-(1–330) was totally blocked with the MEK1/2 inhibitor, U0126. However, individual Ser/Ala mutations at residues 301 or 319 only slightly inhibited MAPK stimulation, whereas the S282A mutation was without effect. On the other hand, introduction of a S301A,S319A double mutation completely eliminated MAPK responsiveness. In contrast, the S301E,S319E mutant exhibited high basal transcriptional activity in the absence of MAPK stimulation that was not affected by Mek(sp). This is consistent with previous studies showing that addition of the charged amino acid is able to mimic a phosphorylated serine residue (38).

To evaluate the role of phosphorylation sites in the context of the native Runx2 protein, S301A,S319A or S301E,S319E mutations were also introduced into full-length Runx2 and evaluated for Mek(sp) (Fig. 5*B*) or FGF2 responsiveness (Fig. 5*C*) using the same 6OSE2-luc reporter used above. As was the case with Runx2-(1–330), the Mek(sp)-dependent induction of luciferase activity was blocked with U0126, whereas the S301E,S319E mutation resulted in constitutive activation of reporter activity that was not further stimulated by Mek(sp). In contrast to the result obtained with Runx2-(1–330), S301A,S319A mutations only partially blocked the MAPK response (approximately 40% inhibition).

As noted above, FGF2 induction of *Ocn* expression also requires ERK/MAPK activity and is associated with Runx2 phosphorylation (13). A preliminary deletion analysis (not shown) also indicated that FGF2 responsiveness was lost after deletion of the aa 286–330 Runx2 region. To evaluate whether Ser^{301} and Ser^{319} are required for the FGF2 response, wild type

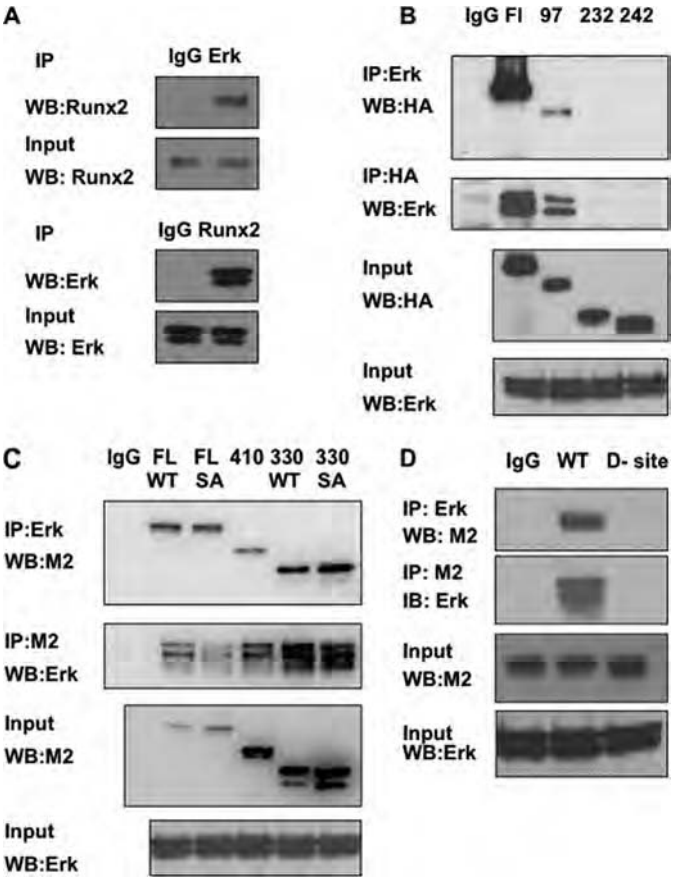

FIGURE 4. **Association of Runx2 with ERK.** *A*, co-immunoprecipitation of endogenous Runx2 and ERK. MC-4 cell nuclear extracts were immunoprecipitated with IgG, ERK, or Runx2 antibodies and blots were probed as indicated. *B–D*, identification of the ERK binding domain in Runx2. Wild type (*WT*) Runx2 or the indicated N-terminal (HA-tagged Runx2, *B*) or C-terminal Runx2 deletions (FLAG-tagged Runx2, *C*) were expressed in COS7 cells and immunoprecipitated (*IP*) with the indicated antibodies. Blots were then probed for Runx2 (HA or M2 antibodies) or total ERK. *Panel C* also shows immunoprecipitation results using either full-length or the 1–330 truncated Runx2 containing either wild type sequence (*WT*) or the S301A,S319A double mutation (*SA*). *Panel D* compares immunoprecipitation activity of WT Runx2 with an internal deletion containing a consensus ERK-binding D site (amino acid residues 201–215).

or S301A,S319A mutant Runx2 were transfected into COS7 cells together with 6OSE2-luc, and luciferase activity was measured after a 24-h treatment with FGF2. Consistent with our previous report (13), FGF2 stimulated 6OSE2-luc activity in a Runx2-dependent manner. However, growth factor activity was significantly reduced, although not eliminated, in cells transfected with the S301A,S319A mutant (Fig. 5*C*). Taken together, studies with full-length Runx2 indicate that Ser^{301} and Ser^{319} phosphorylation sites are important for MAPK responsiveness although more distal sites outside the 1–330 region may also be needed for full transcriptional activation.

Requirement for Ser^{301} and Ser^{319} Phosphorylation Sites for Osteoblast-specific Gene Expression and Differentiation—The studies shown in Fig. 5 demonstrated that S301A,S319A mutations in Runx2-(1–330) completely blocked Mek(sp)-dependent activation of transcriptional activity, whereas the same mutations in the context of the full-length Runx2 molecule only partially eliminated MAPK responsiveness. Because results from transcription assays using constitutively active kinases and artificial reporter constructs often do not mimic those obtained with endogenous genes, we considered it important to show that these mutations also reduce the ability of Runx2 to stimulate endogenous osteoblast gene expression and differentiation. Two approaches were taken to address this issue. In the first, mTERT-immortalized calvarial cells from $Runx2^{-/-}$ mice (34) were transfected with wild type Runx2, S301A,S319A, or S301E,S319E mutants (Fig. 6). After 5 days of growth in ascorbic acid-containing medium to stimulate ECM-dependent differentiation, total RNA was isolated and levels of osteocalcin (*A*) and bone sialoprotein mRNAs (*B*) were measured by quantitative reverse transcription-PCR. As expected, wild type Runx2 transfection strongly induced both mRNAs and this induction was suppressed by the MAPK inhibitor, U0126. In contrast, the S301A,S319A mutant only weakly stimulated mRNA expression and its activity was resistant to further inhibition by U0126. The S301E,S319E mutant, on the other hand, induced *Ocn* and *Bsp* mRNAs to higher levels than those obtained with wild type Runx2 via a mechanism that was largely resistant to MAPK inhibition. As shown in *panel C*, these results cannot be explained by differences in expression levels of wild type and mutant Runx2 proteins.

To examine the requirement for Runx2 phosphorylation sites in osteoblast differentiation over a more prolonged time period, we used an adenovirus expression system in C3H10T1/2 cells. This mesenchymal cell line contains no detectable endogenous Runx2, but will undergo osteoblast differentiation after transduction with an adeno-Runx2 expression vector. Previous studies showed that AdRunx2 vectors continue to produce active transcription factors for at least 7–10 days in this system (36). Wild type and S301A,S319A Runx2 adenovirus were constructed and titered in C3H10T1/2 cells to produce equivalent amounts of Runx2 protein as measured on Western blots. As shown in Fig. 7, wild type Runx2 clearly induced osteoblast differentiation in this system. Sustained induction of alkaline phosphatase activity (*panel A*) as well as *Ocn* and *Bsp* mRNAs (*panels B* and *C*) was observed over a 12-day period. In contrast, cells expressing the Ser/Ala mutant had less than 25% the alkaline phosphatase activity of wild type at all times examined. Induction of *Ocn* and *Bsp* mRNAs was similarly attenuated. Western blot results revealed little or no differences in Runx2 protein levels in the two groups at all times examined, making it unlikely that differences in Runx2 expression or stability could explain these results.

DISCUSSION

In this study, we identified two phosphorylation sites in Runx2 at Ser^{301} and Ser^{319} that are required for MAPK-dependent activation of Runx2 transcriptional activity and osteoblast differentiation. These sites are phosphorylated in a MAPK-dependent manner in intact cells. As shown by MS/MS analysis, at least one, Ser^{319}, is a direct ERK1 substrate. Furthermore, Runx2 can bind ERK using a D site between amino acids 201 and 215 in the runt domain region. Consistent with Ser^{301} and Ser^{319} being important for osteoblast function, inactivating Ser to Ala mutations greatly reduced the ability of Runx2 to stimulate expression of *Ocn* and *Bsp* mRNAs in $Runx2^{-/-}$ calvarial cells and blocked Runx2-dependent induction of osteo-

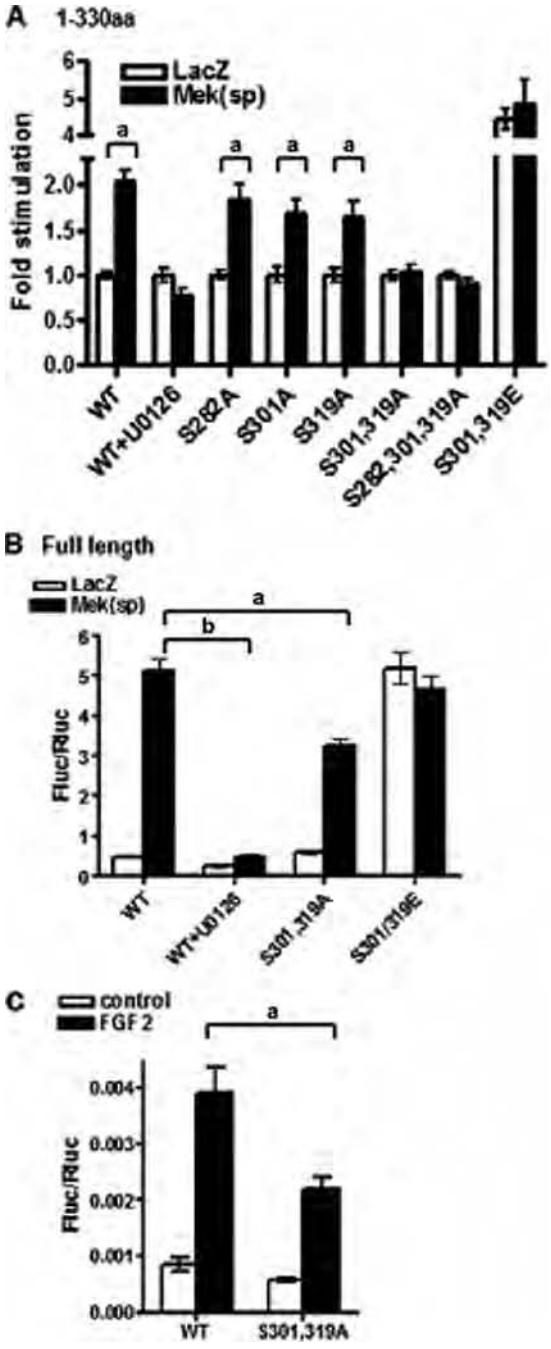

FIGURE 5. **Functional analysis of Runx2 phosphorylation sites.** *A*, identification of phosphorylation sites necessary for MAPK responsiveness using Runx2-(1–330). Specific mutations were created in Runx2-(1–330) to generate S282A, S301A, or S319A mutants or the indicated combinations as well as an S301E,S319E mutant. Runx2 expression plasmids were transfected into COS7 cells in the presence or absence of Mek(sp) vector and luciferase reporters as described in the legend to Fig. 1. *B*, evaluation of requirement for Ser^{301} and Ser^{319} sites in the context of full-length Runx2 protein. S301A,S319A or S301E,S319E mutations were generated in full-length Runx2 and evaluated for Mek(sp) responsiveness as in *panel A*. *C*, FGF2-responsiveness of wild type (*WT*) and mutant Runx2. COS7 cells were transfected with wild type full-length Runx2 or the S301A,S319A mutant. After 24 h, cells were treated for an additional 24 h with FGF2 (50 ηg/ml) before luciferase activity was measured. Statistically significant differences are indicated: *a*, $p < 0.05$; *b*, $p < 0.01$. *Error bars*, ±S.D.

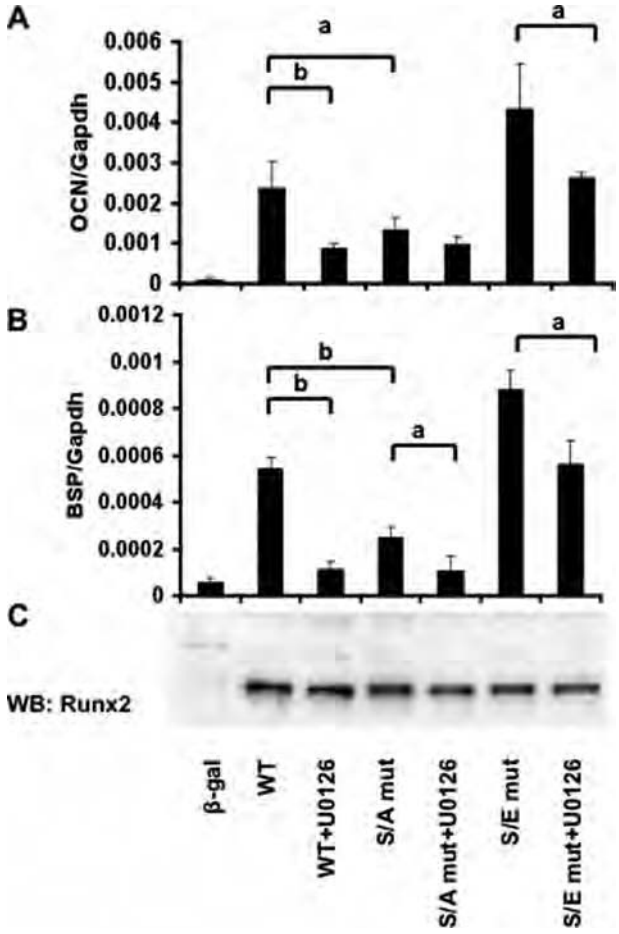

FIGURE 6. **Induction of osteoblast differentiation markers by wild type (*WT*) Runx2 and phosphorylation site mutants.** An mTERT-immortalized cell line derived from $Runx2^{-/-}$ calvaria was transfected with wild type and mutant Runx2 expression vectors and grown for 5 days in ascorbic acid-containing medium before measurement of *Ocn* (*A*) and *Bsp* (*B*) mRNAs by real-time reverse transcription-PCR. Indicated samples were also treated with U0126 12 h before harvest. The mRNA levels were normalized to glyceraldehyde-3-phosphate dehydrogenase (*Gapdh*) mRNA in each sample. Runx2 protein in each group was measured on Western blots (*WB*) (*C*). *S/A mut*, S301A,S319A mutant; *S/E mut*, S301E,S319E mutant. Statistically significant differences are indicated: *a*, $p < 0.05$; *b*, $p < 0.01$. *β-gal*, β-galactosidase. *Error bars*, ±S.D.

blast gene expression and differentiation in a mesenchymal cell line. In contrast, Ser to Glu mutations, which mimic the charge density of phosphorylated amino acids, activated Runx2-dependent transcription. Taken together, these studies emphasize the importance of MAPK-dependent phosphorylation as a means of controlling Runx2 transcriptional activity in bone.

As one of the major signal transduction pathways in bone, the ERK/MAPK pathway is able to integrate stimuli from growth/differentiation factor binding to receptor tyrosine kinases (39), ECM-integrin binding and focal adhesion kinase activation (40), certain non-genomic actions of estrogens (41), and mechanical stimulation mediated by FAK activation (42) and connexin 43 up-regulation (43). It also has important functions in the differentiation of post-mitotic mesenchymal and neuronal cells (44, 45) and regulates the activity of several tissue-specific transcription factors including MyoD (muscle (46)), Sox9 (cartilage (47)) and peroxisome proliferator-activated receptor γ (adipose (48)). Furthermore, as previously shown by this laboratory, *in vivo* transgenic stimulation of ERK/MAPK signaling in osteoblasts accelerates bone development and is able to partially rescue the cleidocranial dysplasia pheno-

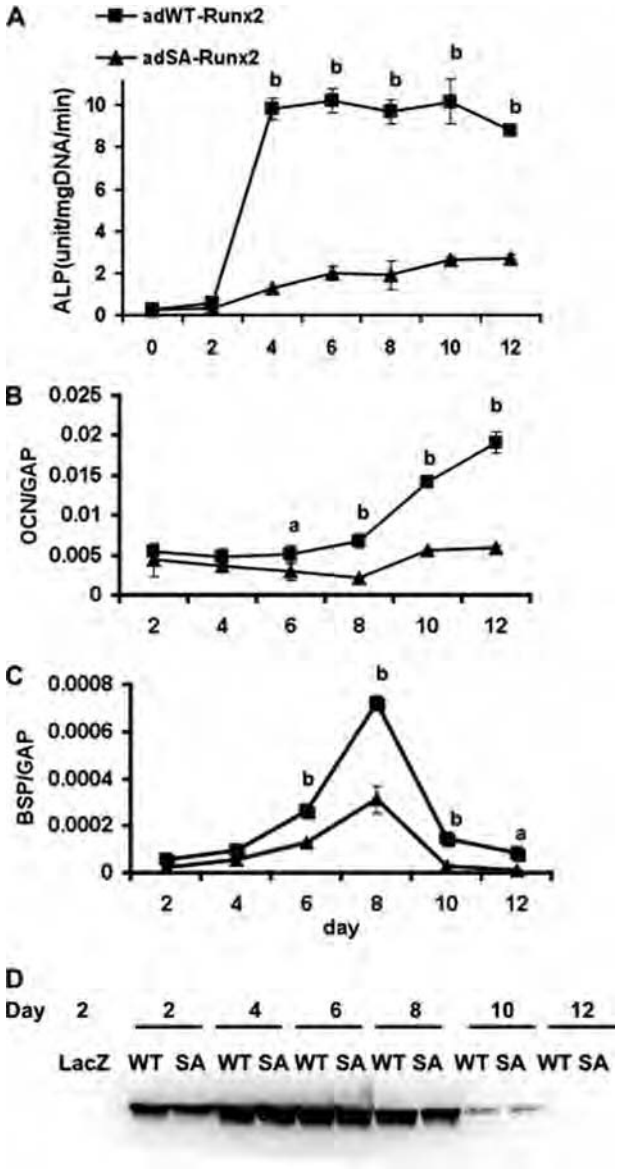

FIGURE 7. **Induction of osteoblast differentiation by wild type Runx2 and the S301A,S319A phosphorylation site mutant.** Adenovirus expression vectors containing wild type and S301A,S319A Runx2 mutants (SA) were used to transduce C3H10T1/2 mesenchymal cells. Cells were then grown in differentiation medium for the indicated times before measurement of alkaline phosphatase activity (*ALP*; *A*) or *Ocn*/*Bsp* mRNA levels (*OCN* and *BSP*; normalized to glyceraldehyde-3-phosphate dehydrogenase (GAP); *C* and *D*). Runx2 protein in each sample was measured on Western blots (*D*). Statistically significant differences are indicated: *a*, $p < 0.05$; *b*, $p < 0.01$. *SA*, S301A,S319A mutant. *Error bars*, ±S.D.

type of Runx2 haploinsufficient mice (14). Based on this work, it is likely that the phosphorylation sites we identified at Ser^{301} and Ser^{319} are critical for regulating Runx2 activity *in vivo* and may function to integrate the osteogenic response to hormonal, mechanical, and environmental stimuli.

Although Ser^{301} and Ser^{319} are clearly very important for Runx2 transcriptional activity, it is possible that other sites also participate in the MAPK response. Specifically, progressively larger C-terminal deletions of Runx2 gradually reduced MAPK-dependent activation of the 6OSE2-luc reporter gene, with the truncated Runx2-(1–330) being the minimal Runx2 truncation that still retained MAPK responsiveness (Fig. 1). It is, therefore, possible that phosphorylation sites in the region between residues 330 and 528 may also participate in the MAPK response, perhaps functioning as secondary sites after priming phosphorylations occur at Ser^{301} and Ser^{319}. Consistent with this idea, our MS/MS analysis, which identified peptides containing all proline-directed serines in Runx2 except Ser^{301}, detected two additional direct MAPK phosphorylation sites at Ser^{43} and Ser^{510} as well as an indirect MAPK site at Ser^{282}. Also, the S301A,S319A mutant Runx2 still retained a MAPK-dependent increase in total P-serine on Western blots as would be expected if additional sites were present (Fig. 3). However, the observation that the high constitutive activity of the S301E,S319E Runx2 mutant was refractory to MAPK inhibition (Fig. 6) argues against these other sites being major contributors to the MAPK response because inhibiting their phosphorylation was not able to prevent the transcriptional activation seen when 301 and 319 sites were in an activated state.

MAPK-dependent phosphorylation of Runx2 is also clearly required for FGF2-dependent induction of *Ocn* expression (13). However, S301A,S319A mutations only partially blocked FGF2 activation of the 6OSE2-luc reporter (Fig. 5*C*). This partial inhibition may be explained by the involvement of additional MAPK sites as well as other kinase sites. In this regard, a recent study by Kim and co-workers (49) reported that FGF2 also activates Runx2 via phosphorylation by PKCγ at Ser^{247}. Thus, it is possible that FGF2 activates Runx2 transcriptional activity by phosphorylating both ERK/MAPK and PKC sites.

Runx family members exhibit a high degree of amino acid sequence conservation, particularly in the DNA binding or Runt domain. Although the C-terminal Pro/Ser/Thr domain of Runx proteins is not highly conserved, the two phosphorylation sites we identified in Runx2 are also present in Runx1 (but not in Runx3). Interestingly, EGF and phorbol ester activation of the ERK/MAPK pathway can stimulate Runx1 transcriptional activity via phosphorylation on these sites (50, 51). Runx1 is essential for hematopoietic cell differentiation (52) and is also a frequent site for chromosomal translocations in acute myelogenous leukemia. Consistent with this oncogenic activity, transfection of Runx1 into fibroblasts stimulates anchorage-independent growth and transformation. Interestingly, Ser/Ala mutations at Ser^{249} and Ser^{266} in Runx1 (equivalent to Ser^{301} and Ser^{319} in Runx2) inhibit growth of NIH 3T3 fibroblasts in soft agar, a common assay for cell transformation (50). Runx2 can also function as an oncogene under certain conditions and has been associated with cell proliferation and migration of breast cancer cells (53, 54). It is, therefore, possible that ERK/MAPK-dependent phosphorylation of Runx2 at Ser^{301} and Ser^{319} could also be associated with this metastasis-related behavior.

It is not presently understood how phosphorylation of Runx2 stimulates transcription. We and others previously observed that the apparent affinity of Runx2 for OSE2-containing DNA increases with differentiation and this increase can be blocked with MAPK inhibition (12, 26, 55). However, it is not known if this is a direct consequence of Runx2 phosphorylation. Interestingly, using chromatin immunoprecipitation assays, we find Runx2 associated with *Ocn* and *Bsp* chromatin in both differentiated and undifferentiated MC3T3-E1 cells even in the pres-

ence of MAPK inhibition (56). Thus, Runx2 does not dissociate from its binding sites on chromatin even though its *in vitro* affinity for DNA may be lower in the unphosphorylated state. Runx2 is also known to serve as a docking site for many nuclear factors that can form active or inactive transcription complexes on chromatin (57). In this regard, we recently showed that the physical association of Runx2 with ERK reported in the present study can also be detected on the chromatin of Runx2 target genes *in vivo* (56). In this case, P-ERK binding to *Ocn* and *Bsp* chromatin required Runx2 and intact Runx2 binding sites in the DNA. Furthermore, this binding was dependent on the elevated MAPK activity associated with osteoblast differentiation. Runx2 can therefore be viewed as providing a docking site for P-ERK on the chromatin of target genes. In addition to phosphorylating Runx2, chromatin-bound P-ERK may also initiate subsequent events such as phosphorylation of other chromatin substrates or the recruitment of additional factors including histone acetyltransferases like p300/cAMP-response element-binding protein to modify chromatin structure, thereby allowing the initiation of transcription. Interestingly, the ERK/MAPK-dependent phosphorylation of Runx1 discussed above is associated with the dissociation of the histone deacetylase co-factor, mSin3a, from Runx1, thereby allowing subsequent increases in histone acetylation (58). Because Runx1 phosphorylation sites are conserved in Runx2, this observation provides a plausible mechanism for how ERK/MAPK phosphorylation could alter Runx2-dependent transcription. This possibility is currently being pursued by this laboratory. Last, Afzal and coworkers (59) showed that MAPK-mediated phosphorylation of Runx2 is also necessary for complex formation with Smads.

In addition to the ERK/MAPK-dependent regulation of Runx2 described herein, several other types of post-translational modifications have been described for this molecule. Phenylthiohydantoin/protein kinase A-mediated phosphorylation of a C-terminal Runx2 site was correlated with induction of MMP13 (60). More recently, Cdk4-mediated phosphorylation at Ser^{472} was shown to target Runx2 for ubiquitination and proteosomal degradation during the cell cycle (61), whereas cdc2 phosphorylation at Ser^{451} was shown to be necessary for cell cycle progression of endothelial cells (62). Also, glycogen synthase kinase 3β-dependent phosphorylation of Runx2 at Ser^{369}-Ser^{373}-Ser^{377} was shown to reduce transcriptional activity (63). Last, Runx2 can be acetylated on critical lysine residues by p300 acetyltransferase. This modification, which is stimulated by BMP2, increases transcription and stabilizes Runx2 against proteosomal degradation (64). Thus, post-translational modification appears to be a common mechanism for regulating Runx2 activity and stability.

In summary, phosphorylation of Runx2 at Ser^{301} and Ser^{319} clearly has an important regulatory role in Runx2-dependent transcription because mutation of these sites in the context of the intact Runx2 molecule severely attenuated the ability of Runx2 to stimulate osteoblast-specific gene expression during differentiation. Ongoing *in vivo* studies will be necessary to assess the full impact of Runx2 phosphorylation to the overall activity of this molecule during skeletal development and remodeling.

REFERENCES

1. Ducy, P., Zhang, R., Geoffroy, V., Ridall, A. L., and Karsenty, G. (1997) *Cell* **89,** 747–754
2. Nakashima, K., Zhou, X., Kunkel, G., Zhang, Z., Deng, J. M., Behringer, R. R., and de Crombrugghe, B. (2002) *Cell* **108,** 17–29
3. Yang, X., Matsuda, K., Bialek, P., Jacquot, S., Masuoka, H. C., Schinke, T., Li, L., Brancorsini, S., Sassone-Corsi, P., Townes, T. M., Hanauer, A., and Karsenty, G. (2004) *Cell* **117,** 387–398
4. Ducy, P., Starbuck, M., Priemel, M., Shen, J., Pinero, G., Geoffroy, V., Amling, M., and Karsenty, G. (1999) *Genes Dev.* **13,** 1025–1036
5. Tou, L., Quibria, N., and Alexander, J. M. (2003) *Mol. Cell Endocrinol.* **205,** 121–129
6. Xiao, G., Jiang, D., Thomas, P., Benson, M. D., Guan, K., Karsenty, G., and Franceschi, R. T. (2000) *J. Biol. Chem.* **275,** 4453–4459
7. Xiao, G., Wang, D., Benson, M. D., Karsenty, G., and Franceschi, R. T. (1998) *J. Biol. Chem.* **273,** 32988–32994
8. Franceschi, R. T., and Iyer, B. S. (1992) *J. Bone Miner. Res.* **7,** 235–246
9. Franceschi, R. T., Iyer, B. S., and Cui, Y. (1994) *J. Bone Miner. Res.* **9,** 843–854
10. Franceschi, R. T., Ge, C., Xiao, G., Roca, H., and Jiang, D. (2007) *Ann. N. Y. Acad. Sci.* **1116,** 196–207
11. Xiao, G., Gopalakrishnan, R., Jiang, D., Reith, E., Benson, M. D., and Franceschi, R. T. (2002) *J. Bone Miner. Res.* **17,** 101–110
12. Xiao, G., Cui, Y., Ducy, P., Karsenty, G., and Franceschi, R. T. (1997) *Mol. Endocrinol.* **11,** 1103–1113
13. Xiao, G., Jiang, D., Gopalakrishnan, R., and Franceschi, R. T. (2002) *J. Biol. Chem.* **277,** 36181–36187
14. Ge, C., Xiao, G., Jiang, D., and Franceschi, R. T. (2007) *J. Cell Biol.* **176,** 709–718
15. Zimmerman, D., Jin, F., Leboy, P., Hardy, S., and Damsky, C. (2000) *Dev. Biol.* **220,** 2–15
16. Takeuchi, Y., Nakayama, K., and Matsumoto, T. (1996) *J. Biol. Chem.* **271,** 3938–3944
17. Takeuchi, Y., Suzawa, M., Kikuchi, T., Nishida, E., Fujita, T., and Matsumoto, T. (1997) *J. Biol. Chem.* **272,** 29309–29316
18. Jikko, A., Harris, S. E., Chen, D., Mendrick, D. L., and Damsky, C. H. (1999) *J. Bone Miner. Res.* **14,** 1075–1083
19. Lai, C. F., Chaudhary, L., Fausto, A., Halstead, L. R., Ory, D. S., Avioli, L. V., and Cheng, S. L. (2001) *J. Biol. Chem.* **276,** 14443–14450
20. Jaiswal, R. K., Jaiswal, N., Bruder, S. P., Mbalaviele, G., Marshak, D. R., and Pittenger, M. F. (2000) *J. Biol. Chem.* **275,** 9645–9652
21. Shui, C., Spelsberg, T. C., Riggs, B. L., and Khosla, S. (2003) *J. Bone Miner. Res.* **18,** 213–221
22. Schmidt, C., Pommerenke, H., Dürr, F., Nebe, B., and Rychly, J. (1998) *J. Biol. Chem.* **273,** 5081–5085
23. Pavalko, F. M., Chen, N. X., Turner, C. H., Burr, D. B., Atkinson, S., Hsieh, Y. F., Qiu, J., and Duncan, R. L. (1998) *Am. J. Physiol. Cell Physiol.* **275,** C1591–C1601
24. Ziros, P. G., Gil, A. P., Georgakopoulos, T., Habeos, I., Kletsas, D., Basdra, E. K., and Papavassiliou, A. G. (2002) *J. Biol. Chem.* **277,** 23934–23941
25. Zayzafoon, M., Abdulkadir, S. A., and McDonald, J. M. (2004) *J. Biol. Chem.* **279,** 3662–3670
26. Qiao, M., Shapiro, P., Kumar, R., and Passaniti, A. (2004) *J. Biol. Chem.* **279,** 42709–42718
27. Celil, A. B., Hollinger, J. O., and Campbell, P. G. (2005) *J. Cell. Biochem.* **95,** 518–528
28. Celil, A. B., and Campbell, P. G. (2005) *J. Biol. Chem.* **280,** 31353–31359
29. Ducy, P., and Karsenty, G. (1995) *Mol. Cell. Biol.* **15,** 1858–1869
30. Thirunavukkarasu, K., Mahajan, M., McLarren, K. W., Stifani, S., and Karsenty, G. (1998) *Mol. Cell. Biol.* **18,** 4197–4208
31. Zheng, C. F., and Guan, K. L. (1993) *J. Biol. Chem.* **268,** 23933–23939
32. de Boer, E., Rodriguez, P., Bonte, E., Krijgsveld, J., Katsantoni, E., Heck, A., Grosveld, F., and Strouboulis, J. (2003) *Proc. Natl. Acad. Sci. U.S.A.* **100,** 7480–7485
33. Hardy, S., Kitamura, M., Harris-Stansil, T., Dai, Y., and Phipps, M. L. (1997) *J. Virol.* **71,** 1842–1849
34. Bae, J. S., Gutierrez, S., Narla, R., Pratap, J., Devados, R., van Wijnen, A. J.,

Stein, J. L., Stein, G. S., Lian, J. B., and Javed, A. (2007) *J. Cell. Biochem.* **100,** 434–449
35. Wang, D., Christensen, K., Chawla, K., Xiao, G., Krebsbach, P. H., and Franceschi, R. T. (1999) *J. Bone Miner. Res.* **14,** 893–903
36. Yang, S., Wei, D., Wang, D., Phimphilai, M., Krebsbach, P. H., and Franceschi, R. T. (2003) *J. Bone Miner. Res.* **18,** 705–715
37. Akella, R., Moon, T. M., and Goldsmith, E. J. (2008) *Biochim. Biophys. Acta* **1784,** 48–55
38. Mansour, S. J., Matten, W. T., Hermann, A. S., Candia, J. M., Rong, S., Fukasawa, K., Vande Woude, G. F., and Ahn, N. G. (1994) *Science* **265,** 966–970
39. Cobb, M. H., Boulton, T. G., and Robbins, D. J. (1991) *Cell Regul.* **2,** 965–978
40. Franceschi, R. T., and Xiao, G. (2003) *J. Cell. Biochem.* **88,** 446–454
41. Kousteni, S., Han, L., Chen, J. R., Almeida, M., Plotkin, L. I., Bellido, T., and Manolagas, S. C. (2003) *J. Clin. Invest.* **111,** 1651–1664
42. Moalli, M. R., Wang, S., Caldwell, N. J., Patil, P. V., and Maynard, C. R. (2001) *J. Appl. Physiol.* **91,** 912–918
43. Lecanda, F., Warlow, P. M., Sheikh, S., Furlan, F., Steinberg, T. H., and Civitelli, R. (2000) *J. Cell Biol.* **151,** 931–944
44. Yao, Y., Li, W., Wu, J., Germann, U. A., Su, M. S., Kuida, K., and Boucher, D. M. (2003) *Proc. Natl. Acad. Sci. U.S.A.* **100,** 12759–12764
45. Kao, S., Jaiswal, R. K., Kolch, W., and Landreth, G. E. (2001) *J. Biol. Chem.* **276,** 18169–18177
46. Zetser, A., Frank, D., and Bengal, E. (2001) *Dev. Biol.* **240,** 168–181
47. Murakami, S., Kan, M., McKeehan, W. L., and de Crombrugghe, B. (2000) *Proc. Natl. Acad. Sci. U.S.A.* **97,** 1113–1118
48. Adams, M., Reginato, M. J., Shao, D., Lazar, M. A., and Chatterjee, V. K. (1997) *J. Biol. Chem.* **272,** 5128–5132
49. Kim, B. G., Kim, H. J., Park, H. J., Kim, Y. J., Yoon, W. J., Lee, S. J., Ryoo, H. M., and Cho, J. Y. (2006) *Proteomics* **6,** 1166–1174
50. Tanaka, T., Kurokawa, M., Ueki, K., Tanaka, K., Imai, Y., Mitani, K., Okazaki, K., Sagata, N., Yazaki, Y., Shibata, Y., Kadowaki, T., and Hirai, H. (1996) *Mol. Cell. Biol.* **16,** 3967–3979
51. Zhang, Y., Biggs, J. R., and Kraft, A. S. (2004) *J. Biol. Chem.* **279,** 53116–53125
52. Tanaka, T., Tanaka, K., Ogawa, S., Kurokawa, M., Mitani, K., Nishida, J., Shibata, Y., Yazaki, Y., and Hirai, H. (1995) *EMBO J.* **14,** 341–350
53. Barnes, G. L., Hebert, K. E., Kamal, M., Javed, A., Einhorn, T. A., Lian, J. B., Stein, G. S., and Gerstenfeld, L. C. (2004) *Cancer Res.* **64,** 4506–4513
54. Pratap, J., Lian, J. B., Javed, A., Barnes, G. L., van Wijnen, A. J., Stein, J. L., and Stein, G. S. (2006) *Cancer Metastasis Rev.* **25,** 589–600
55. Fujita, T., Azuma, Y., Fukuyama, R., Hattori, Y., Yoshida, C., Koida, M., Ogita, K., and Komori, T. (2004) *J. Cell Biol.* **166,** 85–95
56. Li, Y., Ge, C., and Franceschi, R. (2009) *J. Bone Miner. Res.,* in press
57. Lian, J. B., Javed, A., Zaidi, S. K., Lengner, C., Montecino, M., van Wijnen, A. J., Stein, J. L., and Stein, G. S. (2004) *Crit. Rev. Eukaryot. Gene Expr.* **14,** 1–41
58. Imai, Y., Kurokawa, M., Yamaguchi, Y., Izutsu, K., Nitta, E., Mitani, K., Satake, M., Noda, T., Ito, Y., and Hirai, H. (2004) *Mol. Cell. Biol.* **24,** 1033–1043
59. Afzal, F., Pratap, J., Ito, K., Ito, Y., Stein, J. L., van Wijnen, A. J., Stein, G. S., Lian, J. B., and Javed, A. (2005) *J. Cell. Physiol.* **204,** 63–72
60. Selvamurugan, N., Pulumati, M. R., Tyson, D. R., and Partridge, N. C. (2000) *J. Biol. Chem.* **275,** 5037–5042
61. Shen, R., Wang, X., Drissi, H., Liu, F., O'Keefe, R. J., and Chen, D. (2006) *J. Biol. Chem.* **281,** 16347–16353
62. Qiao, M., Shapiro, P., Fosbrink, M., Rus, H., Kumar, R., and Passaniti, A. (2006) *J. Biol. Chem.* **281,** 7118–7128
63. Kugimiya, F., Kawaguchi, H., Ohba, S., Kawamura, N., Hirata, M., Chikuda, H., Azuma, Y., Woodgett, J. R., Nakamura, K., and Chung, U. I. (2007) *PLoS ONE* **2,** e837
64. Jeon, E. J., Lee, K. Y., Choi, N. S., Lee, M. H., Kim, H. N., Jin, Y. H., Ryoo, H. M., Choi, J. Y., Yoshida, M., Nishino, N., Oh, B. C., Lee, K. S., Lee, Y. H., and Bae, S. C. (2006) *J. Biol. Chem.* **281,** 16502–16511

IDENTIFICATION AND FUNCTIONAL CHARACTERIZATION OF EXTRACELLULAR-REGULATED KINASE/MAPK PHOSPHORYLATION SITES IN THE RUNX2 TRANSCRIPTION FACTOR

Chunxi Ge[1,4], Guozhi Xiao[3,4], Di Jiang[1], Qian Yang[1], Nan E. Hatch[1] and Renny T. Franceschi[1,2].
From Department of Periodontics and Oral Medicine, School of Dentistry[1] and Department of Biological Chemistry, School of Medicine[2], University of Michigan, Ann Arbor, MI 48109-1078, [3]Department of Medicine, University of Pittsburgh, Pittsburgh, PA 15240. [4]Both authors contributed equally to this study.

Supplementary Figure S1

Supplementary Figure Legend

Address Correspondence to : Renny T. Franceschi, Department of Periodontics and Oral Medicine, University of Michigan School of Dentistry, 1011 N. University Ave., Ann Arbor, MI 48109-1078; Tel. 734 763-7381; FAX 734 763-5503; email: rennyf@umich.edu

Supplementary Figure S1

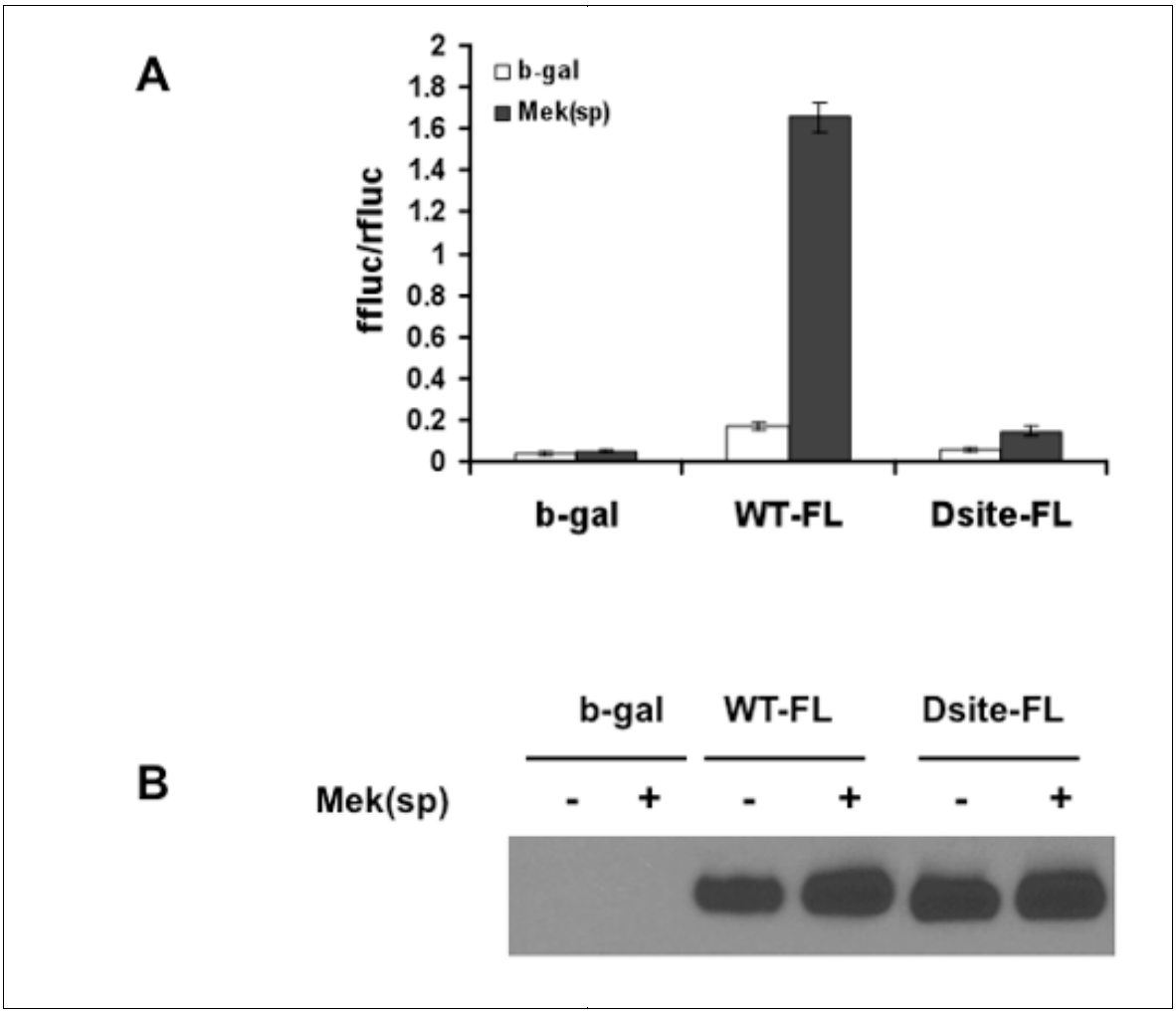

SUPPLEMENTARY FIGURE LEGEND

Supplementary Figure S1. Effect of D site deletion on MAPK-stimulated Runx2 transcriptional activity. Wild type full-length Runx2 (WT-FL) or Runx2 containing a 15 amino acid residue deletion (Δ201-215) spanning the Erk-binding D site (D site-FL) was transfected into COS7 cells with a 6OSE2-luc reporter and renilla normalization vector in the presence or absence of constitutively-active Mek1 (Meksp). After 48 h, cells were harvested for measurement of luciferase activity (A) or total transfected Runx2 protein as measured by immunoblotting (B).

A1

Activating Transcription Factor 4 Mediates the Anabolic Actions of Parathyroid Hormone in Bone

S. Yu[1], R.T. Franceschi[4,5], M. Luo[1], J. Fan[2], D. Jiang[4], H. Cao[1], Y. Lai[3], J. Zhang[1], K. Patrene[1], K. Hankenson[6], G. D. Roodman[1], G. Xiao[1]. Department of Medicine[1], Surgery[2], and Pharmacology and Chemical Biology[3], University of Pittsburgh, Pittsburgh, PA 15240; [4]Department of Periodontics and Oral Medicine, School of Dentistry, [5]Department of Biological Chemistry, School of Medicine, University of Michigan, Ann Arbor, MI 48109; [6]Department of Animal Biology, School of Veterinary Medicine, University of Pennsylvania, Philadelphia, PA 19104-6010.

Parathyroid hormone (PTH) is a potent anabolic agent for the treatment of osteoporosis. However, its mechanism of action in osteoblast and bone is not completely understood. In this study, we show that the anabolic actions of PTH in bone are severely impaired in both growing and adult ovariectomized mice lacking bone-related activating transcription factor 4 (ATF4). Our study demonstrates that inactivation of the *Atf4* gene in mice i) suppresses PTH-stimulated osteoblast proliferation and survival; and ii) abolishes PTH-induced osteoblast differentiation, which, together, compromise the anabolic response. We further demonstrate that intermittent PTH increases osteoblast differentiation in vivo at least in part through an ATF4-dependent up-regulation of Osterix (Osx). ATF4 stimulates Osx expression by activating Osx gene transcription. PTH activates Osx transcription through an ATF4 responsive element in the proximal promoter. ATF4 binds to an endogenous Osx promoter in a PTH-dependent manner. Taken together these experiments establish a novel role for ATF4 in the regulation of the anabolic response of osteoblast and bone to PTH.